

# Sharp Ellipsoid Embeddings and Toric Mutations

ROGER CASALS  
RENATO VIANNA

**ABSTRACT:** This article introduces a new method to construct volume-filling symplectic embeddings of 4-dimensional ellipsoids by employing polytope mutations in toric and almost-toric varieties. The construction uniformly recovers the sharp sequences for the Fibonacci Staircase of McDuff-Schlenk, the Pell Staircase of Frenkel-Müller and the Cristofaro-Gardiner-Kleinman's Staircase, and adds new infinite sequences of sharp ellipsoid embeddings. In addition, we initiate the study of symplectic tropical curves for almost-toric fibrations and emphasize the connection to quiver combinatorics.

## Contents

<b>1</b>	<b>Introduction</b>	<b>2</b>
1.1	Context and Results . . . . .	2
<b>2</b>	<b>Preliminaries</b>	<b>6</b>
2.1	Symplectic Almost-Toric Geometry . . . . .	6
2.2	Polytope Mutations in Almost-Toric Diagrams . . . . .	8
<b>3</b>	<b>Existence of Sharp Sequences of Ellipsoid Embeddings</b>	<b>10</b>
3.1	Realization of a Symington Sequence . . . . .	12
3.2	Arithmetic of Symington Sequences for $(\mathcal{P}, \mathcal{S}) \in \mathcal{H}$ . . . . .	14
3.3	Proof of Theorem 1.3 . . . . .	17
<b>4</b>	<b>Symplectic Tropical Curves in Almost Toric Fibrations</b>	<b>21</b>
4.1	An Introduction to Almost-Toric Tropical Curves . . . . .	22
4.2	Almost-toric Fibrations . . . . .	24
4.3	Symplectic-tropical curves . . . . .	26
4.4	Combinatorial background for triangular shaped ATFs . . . . .	36
4.5	Required Symplectic-Tropical Curves in the $\mathfrak{N}$ for Theorem 1.3 . . . . .	44
4.6	Further Deformations of Symplectic Tropical Curves . . . . .	45
4.7	Getting chains of symplectic-tropical curves . . . . .	50
<b>5</b>	<b>Quiver Combinatorics and Ellipsoid Embeddings</b>	<b>54</b>
5.1	The algebraic recipe . . . . .	55
	<b>Bibliography</b>	<b>58</b>

# 1 Introduction

The novel contribution of the article is the use of polytope mutations as a method for generating sharp ellipsoid embeddings in infinite staircases. In particular, we give a uniform toric mutation explanation for the sharp embeddings in the two classical staircases: the McDuff-Schlenk's Fibonacci Staircase [41, 42] and the Frenkel-Müller's Pell Staircase [14], as well as the more recent discovery by Cristofaro-Gardiner-Kleinman [8]. In addition, we discuss nine 4-dimensional symplectic toric domains  $(X, \omega)$  with a sharp infinite staircase in its symplectic ellipsoid embedding function. These are conjecturally all such domains with this property, as formulated in [9, Conjecture 6.1]. This is the content of the first part of the article, in Sections 2 and 3.

The manuscript also develops new techniques in the study of symplectic tropical curves in almost-toric fibrations, incorporating the works of M. Symington [34, 52] and G. Mikhalkin [45, 46] into the study of symplectic ellipsoid embeddings, and the connections with the theory of cluster algebras and quiver mutations. This is the content of the second part of the article, developed in Sections 4 and 5.

## 1.1 Context and Results

Let  $(\mathbb{R}^4, \omega_{\text{st}})$  be standard symplectic 4-space,  $a, b \in \mathbb{R}^+$ , and consider the symplectic ellipsoid

$$E(a_1, a_2) := \left\{ (x_1, y_1, x_2, y_2) \in \mathbb{R}^4 : \frac{x_1^2 + y_1^2}{a_1} + \frac{x_2^2 + y_2^2}{a_2} \leq 1 \right\} \subseteq (\mathbb{R}^4, \omega_{\text{st}}).$$

Let  $(X, \omega_X)$  be a 4-dimensional symplectic almost-toric domain, as introduced in Section 2. The first goal of this article is to discuss the existence of infinite staircases for the function

$$c_X(a) := \inf \{ \sigma \text{ such that } \exists i : (E(1, a), \omega_{\text{st}}) \hookrightarrow (X, \sigma \cdot \omega_{\text{st}}) \},$$

where  $i$  denotes a *symplectic* embedding, i.e.  $i^* \omega_X = \omega_{\text{st}}$ . A *symplectic* embedding is volume preserving, and thus the volume bound  $\pi^2 a \leq 2\sigma^2 \cdot \text{Vol}(X, \omega_{\text{st}})$  implies

$$\frac{\pi \sqrt{a}}{\sqrt{2 \text{Vol}(X, \omega_{\text{st}})}} \leq c_X(a).$$

The function  $c_X(a)$  is non-decreasing and continuous. The symplectic non-squeezing phenomenon [18] states the existence of values  $a \in \mathbb{R}^+$  for which the above inequality is actually strict. The ground-breaking work of D. McDuff and F. Schlenk [42] establishes for  $(X, \omega_{\text{st}}) = (E(1, 1), \omega_{\text{st}})$  the existence of a non-zero interval  $I_X = [\alpha_X, \Omega_X] \subseteq \mathbb{R}^+$  and a convergent sequence  $S = \{s_n\}_{n \in \mathbb{N}} \subseteq I_X$  such that  $c_X(s_n)$  coincides with the volume lower bound and  $c_X|_{I_X \setminus S}$  is strictly larger than the volume bound. The exact graph for the function  $c_X$  in this case is depicted in [42, Figure 1.1].

**Definition 1.1** A 4-dimensional symplectic domain  $(X, \omega_{\text{st}})$  is said to admit a *sharp infinite staircase* if there exists a non-zero interval  $I_X = [\alpha_X, \Omega_X] \subseteq \mathbb{R}^+$  and an infinite sequence  $S = \{s_n\}_{n \in \mathbb{N}} \subseteq I_X$  of distinct points converging to  $\Omega_X$ , such that  $c_X(s_n)$  coincides with the volume lower bound and  $c_X|_{(I_X \setminus S)}$  is strictly greater than the volume bound. The *sharp points* of a sharp infinite staircase  $(I_X, S)$  are the points  $S = \{s_n\}_{n \in \mathbb{N}}$  where the volume bound for  $c_X|_{I_X}$  is sharp.  $\square$

The existence of a sharp infinite staircase for a 4-dimensional symplectic domain  $(X, \omega_{\text{st}})$  has been a central question in the study of low-dimensional quantitative symplectic geometry, as beautifully developed by D. McDuff, R. Hind, M. Hutchings, F. Schlenk and many others [5, 7, 41, 42, 51].

In the first crucial discovery [42], it is shown that  $(X, \omega_{\text{st}}) = (\mathbb{D}^4(1), \omega_{\text{st}})$ , the standard unit ball, admits an infinite staircase. Two additional results were obtained for the polydisk  $(X, \omega_{\text{st}}) = (\mathbb{D}^2(1) \times \mathbb{D}^2(1), \omega_{\text{st}} \oplus \omega_{\text{st}})$  by Frenkel-Müller [14], and for the ellipsoid  $(X, \omega_{\text{st}}) = (E(2, 3), \omega_{\text{st}})$  by Cristofaro-Gardiner-Kleinman [8].

**Remark 1.2** Definition 1.1 is the notion we use in this manuscript, we refer to M. Usher's [53, Section 1.3] for comparison. The article [9] also consider *non-sharp* staircases where the volume lower-bound is not sharp. This corresponds to their  $J = 3$  case, which would not abide by Definition 1.1.  $\square$

Let  $\mathcal{H}$  be the set of symplectic domains listed in Figure 1. The domains  $(X, \omega_X) \in \mathcal{H}$  are obtained from one of the monotone closed symplectic 4-manifolds  $\mathbb{CP}^2, \mathbb{CP}^1 \times \mathbb{CP}^1, Bl_3(\mathbb{CP}^2)$  and  $Bl_4(\mathbb{CP}^2)$  by removing a configuration of surfaces. These surfaces depend on each item in Figure 1, and thus the choice of  $(X, \omega_X) \in \mathcal{H}$ . Each of these configurations consists of a union of symplectic 2-sphere, lying above the *blue sides* of the almost-toric base, and Lagrangian 2-spheres, located above the *red cuts*. These Lagrangian 2-spheres can be Hamiltonian isotoped to lie above the vertices where the cut starts, and thus  $(X, \omega_X) \in \mathcal{H}$  can also be directly interpreted as the convex domain defined by the polytopes in Figure 1, without taking the red cuts into account.

First, let us state our main result on the construction of sharp ellipsoid embeddings:

**Theorem 1.3** *Let  $(X, \omega_X) \in \mathcal{H}$  be a 4-dimensional symplectic domain. Then the non-decreasing function  $c_X : \mathbb{R} \rightarrow \mathbb{R}$  admits a sequence of sharp points  $S \subseteq I_X$ .*  $\square$

Theorem 1.3 establishes the existence of *sharp* points, which is the constructive ingredient towards infinite staircases. Indeed, the existence of sharp infinite staircases consists of two independent arguments. First, a *constructive* result showing the existence of a sequence of *sharp* points  $S \subseteq I_X$ . Second, an *obstructive* result stating that the volume bound is *not* an equality for the non-sharp points  $I_X \setminus S$ . Our Theorem 1.3 strictly contributes with the constructive part, which is the part that the present manuscript geometrically establishes.

**Remark 1.4** Even if we find the obstructive part equally interesting, our geometric argument is only constructive, not obstructive. The manuscript [9] uses the symplectic capacities from Embedded Contact Homology (ECH), as developed by M. Hutchings [25, 26], to provide the desired obstructions. The combination of our Theorem 1.3, being constructive, and the ECH obstructions in [9] imply that the sequence of sharp points  $S \subseteq I_X$  are indeed part of an infinite staircase. We refer to [9] for a detailed discussion and computation of these ECH capacities.  $\square$

**Example 1.5** The three domains  $(X, \omega_X) \in \mathcal{H}$  in the first row of Figure 1 are the unit ball  $\mathbb{D}^4(1)$ , presented as the complement of a symplectic sphere  $\mathbb{CP}^1 \subseteq (\mathbb{CP}^2, \omega_{\text{st}})$ , the polydisk  $\mathbb{D}^2(1) \times \mathbb{D}^2(1)$ , arising as the complement of the two symplectic sphere  $\mathbb{CP}^1 \times \{pt\}, \{pt\} \times \mathbb{CP}^1 \subseteq (\mathbb{CP}^1 \times \mathbb{CP}^1, \omega_{\text{st}} \oplus \omega_{\text{st}})$ , and  $E(1, 2)$ , presented as the complement of a symplectic sphere  $\mathbb{CP}^1 \times \{pt\} \subseteq (\mathbb{CP}^1 \times \mathbb{CP}^1, \omega_{\text{st}} \oplus \omega_{\text{st}})$  and a Lagrangian 2-sphere  $S^2 \subseteq (\mathbb{CP}^1 \times \mathbb{CP}^1, \omega_{\text{st}} \oplus \omega_{\text{st}})$  in the homology class of the anti-diagonal. Theorem 1.3 for these three domains recovers the Fibonacci stairs [42] and Frenkel-Müller's Pell stairs [14]. The Cristofaro-Gardiner-Kleinman staircase [9] for  $E(2, 3)$  correspond to the rightmost almost-toric base in the second row.  $\square$

The symplectic domains  $(X, \omega_X) \in \mathcal{H}$  not discussed in Example 1.5 do not have particular names, with the exception of the rightmost domain in the second row. For instance, the leftmost domain  $(X, \omega_X) \in \mathcal{H}$  in the second row is the complement in  $Bl_3(\mathbb{CP}^2)$ ,  $\mathbb{CP}^2$  blown-up at three generic points  $p_1, p_2, p_3 \in \mathbb{CP}^2$ , of a configuration of four symplectic 2-spheres: two of the exceptional divisors and the proper transforms of the projective line through  $p_1, p_2$ , and the projective line through  $p_2, p_3$ . These complements do not typically have a given name, except for  $E(2, 3)$ , which appears as the complement of an exceptional divisor and *three* Lagrangian 2-spheres in  $Bl_3(\mathbb{CP}^2)$ .

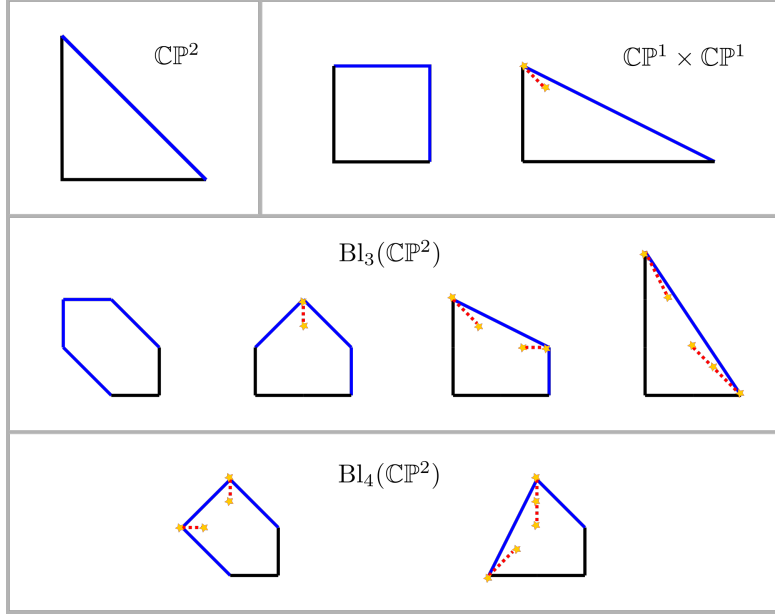


Figure 1: The almost-toric base diagrams for the symplectic domains  $(X, \omega_X)$  in Theorem 1.3. The domains  $(X, \omega_X)$  are the complements of symplectic 2-spheres, in blue, and Lagrangian 2-spheres, in red, in the closed almost-toric symplectic manifold corresponding to each diagram. Note that the same closed symplectic manifold might yield different symplectic domains  $(X, \omega_X)$ , as the choices of symplectic and Lagrangian 2-spheres depend on the almost-toric base diagram.

Second, our method for showing the existence of sharp points requires applying symplectic techniques coming from *tropical* combinatorics in almost-toric diagrams [34, 52]. In particular, our method – including the proof for Theorem 1.3 – requires the introduction and study of *symplectic-tropical curves* in almost-toric fibrations, which represent (configurations of) smooth symplectic curves in 4-dimensional almost-toric symplectic manifolds. In a nutshell, our construction in Section 4 yields the following result:

**Theorem 1.6** *Let  $\pi : (X, \omega_X) \rightarrow B$  be an almost-toric fibration and  $\mathcal{C} \subseteq B$  a symplectic-tropical curve<sup>1</sup> Then there exists a symplectic curve  $C \subseteq X$  with  $\pi(C) = \mathcal{C}$ .*

<sup>1</sup>See Definition 4.6 for a precise description of symplectic tropical curves. They are a generalization of the tropical diagrams in [45, 46] for symplectic surfaces and Lagrangian fibrations with singular nodal fibers.

The statement of Theorem 1.6, as well as the methods we introduce for its proof, are hopefully of interest on their own terms, as they extend the algebraic geometric tropical methods [45, 46] into almost-toric symplectic context. Symplectic tropical curves will be defined in Section 4, where we shall develop the diagrammatics, arithmetic and symplectic geometry associated to symplectic-tropical diagrams in almost-toric polytopes. In fact, the tropical diagrams  $\mathcal{C} \subseteq B$  in Theorem 1.6 allow us to readily compute homological (and geometric) intersection numbers. The construction of the infinite staircases in Theorem 1.3 relies on our study of the symplectic isotopy classes of the symplectic curves  $C_X \subseteq (\bar{X}, \omega_{\bar{X}})$  associated to specific tropical diagrams  $\mathcal{C}$ . Theorem 1.6 further develops the work of M. Symington [52] in line with G. Mikhalkin's study of complex tropical geometry [45]. Section 4 contains a detailed study of the required local models, in Subsections 4.3-4.5, as well as the construction of symplectic chains of embedded curves associated to symplectic-tropical diagrams, in Subsections 4.6 through 4.7.

Finally, the combinatorics and numerics appearing in the infinite staircases from Theorem 1.3 strongly intertwine with the recent developments in the study of cluster algebras [11, 12] and quiver mutations [2, 29]. This connection, and thus a direct relation with homological mirror symmetry, is succinctly illustrated in Section 5.

**Organization.** The article is organized as follows. Section 2 introduces the basic ingredient in almost-toric symplectic geometry. Section 3 proves Theorem 1.3 by constructing the required infinite staircases with the results from Section 4. Section 4 proves Theorem 1.6, and Section 5 describes the combinatorics used for our infinite staircases in terms of quiver mutations.  $\square$

**Acknowledgements.** We are grateful to Dan Cristofaro-Gardiner, Richard Hind, Liana Heuberger, Jeff Hicks, Tara Holm, Alessia Mandini, Dusa McDuff, Navid Nabijou, Ana Rita Pires, Laura Starkston and Weiwei Wu for valuable discussions.

R. Casals is supported by the NSF grant DMS-1841913, an Alfred P. Sloan Fellowship and a BBVA Research Fellowship. R. Vianna's participation at the Matrix program on the Mirror Symmetry and Tropical Geometry at Creswick, Australia was significant for the development of technical aspects of symplectic-tropical curves in Section 4. R. Vianna is supported by Brazil's National Council of scientific and technological development CNPq, via the research fellowships 405379/2018-8 and 306439/2018-2, and by the Serrapilheira Institute grant Serra-R-1811-25965.  $\square$

**Relation to [9].** This article has been posted in parallel with the manuscript [9]. We are grateful to each of its authors, Dan Cristofaro-Gardiner, Tara Holm, Alessia Mandini and Ana Rita Pires, for the fluid and helpful communication with us. It is our understanding that both groups of authors came to the study of this problem from different perspectives, with the idea of using polytope mutations originating with the first author of the present manuscript. Both collaborations have benefited from our exchanges of ideas.

We encourage the reader to study the manuscript [9], which we find to be a very valuable contribution to the theory of symplectic ellipsoid embeddings as well. The results in our article, especially Theorem 1.3 are strengthened by their contributions to the *obstructive* side of the theory, as their manuscript [9] shows that ECH obstructions make the volume bound not sharp away from the required sequences. This clearly highlights the importance of the sharp ellipsoid embeddings we construct, and we gladly acknowledge the relevance and non-triviality of these ECH computations. Their manuscript [9] also

proves Theorem 1.3, equally based on polytope mutations but concluding in a more succinct abstract manner, and formulates a compelling conjecture regarding infinite staircases of rational convex toric domains. Each of the articles addresses the arithmetic of staircases from a different perspective: in this manuscript we directly use the Diophantine implicit equations, and the manuscript [9] proceeds parametrically, in terms of recursions. Even though both manuscripts could potentially be joined, we find that having both articles available is also enriching for the literature, as they discuss different techniques and perspectives.  $\square$

## 2 Preliminaries

In this section we develop notations for the base diagrams of almost-toric fibrations, also known as ATFs [52], which we use in our description of symplectic ellipsoid embeddings. The present section is focused on understanding combinatorial mutations of polytopes that describe these almost-toric fibrations – particularly from the viewpoint of smoothing, and degenerating, toric orbifolds. The more technical aspects of the symplectic topology shall be presented in Subsection 4.2.

### 2.1 Symplectic Almost-Toric Geometry

Let  $\mathcal{P}$  be an integral affine surface with singularities [19, Definition 1.24]. In this article, the regular part  $\mathcal{P}^{reg}$  is always presented as integrally embedded in the standard integral affine structure for  $\mathbb{R}^2$ , given by the standard inclusion  $\mathbb{Z}^2 \subseteq \mathbb{R}^2$ . For our purposes, we define:

**Definition 2.1** An almost-toric base content  $\mathcal{P} = (P, \mathcal{B})$  is a pair where

$$P = \text{conv}(v_1, \dots, v_{|V(P)|}) \subseteq \mathbb{R}^2$$

is the polytope defined by the convex hull of counter-clockwise cyclically ordered  $|V(P)|$  vertices  $v_i \in \mathbb{R}^2$ ,  $1 \leq i \leq |V(P)|$  and  $\mathcal{B}$  is the cut content of  $\mathcal{P}$ . The cut content  $\mathcal{B}$  is defined as the union of pairs  $B_i$ ,  $1 \leq i \leq |V(P)|$ , where  $B_i = (c_i, n_i) \in \mathbb{R}^2 \times \mathbb{N}$  consists of a primitive vector  $c_i \in \mathbb{Z}_2 \subset \mathbb{R}^2$ , pointing inside  $P$  from  $v_i$ , and a non-negative number  $n_i \in \mathbb{N}$ , which accounts for the total number of nodes along  $c_i$ . The primitive vectors must satisfy the consistency condition

$$M_i^{n_i}(v_i - v_{i-1}) = v_{i+1} - v_i,$$

where  $M_i \in GL(2, \mathbb{Z})$  denotes the shear in  $\mathbb{R}^2$  with respect to  $c_i$ .

By definition, an almost-toric base is an almost-toric base content  $\mathcal{P} = (P, \mathcal{B})$ , together with choices of  $r_{i,j} \in \mathbb{R}^+$ , for  $j = 1, \dots, n_i$ ,  $r_{i,j} < r_{i,j-1}$ , so that the cuts  $v_i + tc_i$ ,  $t \in [0, r_{i,1}]$  are disjoint and inside  $P$ . The  $n_i$  nodes associated with  $v_i$  are said to be positioned at  $v_i + r_{i,j}c_i$ .  $\square$

Definition 2.1 is suitable for almost toric fibrations [52, 34] whose base is topologically a disk, as shall be the case in this manuscript. In the case that  $(X, \omega)$  is a Del Pezzo surface, we can and shall take  $c_i = -v_i$ . The vector  $c_i \in \mathbb{R}^2$  in the cut content indicates the direction of the cut at the vertex  $v_i$  and the number  $n_i \in \mathbb{N}$  is the number of singular nodes along the cut at  $v_i$ , placed in the positions  $v_i + r_{i,j}c_i$ , for  $j = 1, \dots, n_i$ . For instance, if  $v_i$  is a toric vertex then  $B_i = (c_i, 1)$  and  $r_{i,1} = 0$ . We have chosen the notation *cut content* in line with the *singular content* as defined in [29]. From now

onwards, we informally refer to  $\mathcal{P} = (P, \mathcal{B})$  as an almost-toric base, referring to an almost toric base with almost-toric base content  $\mathcal{P} = (P, \mathcal{B})$ .

Let us define *mutation* of an almost toric base, which is a different almost toric base that represents the *same* symplectic 4-manifold [52] – for the basics on cut transfers, see [54, 55].

**Definition 2.2** An almost toric base content  $\mu_{v_i}^k \mathcal{P} = (\mu_{v_i}^k P, \mu_{v_i}^k \mathcal{B})$  is said to be *mutated* from the almost toric base content  $\mathcal{P} = (P, \mathcal{B})$  at the vertex  $v_i$  with order  $k \in \{1, \dots, n_i\}$  if it satisfies the following:

- Consider the ray  $\gamma_i$  that leaves  $v_i$  in the direction of  $c_i$ , and  $\tilde{v}$  the intersection with  $\partial P$ . The polytope is divided by  $\gamma_i$  into  $P = P^{(1)} \cup P^{(2)}$ , with  $v_{i-1} \in P^{(1)}$  and  $v_{i+1} \in P^{(2)}$ . Then  $\mu_{v_i}^k P = P^{(1)} \cup M_i^k(P^{(2)})$  or  $\mu_{v_i}^k P = M_i^{-k}(P^{(1)}) \cup P^{(2)}$ .
- The consistency condition for  $\mu_{v_i}^k \mathcal{P}$  implies that, if  $k < n_i$ ,  $v_i$  is a vertex of  $\mu_{v_i}^k \mathcal{P}$ , with content  $(c_i, n_i - k)$ . If  $k = n_i$ ,  $v_i$  is not a vertex of  $\mu_{v_i}^k \mathcal{P}$ . If  $\tilde{v} = v_j$  for some  $j \neq i$ , we assume that  $c_j = -c_i$ , and the content of  $\tilde{v}$  is  $(c_j, n_j + k)$ , otherwise, the content of  $\tilde{v}$  is  $(-c_i, k)$ .

An almost toric base is said to be mutated from another at the vertex  $v_i$  with order  $k \in \{0, \dots, n_i\}$ , if their almost toric base contents are related as above and the position of all the nodes in  $\gamma_i$  are the same. A mutation of order is 1 is said to be a *single* mutation, and a *full* mutation will refer to a mutation of order  $n_i$  at vertex the  $v_i$ .  $\square$

An almost-toric base  $\mathcal{P} = (P, \emptyset)$  with empty cut content yields a complex 2-dimensional toric variety  $X(P)$ , as constructed in [6, 15]. In particular,  $(P, \emptyset)$  gives rise to a real 4-dimensional symplectic toric variety  $(X(P), \omega_{\text{st}})$ , as reviewed in our Section 4. The introduction of non-empty cut content  $\mathcal{B}$  geometrically corresponds to  $\mathbb{Q}$ -Gorenstein smoothing  $X(P, \mathcal{B})$  of  $X(P)$  [29, 31]. Equivalently, there exists a degeneration of  $X(P, \mathcal{B})$  into  $X(P)$ .

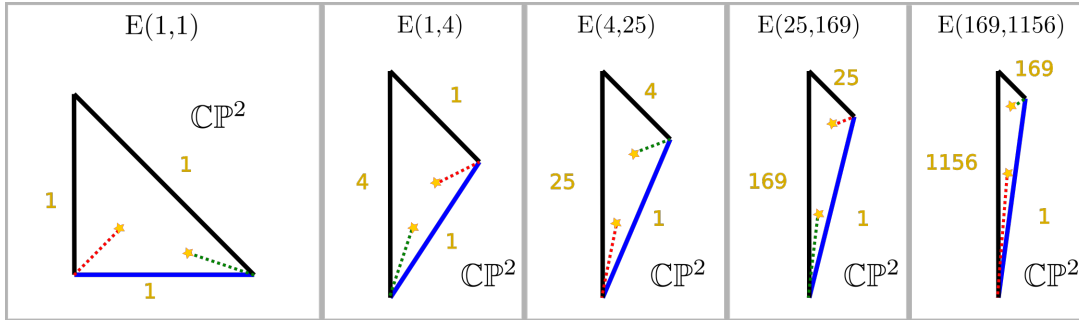


Figure 2: Almost-toric bases for rescalings of  $(\mathbb{CP}^2, \omega_{\text{st}})$ .

**Remark 2.3** It is possible to adapt this definition to incorporate partial smoothing, adjusting the monodromy condition with additional data given by a residual vector associated to the vertex  $v_i$ . That would give rise to almost toric fibrations on orbifolds.  $\square$

**Example 2.4** Consider the five almost-toric bases  $\mathcal{P}_i = (P_i, \mathcal{B}_i)$ ,  $1 \leq i \leq 5$ , depicted in Figure 2, increasingly ordered left to right. In this case, the five symplectic almost-toric varieties  $X(\mathcal{P})$  are



smooth 4-manifolds and, in fact, rescalings of  $(\mathbb{CP}^2, \omega_{\text{st}})$ . The toric varieties  $X(P_i) = X(P_i, \emptyset)$  are singular for  $2 \leq i \leq 5$ , respectively corresponding to the weighted projective spaces  $\mathbb{CP}^2(1, 1, 4)$ ,  $\mathbb{CP}^2(1, 4, 25)$ ,  $\mathbb{CP}^2(1, 25, 169)$  and  $\mathbb{CP}^2(1, 169, 1156)$ . These correspond to the fact that  $\mathbb{CP}^2$  is a  $\mathbb{Q}$ -Gorenstein smoothing of each of these weighted projective spaces.  $\square$

In Example 2.4, the addition of the cut contents  $\mathcal{B}_i$  removes the singularities of the symplectic toric variety  $X(P_i, \emptyset)$ ,  $2 \leq i \leq 5$ . The singularities of the toric varieties we study in this article are cyclic quotient singularities. In general, these singularities cannot be smoothed via a  $\mathbb{Q}$ -Gorenstein deformation, and a singular residue typically persists upon such a deformation [29].

The symplectic domains  $(X, \omega_X) \in \mathcal{H}$  featured in Theorem 1.3 are open subsets of the symplectic 4-manifolds  $X(\mathcal{P})$  obtained by removing collections of symplectic and Lagrangian 2-spheres. Let us introduce the combinatorial structure to encode these surface configurations.

**Definition 2.5** A relative almost-toric base consists of a pair  $(\mathcal{P}, \mathcal{S})$  where  $\mathcal{P} = (P, \mathcal{B})$  is an almost-toric base, and  $\mathcal{S} = S \cup \mathcal{L}$  is a set consisting of sides of the polytope  $P$ , forming a subset  $S \subseteq \mathcal{S}$ , and segments  $l \subseteq \mathcal{S}$  within each cut, a segment being bounded by two consecutive nodes, forming a subset  $\mathcal{L} \subseteq \mathcal{S}$ .  $\square$

In the cases of Theorem 1.3, the sides  $S \subseteq \mathcal{S}$  yield symplectic 2-spheres [34, 52] and the segments  $\mathcal{L} \subseteq \mathcal{S}$  give rise to Lagrangian 2-spheres, as visible surfaces [52]. Indeed, the cut content  $\mathcal{B}$  of an almost-toric base defines a sequence of Lagrangian 2-spheres  $L^j(B_i)$ ,  $0 \leq j \leq n_i, 1 \leq i \leq |V(P)|$ . By definition,  $L^j(B_i)$ ,  $1 \leq j \leq n_i$ , will be the exact Lagrangian 2-sphere with matching cycle the segment in the direction  $c_i \in \mathbb{R}^2$  from the  $j$ th node to the  $(j+1)$ th node, where nodes are ordered increasingly from the vertex  $v_i$  outwards.

Consider a relative almost-toric base  $(\mathcal{P}, \mathcal{S})$ , we denote by  $D(\mathcal{S}) \subseteq X(\mathcal{P})$  the configuration of symplectic divisors  $D(S)$ , associated to the pre-image of the sides of  $S \subseteq \mathcal{S}$  under the almost-toric fibration, and by  $L(\mathcal{L})$  the Lagrangian spheres associated to the segments in  $\mathcal{L} \subseteq \mathcal{S}$ . Note that for the same choice of sides  $S$  in  $P$ , the topology of  $D(S)$  typically depends on the cut content  $\mathcal{B}$  of  $\mathcal{P}$ . We shall denote

$$X(\mathcal{P}, \mathcal{S}) := X(\mathcal{P}) \setminus (D(S) \cup L(\mathcal{L})),$$

the symplectic complement of the symplectic divisors  $D(S)$  and the Lagrangian spheres  $L(\mathcal{L})$  in  $X(\mathcal{P})$ .

**Example 2.6** The unique cut in the rightmost relative almost-toric base  $(\mathcal{P}, \mathcal{S})$  of the first row on Figure 1 yields a Lagrangian 2-sphere  $S^2 \subseteq X(\mathcal{P}) \cong \mathbb{CP}^1 \times \mathbb{CP}^1$ . This is the unique Lagrangian sphere in  $\mathbb{CP}^1 \times \mathbb{CP}^1$ , in the same Hamiltonian isotopy class as the anti-diagonal [23]. The blue side  $S$  in this almost-toric base gives a symplectic divisor in the homology class of  $D(S) = \mathbb{CP}^1 \times \{pt\} \subseteq X(\mathcal{P})$ , and thus  $X(\mathcal{P}, S) \cong \mathbb{CP}^1 \times \mathbb{D}^2(1)$ . Finally, the complement of the anti-diagonal Lagrangian and the symplectic 2-sphere  $D(S)$  is  $X(\mathcal{P}, \mathcal{S}) \cong E(1, 2)$ .  $\square$

## 2.2 Polytope Mutations in Almost-Toric Diagrams

Let  $(X, \omega_X)$  be a 4-dimensional closed *toric* symplectic variety. The moment map  $m : X \rightarrow \mathbb{R}^2$  associated to the Hamiltonian  $T^2$ -action yields a convex polytope  $m(X) = P_X \subseteq \mathbb{R}^2$  [15]. This polytope is the base  $\mathcal{P} = (P, \emptyset)$  of the Lagrangian toric fibration  $m : X \rightarrow m(X)$ , which is a



singular fibration at the boundary  $\partial(P_X) = \mathfrak{m}(X) \setminus \text{Int}(\mathfrak{m}(X))$ , with isotropic fibers. The standard affine structure  $\mathbb{Z}^2 \subseteq \mathbb{R}^2$  in the real plane endows the base of this fibration with an affine structure, which itself coincides with the affine structure associated to the Lagrangian fibration [3].

An *almost-toric* fibration on  $(X, \omega_X)$  is a smooth map  $\pi : X \rightarrow B$ , with allowed singularities being toric and nodal. The precise models are explained in Section 4.2. The regular values of  $\pi$  endows an standard affine structure. A suitable choice of cuts give rise to an almost toric base  $\mathcal{P} = (P_X, \mathcal{B})$  with a continuous map  $B \rightarrow P_X$ , which is affine away from the cuts in  $P_X$ . The composition  $X \xrightarrow{\pi} B \rightarrow P_X$  can be regarded as an analogue of the moment map  $\mathfrak{m} : X \rightarrow \mathbb{R}^2$  and also yields a convex polytope  $\mathfrak{m}(X) = P_X \subseteq \mathbb{R}^2$ , see [52].

Let  $(X, \omega_X) = X(P, \mathcal{B})$  be an almost-toric symplectic variety with almost-toric base  $(P, \mathcal{B})$ , and  $v \in P$  be a vertex of its polytope  $P = \mathfrak{m}(X)$ , with content  $(c_v, n_v)$ . Let us construct a family of Lagrangian *almost-toric* fibrations

$$\mathfrak{m}^t : (X, \omega) \longrightarrow \mathbb{R}^2, \quad t \in [0, 1],$$

with  $\mathfrak{m}^0 = \mathfrak{m}$  and the image  $\mathfrak{m}^1(X)$  being the polytope  $\mu_v^1(P_X)$  obtained by combinatorially mutating  $P_X$  at  $v \in P_X$ , as defined in [1, Section 3], which corresponds to an order one mutation in Definition 2.2 above. This shall be denoted  $\mathfrak{m}^1 = \mu_v^1(\mathfrak{m})$ .

The crucial fact is that these are all fibrations of the *same* symplectic variety  $(X, \omega_X)$ . It is only the presentation of  $(X, \omega_X)$  as an almost-toric symplectic domain that varies. In a nutshell, the geometric idea behind Theorem 1.3 is that different almost-toric fibrations for  $(X, \omega_X)$  make different sharp embeddings of symplectic ellipsoids in  $(X, \omega_X)$  visible.

Let us detail the steps producing the family of maps  $\mathfrak{m}^t$ , which will be discontinuous at  $t = 1$ , but still represents a smooth change of almost toric fibrations on  $(X, \omega_X)$ :

1. First, the introduction of a *nodal trade* at  $v$  (if  $n_v = 1$  and  $r_{1,1} = 0$ ) and subsequent *nodal slides* at the  $n_v$ -th node in direction  $c_v$ , as defined by M. Symington [52], produces a family of almost-toric fibrations, described by  $\mathfrak{m}^t$ ,  $t \in [0, 1)$ , with  $\mathfrak{m}^0 = \mathfrak{m}$ , converging to  $\mathfrak{m}^1$  as  $t \rightarrow 1$ , all with polytope  $P_X$ .
2. Second, apply a single mutation of almost toric base for  $\mathfrak{m}^1(X)$ , obtaining another map  $\mathfrak{m}^1 : (X, \omega) \longrightarrow \mathbb{R}^2$ , by composing  $\mathfrak{m}^1$  with the map  $P_X \longrightarrow \mu_v^1(P_X)$  in Definition 2.2.

We assume that we slide the  $n_v$ -th node long enough so that it is very close to the (often new) vertex  $\tilde{v}$  coming from mutation. In particular, in the case  $X$  is Del Pezzo, we also assume that the node crossed  $0 \in \mathbb{R}^2$ , which represents the monotone fibre. For now, let us assume that  $P_X$  is a triangle, which will simplify our notation and we apply full mutations, so we consider  $\mu_v := \mu_v^1 \circ \dots \circ \mu_v^1 = \mu_v^{n_v}$ .

The process described in the steps above can be iterated for the initial symplectic domain  $(X, \omega_X)$ , as follows. Let  $V = (v_n)_{n \in \mathbb{N}}$  be a sequence of vertices, with  $v_1, v_2$  distinct, such that

$$v_i \in \mu_{v_{i-1}} \mu_{v_{i-2}} \circ \dots \circ \mu_{v_1}(P_X), i \in \mathbb{N},$$

and  $v_j = \tilde{v}_{j-2}$  for all  $j \in \mathbb{N}$ . In short, we choose two vertices  $v_1, v_2 \in P_X$  in a triangle and we first mutate at  $v_1, v_2$ . Then we mutate at the new vertex  $v_3 = \tilde{v}_1 \in \mu_{v_2} \mu_{v_1}(P_X)$  which was first opposite to  $v_1$  in  $P_X$ , and then at  $v_4 = \tilde{v}_2 \in \mu_{v_3} \mu_{v_2} \mu_{v_1}(P_X)$ , which was initially opposite to  $v_2$  in  $\mu_{v_1}(P_X)$ . Note that the triangle  $P_X$  has a vertex  $v_f \in P_X$  which remains fixed under these iterative mutations.

**Example 2.7** Figure 2 shows a sequence of rescaled almost-toric fibrations  $\{\mathbf{m}'\}_{t \in [0,4]}$  at the values  $t = 0, 1, 2, 3, 4$ , on the symplectic manifold  $(\mathbb{CP}^2, \omega_{\text{st}})$ . First, there is a mutation from the toric moment polytope  $P$  for  $(\mathbb{CP}^2, \omega_{\text{st}})$  to  $\mathcal{P}_1 = (P_1, \mathcal{B}_1)$ , where  $\mu^1(P)$  is the toric moment polytope for  $\mathbb{CP}^2(1, 1, 4)$ . The second mutations moves from  $\mathcal{P}_1 = (\mu^1(P), \mathcal{B}_1)$  to  $\mathcal{P}_2 = (\mu^2(P), \mathcal{B}_2)$ , where  $\mu^2(P)$  is the toric moment polytope for  $\mathbb{CP}^2(1, 4, 25)$ . The third mutation leads to the almost-toric base with polytope  $\mu^3(P)$ , the toric moment polytope for  $\mathbb{CP}^2(1, 25, 169)$ , and the fourth mutation arrives at  $\mu^4(P)$ , the toric moment polytope for  $\mathbb{CP}^2(1, 169, 1156)$ . This procedure can be iterated indefinitely, yielding almost-toric bases with their polytope  $\mu^n(P)$  being the toric moment polytope for  $\mathbb{CP}^2(1, a_n, b_n)$ , where  $(a_n, b_n)$  will always be squares of consecutive odd Fibonacci numbers. A clear understanding of this sequence of almost-toric mutations makes Theorem 1.3 for the unit 4-ball  $\mathbb{D}^4(1)$  much more intuitive.  $\square$

### 3 Existence of Sharp Sequences of Ellipsoid Embeddings

The central idea that this manuscript introduces is the use of *almost-toric mutations* in the study of symplectic ellipsoid embeddings. In this section we prove our main result Theorem 1.3, assuming Theorem 3.12, whose proof will require the tropical symplectic techniques developed in Section 4.

Let us start by explaining how to construct symplectic ellipsoid embeddings in an almost-toric domain  $X(\mathcal{P}, \mathcal{S})$  with  $(\mathcal{P}, \mathcal{S})$  a relative almost-toric base.

**Definition 3.1** Let  $P \subseteq \mathbb{R}^2$  be a convex polygon and  $v_0, v_1, v_2 \in V(P)$  three vertices of  $P$ . The triangle  $\bar{T}_{v_0, v_1, v_2} \subseteq P$  is the convex hull of  $v_0, v_1, v_2$ . For  $\varepsilon \in \mathbb{R}_{\geq 0}$ , the open  $\varepsilon$ -triangle  $T_{v_0, v_1, v_2}^\varepsilon \subseteq P$  is the complement  $\bar{T}_{v_0, v_1, v_2} \setminus t^\varepsilon$ , where  $t^\varepsilon \subseteq \bar{T}_{v_0, v_1, v_2}$  is an  $\varepsilon$ -neighborhood of the (open) side  $\text{conv}(v_0, v_2)$  connecting  $v_0, v_2 \in V(P)$ .  $\square$

Let  $(X, \omega) = X(\mathcal{P}, \mathcal{S})$  be symplectic almost-toric manifold with polytope  $P \subseteq \mathcal{P}$ , and assume that  $v_1 \in V(P)$  is a smooth toric vertex. Let  $v_0, v_2$  be the two vertices in  $P$  closest to  $v_1$ . If the open triangle  $T_{v_0, v_1, v_2}^\varepsilon \subseteq P$  does not contain any critical values for the almost-toric fibration  $\mathbf{m}_X : X \rightarrow P$ , the pre-image of  $T_{v_0, v_1, v_2}^\varepsilon$  under  $\mathbf{m}$  yields a symplectic embedding

$$i_{v_1} : E(a, b) \rightarrow (X, \omega),$$

where  $a, b$  are the affine lengths of the two sides  $\text{conv}(v_0, v_1) \cap T_{v_0, v_1, v_2}^\varepsilon$ ,  $\text{conv}(v_1, v_2) \cap T_{v_0, v_1, v_2}^\varepsilon$  respectively. This construction is a potential method for construction symplectic ellipsoid embeddings, but it has the following two disadvantages.

First, for a given  $\varepsilon \in \mathbb{R}^+$ , there are only finitely many open triangles in a moment polytope  $P \subseteq \mathbb{R}^2$  for  $(X, \omega)$  and thus, even if we considered the  $\text{GL}(2, \mathbb{Z})$  action, this observation on its own is not sufficient to build an infinite sequence of ellipsoid embeddings. Second, unless  $P$  is a triangle, i.e.  $|V(P)| = 3$ , the symplectic ellipsoid embeddings of the form  $i_{v_1}$  will not be volume-filling.

The first new geometric idea is that the symplectic manifold  $(X, \omega)$  admits a sequence of *almost-toric* fibrations  $(\mathbf{m}_n)_{n \in \mathbb{N}} : X \rightarrow \mathbb{R}^2$ , as introduced in Section 2.2, which themselves can be used to construct a sequence of symplectic ellipsoid embeddings. The images  $\mathbf{m}_n(X)$  of these almost-toric fibrations are also convex polytopes  $P_n \subseteq \mathbb{R}^2$ . In this almost-toric case, the symplectic embeddings  $i_{v_1}$  are built as above, where the main condition is that the open triangles  $T_{v_0, v_1, v_2}^\varepsilon \subseteq P$  do not include any interior singular values of  $\mathbf{m}_n$ . (This condition is always satisfied in the toric case, as there are no interior singular values for the Lagrangian fibration.)

In Subsection 3.1, we describe the properties for a sequence of almost-toric fibrations  $(\mathbf{m}_n)_{n \in \mathbb{N}} : X \longrightarrow \mathbb{R}^2$  such that each almost-toric fibration admits a volume-filling open triangle  $T_{v_0, v_1, v_2}^\varepsilon \subseteq P$ , for arbitrarily small  $\varepsilon \in \mathbb{R}^+$ . These open triangles give rise to symplectic embeddings

$$i_{v_1}^{(n)} : E(a_n, b_n) \longrightarrow (X, \omega).$$

The arithmetic of the sequence of pairs  $(a_n, b_n) \in \mathbb{N}^2$  is governed by a diophantine equation which depends on the initial choice of  $(\mathcal{P}, \mathcal{S})$ . These equations have featured prominently in birational geometry [21, 27, 28] and the study of coherent sheaves [17, 49, 50], and we present them systematically in Subsection 3.2.

The use of almost-toric fibrations has many advantages, including the fact that we can build sequences of almost-toric fibrations using the theory of *mutations* in algebraic geometry [1, 2, 21]. Nevertheless, the standard techniques have the disadvantage that it requires our symplectic almost-toric manifold  $(X, \omega)$  to be closed. That said, the known tools for polytope mutations and algebraic degenerations do not include the relative case of symplectic divisors and Lagrangian submanifolds. This article starts developing techniques in this direction.

In Theorem 1.3, we are interested in open symplectic toric domains  $X(\mathcal{P}, \mathcal{S})$ , with  $\mathcal{S} \neq \emptyset$ . In order to address this dissonance, we first compactify  $X(\mathcal{P}, \mathcal{S})$  to the closed symplectic toric manifold  $X(\mathcal{P})$  by adding the surface configuration  $D(\mathcal{S}) \subseteq (X, \omega)$ . Then we construct the sequence of almost-toric fibrations  $(\mathbf{m}_n)_{n \in \mathbb{N}} : X(\mathcal{P}) \longrightarrow \mathbb{R}^2$  and, at the same time, keep track of the images of  $D(\mathcal{S}) \subseteq (X, \omega)$  under these almost-toric fibrations. We achieve this latter step by developing a new theory of tropical symplectic curves, in Section 4, and use the uniqueness of certain symplectic isotopy classes in symplectic 4-manifolds [32, 39, 40] and the classification of Lagrangian 2-sphere in the monotone symplectic 4-manifolds  $\mathbb{CP}^1 \times \mathbb{CP}^1, Bl_3(\mathbb{CP}^2), Bl_4(\mathbb{CP}^2)$  [4, 23, 35, 36].

In conclusion, the two main ingredients to execute the above scheme, and thus prove Theorem 1.3, are:

- (i) The construction of a sequence  $(\mathbf{m}_n)_{n \in \mathbb{N}} : X \longrightarrow \mathbb{R}^2$  of almost-toric fibrations, and its associated volume-filling symplectic ellipsoid embeddings  $i^{(n)} : E(a_n, b_n) \longrightarrow (X, \omega)$ . This is the content of Subsections 3.1 and 3.2.
- (ii) Showing that the images  $i^{(n)}(E(a_n, b_n))$  of the symplectic embeddings in Part (i) lie in the complement of the compactifying divisor  $D(\mathcal{S}) \subseteq X(\mathcal{P}, \mathcal{S})$ . This will be argued in Subsection 3.3.

The proof of Theorem 1.3 then proceeds in the following three steps. First, the existence and choice of a Symington Sequence, which addresses the first item above. Second, the construction of tropical configurations realizing  $D(\mathcal{S})$  at each stage of the Symington Sequence, in Section 4. Third, the study of the Hamiltonian isotopy class of these configurations in  $X(\mathcal{P})$ , which is the content of Subsection 3.3. The second and third steps address the second item above.

### 3.0.1 The symplectic domains in Figure 1

The combinatorial reason that sharp ellipsoid staircases can be constructed for the domains in Figure 1 is that they have almost-toric basis with a smooth toric vertex, which admit infinitely many polytope mutations to triangular almost-toric polytopes, with the smooth toric vertex fixed. The nine polytopes in Figure 1 are a subset of the 16 reflexive polytope [29].

These reflexive polytopes also yield one symplectic domains inside of  $Bl_1(\mathbb{CP}^2)$ , and two symplectic domains inside of  $Bl_2(\mathbb{CP}^2)$ , the three of them with infinitely many triangular polytope mutations. The same arguments presented in this article construct infinitely many ellipsoid embeddings  $E(1, a_n)$ , with  $(a_n)_{n \in \mathbb{N}}$  a convergent sequence. Nevertheless, these ellipsoid embeddings are *not* sharp. The twelve symplectic domains presented in [8] are precisely the nine domains in Figure 1 with the addition of these three domains. At this stage, it seems rather natural to ask about the remaining four, of the sixteen, reflexive polytopes. It might be possible to extract interesting staircases using our polytope mutation methods, however, the sequence of polytope mutations shall *not* be of triangular polytopes. The reader is referred to [1, 29] for a thorough study of the mutation classes of reflexive polytopes.  $\square$

### 3.1 Realization of a Symington Sequence

Given an almost-toric symplectic 4-manifold  $X(\mathcal{P})$ , it is possible to mutate an almost-toric fibration for  $X(\mathcal{P})$  as in Subsection 2.2 in many ways. It is *not* true that *any* mutation, even if the underlying polytope is always triangular, will yield a sharp symplectic ellipsoid embedding.

**Example 3.2** We can mutate the triangular polytope  $P_{\mathbb{CP}^2}$  for  $\mathbb{CP}^2 = X(P_{\mathbb{CP}^2}, \emptyset)$  to the toric moment polytope for the weighted projective space  $\mathbb{CP}^2(2, 5, 29)$ . In fact, there are infinitely many  $\mathbb{Q}$ -Gorenstein degenerations of  $\mathbb{CP}^2$  obtained by mutating the triangular polytope  $P_{\mathbb{CP}^2}$ , including  $\mathbb{CP}^2(5, 29, 433)$  and  $\mathbb{CP}^2(2, 29, 169)$  [2, 21]. Neither of these weighted projective spaces readily admits a sharp symplectic ellipsoid embedding, since the three vertices of their toric moment polytopes are singular.  $\square$

Example 3.2 illustrates that a specific choice of sequence of mutations is needed in order to construct sharp ellipsoid embeddings with our method. This leads to the following definition, which we have named after M. Symington, after her exemplary article [52].

**Definition 3.3** A *Symington sequence* for an almost-toric symplectic manifold  $X(\mathcal{P}, \mathcal{S})$  consists of a sequence of pairs  $\{(\mathcal{P}_n, v_n)\}_{n \in \mathbb{N}}$  such that:

- (S1)  $X(\mathcal{P}_n) = X(\mathcal{P})$  for all  $n \in \mathbb{N}$ ,
- (S2)  $P_n$  is a triangle and  $v_n \in V(P_n)$  is a vertex,
- (S3)  $P_{n+1} = \mu_{v_n}(P_n)$ , where  $\mu_{v_n}(P_n)$  is the polytope mutation of  $P_n$  at  $v_n$ ,
- (S4) There exists  $v_f \in \mathbb{R}^2$  such that  $v_f \in V(P_n)$  is a smooth toric vertex, for all  $n \in \mathbb{N}$ .

The vertex  $v_f$  in (S4) will be referred to as a *frozen* vertex, as it does not appear in the sequence  $(v_n)_{n \in \mathbb{N}}$  specifying the sequence of mutations  $(\mu_{v_n})_{n \in \mathbb{N}}$ .  $\square$

The crucial geometric properties in Definition 3.3 are (S1) and (S3), and the fact that we are interested in *ellipsoid* embeddings leads to requiring (S2) and (S4).

**Proposition 3.4** Let  $X(\mathcal{P}, \mathcal{S})$  be a symplectic domain with relative almost-toric base  $(\mathcal{P}, \mathcal{S}) \in \mathcal{H}$ . Then there exists a Symington sequence  $X(\mathcal{P}, \mathcal{S})$ .

**Proof** The statement readily holds for those  $X(\mathcal{P}, \mathcal{S})$  such that  $P \in \mathcal{P}$  is a triangle with a smooth toric vertex. Indeed, if  $P$  is a triangle, a Symington sequence is obtained by choosing one of the two vertices in  $P$  different from  $v_f$ , and iteratively mutating and choosing the only vertex in the mutated polytope which differs from  $v_f$  and the newly created vertex. In case  $P \in \mathcal{P}$  is not a triangle, we must directly verify that the almost-toric diagram  $\mathcal{P}$  can be mutated to triangular almost-toric diagram with a smooth toric vertex. This is explicitly shown in [55], and Figure 1 for  $Bl_3(\mathbb{CP}^2)$ .  $\square$

The arithmetic of the vertices of a Symington sequence for each  $X(\mathcal{P}, \mathcal{S}) \in \mathcal{H}$  is discussed in the subsequent Subsection 3.2. The usefulness of a Symington sequence in the study of the Ellipsoid Embedding function  $c_X$  comes from the following:

**Proposition 3.5** *Let  $P \subseteq \mathbb{R}^2$  be a triangular polytope with a smooth toric vertex  $v_f \in V(P)$ , and let  $(a, b) \in \mathbb{Z}^2$  be the affine length of the two sides of  $P$  incident to  $v_f$ . Then there exists a volume-filling symplectic embedding  $i : E(a, b) \longrightarrow X(P)$ .  $\square$*

Proposition 3.5 follows by noticing that the complement of the symplectic divisor associated to the side in  $P$  non-incident to  $v_f$  is the symplectic domain  $E(a, b)$  [15, 24, 51]. In particular, let  $\{(\mathcal{P}_n, v_n)\}_{n \in \mathbb{N}}$  be a Symington sequence and denote by  $(a_n, b_n) \in \mathbb{Z}^2$  the affine lengths of the sides of  $P_n$  incident to  $v_f$ . Then there exist a sequence of symplectic ellipsoid embeddings

$$i_n : E(a_n, b_n) \longrightarrow X(P_n).$$

This is at the core of the relation between the existence of infinite staircase and polytope mutations. It is a powerful starting point, but it not enough to conclude Theorem 1.3 since the symplectic varieties  $X(P_n)$  are not isomorphic. As emphasized,  $X(P_n)$  are typically singular algebraic varieties, and their algebraic isomorphic type strongly depends on  $n \in \mathbb{N}$ . That said, the fundamental defining property (S1) of a Symington sequence states that  $X(\mathcal{P}_n) = X(\mathcal{P})$  for all  $n \in \mathbb{N}$ .

The difference between the equalities  $X(\mathcal{P}_n) = X(\mathcal{P})$ , for all  $n \in \mathbb{N}$ , and the sequence of algebraic varieties  $X(P_n)$  is contained in the cut content  $\mathcal{B}_n$  in  $\mathcal{P}_n = (P_n, \mathcal{B}_n)$ . In particular, Proposition 3.5 implies the following:

**Proposition 3.6** *Let  $P \subseteq \mathbb{R}^2$  be a triangular polytope with a smooth toric vertex  $v_f \in V(P)$ , and let  $(a, b) \in \mathbb{Z}^2$  be the affine length of the two sides of  $P$  incident to  $v_f$ . Suppose that  $\mathcal{P} = (P, \mathcal{B})$  has empty cut content at  $v_f$ . Then there exists a volume-filling symplectic embedding  $i : E(a, b) \longrightarrow X(\mathcal{P})$ .  $\square$*

Indeed, introducing cut content  $\mathcal{B}$  can be achieved by choosing arbitrarily short cuts at the vertices of  $P$ . In precise terms, let  $N \subseteq P$  be a neighborhood of the side in  $P$  opposite to  $v_f$  containing the cuts in  $\mathcal{B}$ . The complement in  $X(\mathcal{P})$  of the pre-image of  $N \subseteq P$  is a symplectic ellipsoid  $E(a - \varepsilon, b - \varepsilon)$  for certain  $\varepsilon \in \mathbb{R}^+$  depending on the choice of  $N$ . By choosing  $N \subseteq \mathbb{R}^2$  small enough in Euclidean area,  $\varepsilon \in \mathbb{R}^+$  can be chosen arbitrarily small, thus yielding a volume-filling embedding of  $E(a, b)$ .

Given a Symington sequence  $\{(\mathcal{P}_n, v_n)\}_{n \in \mathbb{N}}$  for  $X(\mathcal{P}, \mathcal{S})$ , Proposition 3.4 and Proposition 3.6 allow us to construct a sequence of sharp symplectic ellipsoid embeddings

$$i_n : E(a_n, b_n) \longrightarrow X(\mathcal{P}).$$

The challenge is now upgrading these absolute ellipsoid embeddings  $(i_n)_{n \in \mathbb{N}}$  to a sequence of relative sharp symplectic ellipsoid embeddings

$$\iota_n : E(a_n, b_n) \longrightarrow X(\mathcal{P}, \mathcal{S}).$$

This would conclude Theorem 1.3 once we study the arithmetic properties of the Symington sequence  $(a_n, b_n)$  associated to  $X(\mathcal{P}, \mathcal{S})$  as in Proposition 3.4. The focus of Subsection 3.3 and Section 4 is the construction of the relative embeddings  $\iota_n$  into  $X(\mathcal{P}, \mathcal{S})$  from the absolute embeddings  $i_n$  into  $X(\mathcal{P})$ .

The central difficulty in arguing the existence of  $\iota_n$  is understanding the surface configuration  $D(\mathcal{S}) \subseteq X(\mathcal{P})$  under the identifications  $X(\mathcal{P}) \cong X(\mathcal{P}_n)$ , for each  $n \in \mathbb{N}$ . In order to achieve that, we will

develop a diagrammatic tropical calculus for surface configurations  $D(\mathcal{S}) \subseteq X(\mathcal{P})$  in almost-toric symplectic manifolds. In particular, such tropical calculus starts with a configuration  $D(\mathcal{S}) \subseteq X(\mathcal{P}_n)$  and describes a diagram  $\Delta_n \subseteq \mathcal{P}_n$  such that the Hamiltonian isotopy class of the configuration  $D(\mathcal{S})$  admits a representative contained in the pre-image of this diagram  $\Delta_n$ .

**Remark 3.7** There is an alternative course of action to construct  $\iota_n$ . It should be possible to understand how the surface configuration  $D(\mathcal{S})$  is explicitly carried along a polytope mutation through almost-toric diagrams [52, 55]. Starting with  $D(\mathcal{S}) \subseteq X(\mathcal{P})$ , this would yield an understanding of the inclusions  $D(\mathcal{S}) \subseteq X(\mathcal{P}_n)$ , upon identifying  $X(\mathcal{P}_n) \cong X(\mathcal{P})$  along the mutation sequence. This is an interesting line of research, but we shall not discuss it in the present manuscript.  $\square$

Let us now provide a detailed and self-contained account of the numerics appearing in Symington sequences for  $X(\mathcal{P}, \mathcal{S})$  for  $(\mathcal{P}, \mathcal{S}) \in \mathcal{H}$ . After that, we proceed with Subsection 2.1, which states the main result from Section 4, and Subsection 3.3, which constructs  $(\iota_n)_{n \in \mathbb{N}}$ , leading to the conclusion of Theorem 1.3.

### 3.2 Arithmetic of Symington Sequences for $(\mathcal{P}, \mathcal{S}) \in \mathcal{H}$

The polytope  $P \in \mathcal{P}$  in an almost-toric base contains all the arithmetic information for its mutations. The useful property of polytopes in Figure 1 is the following:

**Lemma 3.8** *Each of the polytopes in Figure 1 is mutation equivalent to a triangular polytope.*

**Proof** This is immediate for the first two rows: the toric moment polytope for  $\mathbb{CP}^2$  is triangular, the square toric moment polytope for the monotone  $\mathbb{CP}^1 \times \mathbb{CP}^1$  is mutation equivalent to the triangular moment polytope for  $\mathbb{CP}^2(1, 1, 2)$ , and hexagonal moment polytope for the monotone  $Bl_3(\mathbb{CP}^2)$  is mutation equivalent to the triangular moment polytope for  $\mathbb{CP}^2(1, 2, 3)$ . These triangular polytopes are depicted in Figure 1 at the rightmost part for each region corresponding to each symplectic 4-manifold. Finally, the almost-toric polytope  $Bl_4(\mathbb{CP}^2)$  can be mutated to  $\mathbb{CP}^2(1, 4, 5)$  as shown in [55].  $\square$

This allows us to reduce the arithmetic of Symington sequences for the polytopes in Figure 1 to those for the weighted projective spaces  $\mathbb{CP}^2(1, 1, 1)$ ,  $\mathbb{CP}^2(1, 1, 2)$ ,  $\mathbb{CP}^2(1, 2, 3)$  and  $\mathbb{CP}^2(1, 4, 5)$ . The following result covers all the necessary arithmetic for our Theorem 1.3:

**Proposition 3.9** Let  $P(\alpha, \beta, \gamma)$  the toric moment polytope for  $\mathbb{CP}^2(\alpha, \beta, \gamma)$ .

- (i) Suppose that  $\alpha$  corresponds to a smoothable singularity of  $\mathbb{CP}^2(\alpha, \beta, \gamma)$  and divides  $(\beta + \gamma)^2$ , with  $\alpha \cdot \delta = (\beta + \gamma)^2$ . Then the polytope  $P(\alpha, \beta, \gamma)$  admits a polytope mutation to the triangle  $P(\beta, \gamma, \delta)$ .

- (ii) (*Vieta jumping*) Suppose that  $(p, q, r) \in \mathbb{Z}^3$  solves the Diophantine equation

$$C_0 p^2 + C_1 q^2 + C_2 r^2 = mpqr.$$

Suppose that the  $C_i$  divide  $m$ ,  $1 \leq i \leq 3$ , then either of the three triples  $(p, q, mpq/C_2 - r)$ ,  $(p, mpr/C_1 - q, r)$  and  $(mqr/C_0 - p, q, r)$  solves this Diophantine equation.  $\square$



**Remark 3.10** A toric orbifold singularity being smoothable is equivalent to being a  $T$ -singularity [2, 29]. If  $\mathbb{CP}^2(\alpha, \beta, \gamma)$  is smoothable, then it is of the form  $\mathbb{CP}^2(C_0 p^2, C_1 q^2, C_2 r^2)$ , where  $(p, q, r) \in \mathbb{Z}^3$  solves the Diophantine equation above. Vieta jumping is then equivalent to the change  $\alpha \leftrightarrow \delta$  in Proposition 3.9(i), with  $\delta = C_0(mqr/C_0 - p)$ . Note that Proposition 3.9 is proven in [2] for more general toric orbifolds with triangular moment map and smoothable corner, and it appears in the context of Del Pezzo surfaces in [55] as Lemma 4.2.  $\square$

**Arithmetic for**  $(\mathbb{CP}^2, \omega_{\text{st}})$ . The toric moment polytope for  $(\mathbb{CP}^2, \omega_{\text{st}})$  is mutation equivalent to the toric moment polytope for  $\mathbb{CP}^2(p^2, q^2, r^2)$  if and only if  $(p, q, r) \in \mathbb{Z}^3$  is a Markov triple, i.e.

$$p^2 + q^2 + r^2 = 3pqr.$$

This explains the numerics in Example 3.2. An arbitrary sequence of Markov triples, even if they differ only in one component, does *not* yield a Symington Sequence, since condition (S4) in Definition 3.3 imposes a non-trivial constraint. Indeed,  $\mathbb{CP}^2(p^2, q^2, r^2)$  has a smooth toric vertex if and only if one of the numbers  $p, q, r \in \mathbb{Z}$  equals one. Thus a Symington Sequence for  $(\mathbb{CP}^2, \omega_{\text{st}})$  can be obtained using the construction in the proof of Proposition 3.4 yielding any of the toric polytopes for  $\mathbb{CP}^2(1, q^2, r^2)$ , if  $(q, r) \in \mathbb{Z}^2$  satisfy

$$1 + q^2 + r^2 = 3qr.$$

Let  $F_n$  be the  $n$ th odd Fibonacci number, starting at  $F_1 = 1$ . The recursion  $F_{n+2} = 3F_{n+1} - F_n$  implies that  $(1, F_n, F_{n+1})$  is a Markov triple with  $p = 1$ , as required. Hence, a Symington Sequence for  $(\mathbb{CP}^2, \omega_{\text{st}})$  yields the sequence of toric polytopes  $\mathbb{CP}^2(1, F_n^2, F_{n+1}^2)$  for all  $n \in \mathbb{N}$ . Conversely, all positive integral solutions  $(1, q, r)$  of the Markov equation are of the form  $(1, F_n, F_{n+1})$ . These Fibonacci solutions are directly obtained by iteratively applying the Vieta jumping in Proposition 3.9 starting with the minimal solution  $(p, q, r) = (1, 1, 1)$ . The ratio  $F_{n+1}/F_n$  is known to converge to  $1 + \varphi$ , where  $\varphi$  is the golden ratio, which is readily extracted from  $1 + q_n^2 + r_n^2 = 3q_n r_n$ , by dividing by  $r_n^2$  and noticing that in the limit  $1/r_n^2 \rightarrow 0$  as  $n \rightarrow \infty$ , i.e., it is the root of  $1 - 3x + x^2$  that is greater than 1.

This is the explanation for the appearance of the odd Fibonacci numbers in D. McDuff's Fibonacci staircase from the viewpoint of polytope mutations. Indeed, this computation shows the  $E(1, F_{n+1}^2/F_n^2)$  admits a sharp symplectic embedding into

$$\left( \mathbb{CP}^2, \sqrt{\frac{2 \text{Vol}(E(1, F_{n+1}^2/F_n^2))}{\pi^2}} \cdot \omega_{\text{st}} \right),$$

and that any symplectic ellipsoid embedding obtained via toric mutations must be of this form.

**Remark 3.11** From the proof of Theorem 6.5 in [33], see [33, Figure 15], we can readily conclude that,  $F_{n+1} > F_n$ , then  $E(1, F_{n+1}^2/F_n^2)$  embeds into

$$\left( Bl_k(\mathbb{CP}^2), \frac{F_{n+1}^2/F_n^2}{3F_{n+1}/F_n - k} \sqrt{\frac{2 \text{Vol}(E(1, F_{n+1}^2/F_n^2))}{\pi^2}} \cdot \omega_{\text{st}} \right), \quad k \leq 5.$$

We learned about staircases in the toric domains related to  $Bl_1(\mathbb{CP}^2)$  and  $Bl_2(\mathbb{CP}^2)$  from [9].  $\square$

**Arithmetic for**  $(\mathbb{CP}^1 \times \mathbb{CP}^1, \omega_{\text{st}} \oplus \omega_{\text{st}})$ . The toric moment polytope for  $(\mathbb{CP}^2(1, 1, 2), \omega_{\text{st}})$  is mutation



equivalent to the toric moment polytope for  $\mathbb{CP}^2(p^2, q^2, 2r^2)$  if and only if  $(p, q, r) \in \mathbb{Z}^3$  satisfies

$$p^2 + q^2 + 2r^2 = 4pqr.$$

As above, these  $\mathbb{CP}^2(p^2, q^2, 2r^2)$  have smooth toric vertex if and only if one of the numbers  $p, q, r \in \mathbb{Z}$  equals one. Thus a Symington Sequence for  $(\mathbb{CP}^1 \times \mathbb{CP}^1, \omega_{\text{st}} \oplus \omega_{\text{st}})$  exists and yields any of the toric polytopes for  $\mathbb{CP}^2(1, q^2, 2r^2)$ , if  $(q, r) \in \mathbb{Z}^2$  satisfy

$$1 + q^2 + 2r^2 = 4qr.$$

Let  $P_n, H_n$  be the  $n$ th Pell number and the  $n$ th half-companion Pell number, starting at

$$P_0 = 1, P_1 = 1, \quad H_0 = H_1 = 1.$$

It is readily verified that the triples  $(1, 2P_n^2, H_{n+1}^2)$ , verify the above Diophantine equation, since  $P_n = 2P_{n-1} + P_{n-2}$  and  $H_n = 2H_{n-1} + H_{n-2}$ . These Pell solutions are also obtained by iteratively applying Proposition 3.9 starting with  $(p, q, r) = (1, 1, 1)$ .

Consider  $c_n = \max \{2P_n^2/H_{n+1}^2, H_{n+1}^2/(2P_n^2)\}$ , this computation shows the symplectic ellipsoid  $E(1, c_n)$  symplectically embeds into  $(\mathbb{CP}^1 \times \mathbb{CP}^1, \widetilde{\text{Vol}}(E(1, c_n)) \cdot (\omega_{\text{st}} \oplus \omega_{\text{st}}))$  for all  $n \in \mathbb{N}$ , where  $\widetilde{\text{Vol}}$  denotes the rescaled volume, as in Remark 3.11. This explains the numerics in Frenkel-Müller's Pell staircase via polytope mutations. The limit of  $c_n$  can be also extracted from  $1 + q_n^2 + 2r_n^2 = 4q_n r_n$ , by dividing by  $r_n^2$  and getting the solution of  $x^2 - 4x + 2 = 0$  that satisfy  $x^2/2 > 1$ , which is  $2 + \sqrt{2}$ . So,  $c_n \rightarrow x^2/2 = 3 + 2\sqrt{2}$ .

**Arithmetic for  $(Bl_3(\mathbb{CP}^2), \omega_{\text{st}})$ .** The toric moment polytope for  $(\mathbb{CP}^2(1, 2, 3), \omega_{\text{st}})$  is mutation equivalent to the toric moment polytope for  $\mathbb{CP}^2(p^2, 2q^2, 3r^2)$  if and only if  $(p, q, r) \in \mathbb{Z}^3$  satisfies

$$p^2 + 2q^2 + 3r^2 = 6pqr.$$

A Symington Sequence for  $(Bl_3(\mathbb{CP}^2), \omega_{\text{st}})$  thus yields any of the toric polytopes for  $\mathbb{CP}^2(1, q, r)$ , if  $(q, r) \in \mathbb{Z}$  satisfy

$$1 + 2q^2 + 3r^2 = 6qr.$$

This Diophantine equation gives rise to the numerics of the Cristofaro-Gardner-Kleinman's staircase. Indeed, Vieta jumping alternately applied to the second and third components of  $(p, q, r) = (1, 1, 1)$  yields the sequence of triples

$$(1, 1, 1) \mapsto (1, 2, 1) \mapsto (1, 2, 3) \mapsto (1, 7, 3) \mapsto \dots$$

which prove the existence of sharp ellipsoid embeddings into the appropriately rescaled  $(Bl_3(\mathbb{CP}^2), \omega_{\text{st}})$ , starting with the corresponding sequence

$$E(1, 3/2), E(1, 8/3), E(1, 27/8), E(1, 98/27), \dots,$$

associated to the triples above. The sequence of ellipsoids  $E(1, k_n)$ , where  $\{k_n\}_{n \in \mathbb{N}}$  is associated to ratios of solutions for the Diophantine equation obtained by Proposition 3.9 is a convergent infinite sequence, limiting to  $2x^2/3 = 2 + \sqrt{3}$ , where  $x = \frac{3+\sqrt{3}}{2}$  is the solution of  $2x^2 - 6x + 3 = 0$  with  $2x^2/3 = 2 + \sqrt{3} > 1$ , which is obtained from dividing  $1 + 2q_n^2 + 3r_n^2 = 6q_n r_n$  by  $r_n^2$  and taking the limit  $n \rightarrow \infty$ .

**Arithmetic for  $(Bl_4(\mathbb{CP}^2), \omega_{\text{st}})$ .** The toric moment polytope for  $(\mathbb{CP}^2(1, 4, 5), \omega_{\text{st}})$  mutates to the toric moment polytope for  $\mathbb{CP}^2(p^2, q^2, 5r^2)$  if and only if  $(p, q, r) \in \mathbb{Z}^3$  satisfies

$$p^2 + q^2 + 5r^2 = 5pqr.$$

In conclusion, a Symington Sequence for  $(Bl_4(\mathbb{CP}^2), \omega_{st})$  yields any of the toric polytopes for  $\mathbb{CP}^2(1, q^2, 5r^2)$ , if  $(q, r) \in \mathbb{Z}^2$  satisfy

$$1 + q^2 + 5r^2 = 5qr.$$

The sharp ellipsoid embeddings comes from the sequence of triples

$$(1, 2, 1) \mapsto (1, 3, 1) \mapsto (1, 3, 2) \mapsto (1, 7, 2) \mapsto (1, 7, 5) \mapsto \dots,$$

which yields the sequence of  $E(1, 5/4), E(1, 9/5), E(1, 20/9), E(1, 49/20), E(1, 125/49) \dots$ , into an optimal rescaling of  $(Bl_4(\mathbb{CP}^2), \omega_{st})$ . This is a new sharp ellipsoid staircase  $E(1, l_n)$ , with sequence  $\{l_n\}_{n \in \mathbb{N}}$  of ratios of solutions converging to  $1 + \varphi$ . Indeed,  $1 + \varphi = x^2/5$ , where

$$x = \frac{5 + \sqrt{5}}{2},$$

is the solution of  $x^2 - 5x + 5 = 0$ , with  $x^2/5 > 1$ , obtained from dividing  $1 + q_n^2 + 5r_n^2 = 5q_n r_n$  by  $r_n^2$  and taking  $n \rightarrow \infty$ .

### 3.3 Proof of Theorem 1.3

Let us now prove Theorem 1.3, building on the Symington sequences discussed in Subsections 3.1 and 3.2. For that, let us first state the result that we need from the theory of symplectic-tropical curves, as developed in Section 4. The following statement is the only tropical ingredient for our proof of Theorem 1.3, its proof will be the content of Section 4.

**Theorem 3.12** *Let  $X(\mathcal{P}, \mathcal{S})$  be a symplectic toric domain, with  $(\mathcal{P}, \mathcal{S}) \in \mathcal{H}$ , an associated Symington sequence  $(\mathcal{P}_n, \mathcal{S}_n)$ , and let*

$$i_n : E(a_n, b_n) \longrightarrow X(\mathcal{P})$$

*be a sharp symplectic ellipsoid embedding. For any  $\varepsilon \in \mathbb{R}^+$ , there exists a tropical symplectic curve  $\tilde{S}_n \subseteq \mathcal{P}_n$  such that*

(i) *The tropical symplectic curve  $\tilde{S}_n \subseteq \mathcal{P}_n$  represents any embedded (configuration of) symplectic surface(s)  $D(\tilde{S}_n) \subseteq X(\mathcal{P}_n)$  in the same homology class as the (configuration of) embedded symplectic curve(s) in  $D(S)$ ,*

(ii) *There exists a neighborhood  $\mathcal{O}_p(\tilde{S}_n) \subseteq P_n$  and a volume-filling symplectic embedding*

$$\iota_n : E(a_n, b_n) \longrightarrow X(\mathcal{P}_n) \setminus D(\tilde{S}_n).$$

□

The inclusion  $\tilde{S}_n \subseteq \mathcal{P}_n$  in Theorem 3.12 is to be understood as  $\tilde{S}_n \subseteq P_n$  for a realization of the cut content  $\mathcal{B}_n$  of  $\mathcal{P}_n$ . The exact realization of the cut content  $\mathcal{B}_n$ , as cuts in  $P_n$ , is a choice and, in Theorem 3.12, this choice depends on the initial value of  $\varepsilon \in \mathbb{R}^+$ . Let us now apply Theorem 3.12 and conclude Theorem 1.3 in each of the cases.

**Remark 3.13** The exact configurations of symplectic curves that we shall use in Theorem 3.12 are specifically constructed in Proposition 4.32, for  $\mathbb{CP}^1 \times \mathbb{CP}^1$ , Proposition 4.34 for  $Bl_3(\mathbb{CP}^2)$  and Proposition 4.35 for  $Bl_4(\mathbb{CP}^2)$ . □

**Complex Projective Plane**  $\mathbb{CP}^2$ . There is a unique almost-toric base  $\mathcal{P} = (P, \mathcal{B})$  in Figure 1, with  $\mathcal{B} = \emptyset$ . The relative almost-toric base  $(\mathcal{P}, \mathcal{S})$  has  $D(\mathcal{S}) = \mathbb{CP}^1$ , the complex projective line, as its unique symplectic divisor. This relative almost-toric base leads to the symplectic toric domain of the standard symplectic 4-ball

$$X(\mathcal{P}, \mathcal{S}) = (\mathbb{D}^4(1), \omega_{\text{st}}) \cong (\mathbb{CP}^2 \setminus \mathbb{CP}^1, \omega_{\text{st}}).$$

Let  $c_n = \text{Vol}(E(1, F_{n+1}^2/F_n^2))$ , with  $\{F_n\}_{n \in \mathbb{N}}$  as in Subsection 3.2, and let us show that there exists a sharp symplectic embedding

$$\iota_n : E(1, F_{n+1}^2/F_n^2) \longrightarrow (\mathbb{D}^4(1), c_n \cdot \omega_{\text{st}}).$$

The sequence of polytope mutations, as discussed in Subsection 2.2, associated to the Symington sequence in Subsection 3.1 yields a sequence of sharp symplectic embeddings

$$i_n : E(1, F_{n+1}^2/F_n^2) \longrightarrow (\mathbb{CP}^2, c_n \cdot \omega_{\text{st}}).$$

This sequence follows the arithmetic in Subsection 3.2 stemming from the Markov Equation with  $a = 1$ . In order to guarantee an embedding into  $X(\mathcal{P}, \mathcal{S})$ , it suffices to show that  $D(\mathcal{S}) = \mathbb{CP}^1$  can be symplectically isotoped to lie above an arbitrarily small  $\varepsilon$ -neighborhood of the side opposite to the frozen vertex  $v_f \in P_n$ ,  $n \in \mathbb{N}$ . This is achieved by first constructing a symplectic  $\mathbb{CP}^1$  above this  $\varepsilon$ -neighborhood, and then arguing that this symplectic  $\mathbb{CP}^1$  can be symplectically isotoped to the standard  $D(\mathcal{S}) = \mathbb{CP}^1 \subseteq X(\mathcal{P})$ . The former part is achieved by Theorem 3.12, the symplectic tropical-curves of which are depicted explicitly in Figure 3, for the first five mutations in the Fibonacci-Symington Sequence. The latter part, constructing a symplectic isotopy from the lift of the symplectic-tropical curve to the standard complex line  $D(\mathcal{S})$ , is now achieved by using M. Gromov's [18], which shows that the symplectic isotopy class of the complex line is unique.

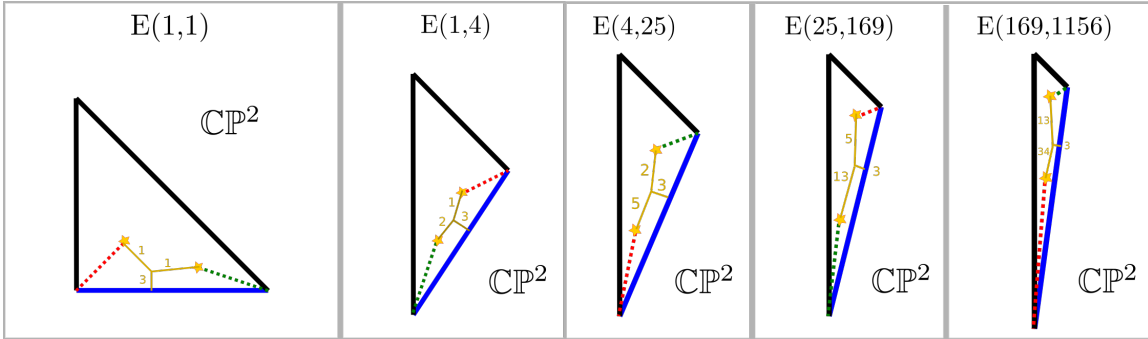


Figure 3: Symplectic-tropicalCurves for  $(\mathbb{CP}^2, \omega_{\text{st}})$ . The weights of the tripods are, from left to right,  $(1, 1, 3)$  for the toric moment polytope,  $(1, 2, 3)$ ,  $(5, 2, 3)$ ,  $(13, 5, 3)$  and  $(34, 13, 3)$ . These five tropical symplectic curves represent symplectic embedded lines  $\mathbb{CP}^1 \subseteq (\mathbb{CP}^2, \omega_{\text{st}})$ .

**The Ruled Surface**  $(\mathbb{CP}^1 \times \mathbb{CP}^1, \omega_{\text{st}} \oplus \omega_{\text{st}})$ . There are two (relative) almost-toric bases  $(\mathcal{P}, \mathcal{S})$  in Figure 1, associated to the symplectic domains  $\mathbb{D}^2(1) \times \mathbb{D}^2(1)$ , the polydisk, and the ellipsoid  $E(1, 2)$ .

The first almost-toric base  $(\mathcal{P}, \mathcal{S})$ , on the right, has underlying polytope  $P \in \mathcal{P}$  the toric moment polytope for the weighted projective plane  $\mathbb{CP}^2(1, 1, 2)$ . The cut content  $\mathcal{B} \in \mathcal{P}$  is non-trivial at one of the vertices, where a Lagrangian 2-sphere  $L(\mathcal{B})$  lies above the segment uniting the two nodal points. This Lagrangian 2-sphere is in the homology class of Lagrangian anti-diagonal in

$X(\mathcal{P}) \cong (\mathbb{CP}^1 \times \mathbb{CP}^1, \omega_{\text{st}} \oplus \omega_{\text{st}})$ , and it is in fact Hamiltonian isotopic to the anti-diagonal. The surface configuration  $D(\mathcal{S})$  consists of two surfaces: a symplectic 2-sphere, in the homology class of the complex line  $\{pt\} \times \mathbb{CP}^1$ , and the Lagrangian 2-sphere  $L(\mathcal{B})$ . The sequence of polytope mutations constructed in Subsection 3.1 yields a sequence of embeddings

$$i_n : E(1, p_n) \longrightarrow (\mathbb{CP}^2(1, 1, 2), \text{Vol}(E(1, p_n)) \cdot (\omega_{\text{st}} \oplus \omega_{\text{st}})),$$

where  $p_n = \max \{2P_n^2/H_{n+1}^2, H_{n+1}^2/(2P_n^2)\}$ , according to the arithmetic discussed in Subsection 3.2, and we are denoting  $\text{Vol} = \widetilde{\text{Vol}}$  onwards to ease notation.

In order for these embeddings to be into  $X(\mathcal{P}) = E(1, 2)$ , instead of  $X(P) = \mathbb{CP}^2(1, 1, 2)$ , we first apply Theorem 3.12 and construct a symplectic-tropical curve inside an  $\varepsilon$ -neighborhood of the edge opposite to the frozen vertex, which includes the cuts in  $\mathcal{B}$ . This tropical curve  $\widetilde{S}_n$  is chosen such that  $D(\widetilde{S}_n)$  is a symplectic 2-spheres in the homology class  $[\{pt\} \times \mathbb{CP}^1]$ . Since the symplectic isotopy class of  $\{pt\} \times \mathbb{CP}^1 \subseteq \mathbb{CP}^1 \times \mathbb{CP}^1$  is unique, there exists a symplectic isotopy from  $D(\widetilde{S}_n)$  to  $\{pt\} \times \mathbb{CP}^1$ . The image of the Lagrangian sphere  $L(\mathcal{B}_n)$  under this symplectic isotopy might not coincide with  $L(\mathcal{B})$ . Nevertheless, since  $L(\mathcal{B}_n)$  and  $L(\mathcal{B})$  are both Lagrangian 2-sphere in  $\mathbb{CP}^1 \times \mathbb{CP}^1$  in the class of the anti-diagonal, there exists a Lagrangian isotopy connecting them, relative to the divisor  $\{pt\} \times \mathbb{CP}^1$ , as shown in [23]. Since an exact Lagrangian isotopy can be realized by a Hamiltonian isotopy, this yields a symplectic isotopy from our surface configuration  $D(\widetilde{S}_n)$  and  $L(\mathcal{B}_n)$  to the standard  $D(S)$  and  $L(\mathcal{B})$ . This constructs the sharp symplectic embeddings

$$i_n : E(1, p_n) \longrightarrow (E(1, 2), \text{Vol}(E(1, p_n)) \cdot \omega_{\text{st}}).$$

The second almost-toric base, on the left, corresponds to the toric moment polytope for  $\mathbb{CP}^1 \times \mathbb{CP}^1$  and has  $\mathcal{B} = \emptyset$ . This data has the polydisk  $X(\mathcal{P}) = \mathbb{D}^2(1) \times \mathbb{D}^2(1)$  as its associated domain. Indeed, the surface configuration  $D(\mathcal{S})$  for this first  $(\mathcal{P}, \mathcal{S})$ , depicted in blue, consists of a chain of two symplectic embedded 2-spheres, corresponding to  $H_1 = \mathbb{CP}^1 \times \{pt\}$  and  $H_2 = \{pt\} \times \mathbb{CP}^1$  respectively. Thus the divisor  $D = H_1 + H_2$  is defined as  $(\mathbb{CP}^1 \times \{pt\}) \cup (\{pt\} \times \mathbb{CP}^1) \subseteq X$ , which represents the element  $(1, 1) \in H^2(\mathbb{CP}^1 \times \mathbb{CP}^1, \mathbb{Z}) \cong \mathbb{Z}^2$ . At this stage, we can directly invoke [7], which states that a symplectic ellipsoid embeds sharply in  $E(1, 2)$  if and only if it embeds sharply in  $\mathbb{D}^2(1) \times \mathbb{D}^2(1)$ . This concludes Theorem 1.3 for these two almost-toric bases.

**Explicit Argument for  $\mathbb{D}^2(1) \times \mathbb{D}^2(1)$ .** Instead of invoking [7], we can directly conclude Theorem 1.3 for this second almost-toric base as follows. In line with our argument in the first case of  $\mathbb{CP}^2$ , the question is whether a symplectic configuration  $D(S) \subseteq \mathbb{CP}^1 \times \mathbb{CP}^1$  of a plumbing of two symplectic 2-spheres, representing the same cohomology class  $[D(S)] = [D]$ , is symplectic isotopic to  $D$ , through symplectic configurations which are plumbing of two symplectic 2-spheres. This is the notion of equisingular isotopy in [16, Definition 2.6], and D. McDuff's work [32, 40] implies the answer in the affirmative.

For completeness, let us directly argue the existence of an equisingular isotopy from  $D(S)$  to  $D = H_1 + H_2$  as follows. Blow-up the intersection point of the two 2-spheres in  $D$ , and blow-down each of the proper transforms of the two original 2-spheres, which are themselves 0-self-intersection 2-spheres in  $Bl_1(\mathbb{CP}^1 \times \mathbb{CP}^1)$ . In the identification  $Bl_1(\mathbb{CP}^1 \times \mathbb{CP}^1) \cong Bl_2(\mathbb{CP}^2)$ , the exceptional divisor  $E \subseteq Bl_1(\mathbb{CP}^1 \times \mathbb{CP}^1)$  blows-down to a (+1)-intersection symplectic 2-sphere  $d(E) \subseteq \mathbb{CP}^2$ . The uniqueness of the symplectic isotopy class of the complex line in  $\mathbb{CP}^2$  gives an isotopy from  $d(E)$  to any standard complex line  $\mathbb{CP}^1 \subseteq \mathbb{CP}^2$ . This yields a symplectic isotopy, after blowing up twice

and down once, from the symplectic configuration  $D(S) \subseteq \mathbb{CP}^1 \times \mathbb{CP}^2$  to the standard configuration  $(\mathbb{CP}^1 \times \{pt\}) \cup (\{pt\} \times \mathbb{CP}^1) \subseteq \mathbb{CP}^1 \times \mathbb{CP}^2$ .

The remainder of the argument is now identical to that of the previous case, with Theorem 3.12 applies to construct symplectic representatives of  $H_1$  and  $H_2$  in an  $\varepsilon$ -neighborhood of the edge opposite to the frozen vertex – see Proposition 4.32. As explained in Subsection 3.2, we obtain sharp symplectic embeddings

$$i_n : E(1, p_n) \longrightarrow (\mathbb{CP}^1 \times \mathbb{CP}^1, \text{Vol}(E(1, p_n)) \cdot (\omega_{\text{st}} \oplus \omega_{\text{st}})),$$

where  $p_n = \max \{2P_n^2/H_{n+1}^2, H_{n+1}^2/(2P_n^2)\}$ . Theorem 3.12 yields tropical representatives arbitrarily near the polytope side opposite from the frozen vertex. The symplectic isotopy discussed above then constructs the required sharp symplectic embeddings

$$\iota_n : E(1, p_n) \longrightarrow (\mathbb{D}^2(1) \times \mathbb{D}^2(1), \text{Vol}(E(1, p_n)) \cdot (\omega_{\text{st}} \oplus \omega_{\text{st}})).$$

**Thrice Blown-up  $Bl_3(\mathbb{CP}^2)$ .** There are four relative almost-toric basis  $(\mathcal{P}, \mathcal{S})$  with  $X(\mathcal{P}) \cong Bl_3(\mathbb{CP}^2)$  symplectomorphic to the blow-up of  $(\mathbb{CP}^2, \omega_{\text{st}})$  at three non-collinear points. In line with the previous case of symplectic domains  $\mathbb{CP}^1 \times \mathbb{CP}^1$ , there exists an infinite sharp sequence of ellipsoids for one of these four symplectic domains  $X(\mathcal{P}, \mathcal{S})$  if and only if it exists for one of them [5]. The numerics of these staircases will also coincide. Let us focus on the leftmost relative almost-toric base  $(\mathcal{P}, \mathcal{S})$  in Figure 1. In this case,  $\mathcal{S}$  is a unique symplectic configuration realized by a linear plumbing of four symplectic 2-spheres each with self-intersection  $(-1)$ , and representing the classes  $E_1, E_2, H - E_1 - E_3$  and  $H - E_1 - E_2$ .

Theorem 3.12 applied to this singular configuration – see Proposition 4.34 – yields a tropical curve in an  $\varepsilon$ -neighborhood of the side opposite of a frozen vertex. Then we need to prove that any such symplectic configuration  $S_1, S_2, S_3, S_4 \subseteq Bl_3(\mathbb{CP}^2)$  is equisingularly symplectic isotopic to a given such configuration  $D$  in the same homology class. For that, blow-down the second and fourth spheres  $S_2, S_4 \subseteq Bl_3(\mathbb{CP}^2)$ . The blow-down of  $S_1$  becomes a 0-self-intersection 2-sphere, and the blow-down of  $S_3$  is a  $(+1)$ -self-intersection 2-sphere in  $Bl_1(\mathbb{CP}^2)$ . The classification of ruled symplectic surfaces [32, 40] gives a symplectomorphism of  $Bl_1(\mathbb{CP}^2)$  that sends the symplectic configuration  $S_1 \cup S_3$  to the union of the proper transform of the complex line  $\mathbb{CP}^1 \subseteq \mathbb{CP}^2$  and the 0-self-intersection fiber of the linear pencil of  $\mathbb{CP}^2$ . Since the symplectomorphism group of  $Bl_1(\mathbb{CP}^2)$  is connected [35], this can be achieved via a symplectic isotopy. This same symplectic isotopy, upon blowing up twice, yields the required symplectic isotopy.

**Remark 3.14** The argument above requires the construction of the 4-chain of symplectic spheres, provided by Theorem 3.12. Nevertheless, it is possible to instead argue with the rightmost relative almost-toric base in Figure 1. This alternative argument requires an understanding of the Lagrangian spheres in  $Bl_3(\mathbb{CP}^2)$  – which fortunately exists – and reads as follows.

The rightmost relative almost-toric base yields the symplectic ellipsoid  $E(2, 3) \cong X(\mathcal{P}, \mathcal{S})$ , with the unique symplectic 2-sphere in  $D(\mathcal{S})$  in the homology class of an exceptional divisor  $E \subseteq Bl_3(\mathbb{CP}^2)$ . Consider the Symington sequence  $\mathcal{P}_n$ , constructed in Subsection 3.2, associated to  $\mathbb{CP}^2(1, 2, 3)$ , which yields a sequence of sharp ellipsoid embeddings

$$i_n : E(1, k_n) \longrightarrow (Bl_3(\mathbb{CP}^2), \text{Vol}(E(1, k_n)) \cdot \omega_{\text{st}}).$$

Theorem 3.12 now constructs an almost-tropical curve  $\tilde{S}_n \subseteq P_n$  such that  $D(\tilde{S}_n)$  is an embedded symplectic 2-sphere in the homology class  $[E]$ . At this stage we proceed as before, by constructing a symplectic isotopy from  $D(\tilde{S}_n)$  to the original exceptional divisor  $E \subseteq Bl_3(\mathbb{CP}^2)$ , which is itself

given by  $D(S)$ , where  $S$  is the side of the toric moment polytope of  $\mathbb{CP}^2(1, 2, 3)$  opposite to the frozen smooth vertex. The symplectic isotopy embeds the complement of  $D(\tilde{S}_n)$  into the complement of  $E$ , by upgrading it to an ambient symplectic isotopy, which is possible since the symplectic 2-spheres are embedded. As in the case of  $E(1, 2)$ , the symplectic ellipsoid  $E(2, 3) = X(\mathcal{P}, \mathcal{S})$  arises as the complement of  $E$  and three Lagrangian 2-spheres; this is the geometric incarnation of  $\mathcal{S}$  containing surfaces above the cuts. Similar to the case of  $\mathbb{CP}^1 \times \mathbb{CP}^1$ , the Hamiltonian isotopy classes of these Lagrangian 2-spheres in  $Bl_3(\mathbb{CP}^2)$  are known to be unique [4, 36] and the Lagrangian isotopy can be taken to be in the complement of a stable symplectic sphere configuration [35]. The composition of our symplectic isotopy with a compactly supported Hamiltonian isotopy, bringing these three Lagrangian 2-spheres to our standard configuration in  $X(\mathcal{P}, \mathcal{S})$ , yields a sharp symplectic embedding

$$\iota_n : E(1, k_n) \longrightarrow (E(2, 3), \text{Vol}(E(1, k_n)) \cdot \omega_{\text{st}}).$$

□

**Four Times Blown-up  $Bl_4(\mathbb{CP}^2)$ .** The argument follows the same pattern as the previous three cases. Consider generators  $\langle H, E_1, E_2, E_3, E_4 \rangle \in H^2(Bl_4(\mathbb{CP}^2), \mathbb{Z})$  given by the proper transform of the complex line in  $\mathbb{CP}^2$ , away from the blow-up points, and  $E_i$  the exceptional divisors,  $1 \leq i \leq 4$ . Let us analyze its leftmost relative almost-toric base  $(\mathcal{P}, \mathcal{S})$  in Figure 1, with  $D(\mathcal{S})$  a surface configuration consisting of a symplectic linear chain  $C$  of three self-intersection- $(-1)$  spheres, in the ordered homology classes  $[E_1], [H] - [E_1] - [E_4], [E_4]$ , and two Lagrangian spheres in the homology classes  $[E_3] - [E_1]$  and  $[E_4] - [E_2]$ . In the same scheme as before, the Symington sequence  $\mathcal{P}_n$  associated to  $Bl_4(\mathbb{CP}^2)$ , with arithmetic as in Subsection 3.2, yields sharp symplectic embeddings

$$i_n : E(1, l_n) \longrightarrow (Bl_4(\mathbb{CP}^2), \text{Vol}(E(1, l_n)) \cdot \omega_{\text{st}}).$$

Theorem 3.12 yields an almost-toric tropical curve  $\tilde{S}_n$  for each of these almost-toric bases  $\mathcal{P}_n$ , which yields the required symplectic configuration  $C \subseteq Bl_4(\mathbb{CP}^2)$  and with each 2-sphere in the same homology class as the 2-spheres in  $C$ . See Proposition 4.35 for the explicit construction of  $\tilde{S}_n$ . Now, the equisingular symplectic isotopy class of these configuration is unique, by the same type of argument as in the cases of  $Bl_3(\mathbb{CP}^2)$  and  $\mathbb{CP}^1 \times \mathbb{CP}^1$ . Indeed, blowing-down the two extremal 2-spheres in the classes  $[E_1]$  and  $[E_4]$  gives a  $(+1)$ -symplectic 2-sphere in  $Bl_2(\mathbb{CP}^2)$  disjoint from the remaining two exceptional divisors. This provides a symplectic isotopy in  $Bl_2(\mathbb{CP}^2)$  from our configuration  $D(\tilde{S}_n)$  to the standard configuration in Figure 1. Since Lagrangian 2-spheres in  $Bl_4(\mathbb{CP}^2)$  are unknotted [35], and unique in their homology classes (up to Hamiltonian isotopy), the two Lagrangian 2-spheres can also be Hamiltonian isotoped to the standard configuration. This yields the required sharp embeddings

$$\iota_n : E(1, l_n) \longrightarrow (Bl_4(\mathbb{CP}^2), \text{Vol}(E(1, l_n)) \cdot \omega_{\text{st}}).$$

This concludes Theorem 1.3, where we have assumed Theorem 3.12. Let us now construct the symplectic tropical curves needed for Theorem 3.12. This is the content of Section 4.

## 4 Symplectic Tropical Curves in Almost Toric Fibrations

This section develops the construction of configuration of symplectic curves in terms of almost-toric tropical diagrams. Theorem 3.12 is the result from the present section used in the proof of Theorem 1.3. In a nutshell, tropical curves in almost-toric diagrams consist of two pieces: tropical curves in toric diagrams, as developed by G. Mikhalkin [45, 46], and tropical local models near the cut singularities of



the affine structure. These new tropical local models are discussed in this section. There are two useful perspectives: from the viewpoint of contact 3-manifolds or directly from the perspective of symplectic 4-manifolds.

#### 4.1 An Introduction to Almost-Toric Tropical Curves

To start, we present the simplest of these local models by studying transverse links in contact 3-manifolds. The rest of the section will emphasize the local models directly in the symplectic 4-manifold. The case of almost-toric tropical curves in mutations of the toric moment polytope for  $(\mathbb{CP}^2, \omega_{\text{st}})$  already contains the fundamental ideas for connected almost-toric tropical diagrams, and thus we now focus on this example.

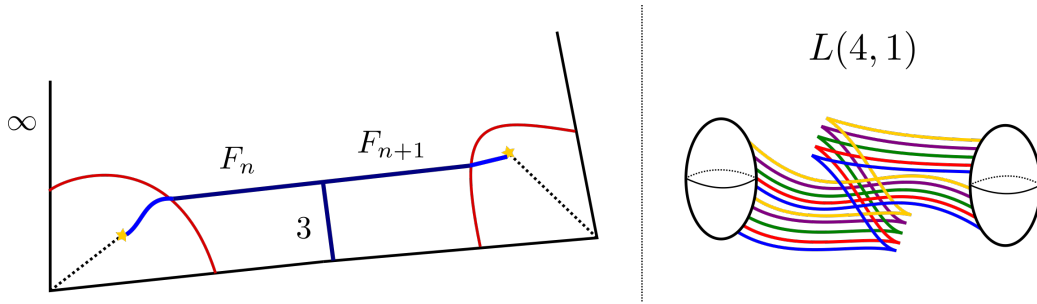


Figure 4: On the left, an almost-toric tropical curve in an almost-toric base for  $(\mathbb{CP}^2, \omega_{\text{st}})$ . The weights of the vertices are determined by the arithmetic of the Symington sequence in Subsection 3.2. The region in dark blue is G. Mikhalkin's model for a holomorphic tropical curve, whereas the region in light blue is the local model we need to discuss. On the right, the Legendrian link whose positive transverse push-off represents the (lift of the) intersection of the tropical curve with the contact 3-dimensional lens space, which is the boundary of a neighborhood of a cut.

Let us explain how to construct an embedded symplectic curve from the almost-toric tropical diagrams  $\tilde{S}$  in Figure 2 and the left of Figure 4. The diagrams for  $\tilde{S}$  are obtained by gluing to parts: a (strictly) tropical diagram and specific diagrams near the nodes and cuts. Since Theorem 3.12 is always applied in an  $\varepsilon$ -neighborhood of the side opposite to the frozen vertex, it suffices to consider a neighborhood of this side. The left of Figure 4 depicts such a neighborhood. In order to represent the symplectic class of the projective line  $\mathbb{CP}^1 \subseteq \mathbb{CP}^2$ , the weight of the tropical trivalent vertex for the leg on that side must be three, since  $[K_{\mathbb{CP}^2}] = 3 \cdot [\mathbb{CP}^1]$ . The remaining two weights are determined by the combinatorics of the polytope, and are readily shown to be  $(F_n, F_{n+1})$ , following the numerics in Subsection 3.2.

The question is now completing the piece of (actual) tropical curve away from the cuts to an almost-toric tropical curve. In terms of Figure 4 (Left), we first construct the dark blue region away from the cuts, and we aim at building an embedded symplectic curve above the light blue pieces. The contact 3-dimensional approach is the following.

Consider the intersection of the tropical piece with the 3-dimensional contact lens space

$$(L(k \cdot n^2, k \cdot nm - 1), \xi_{\text{st}})$$



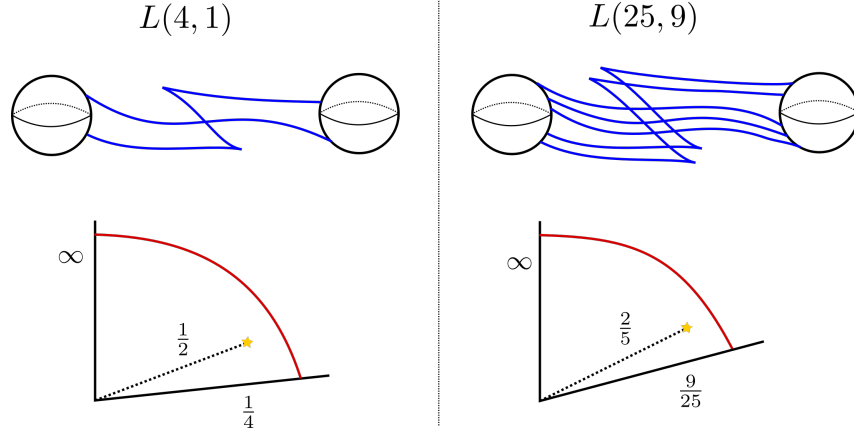


Figure 5: Each column depicts an example of a Legendrian handlebody for a rational homology ball  $B_{n,m}$ , with its contact boundary lens space  $L(n^2, nm - 1)$ . The Legendrian handlebody is a contact surgery diagram for the contact 3-manifold above the red curve in the almost-toric diagram. The left column depicts  $L(4, 1)$  as a boundary of  $B_{2,1} \cong T^*\mathbb{RP}^2$ , and the right column depicts  $L(25, 9)$  as a boundary of  $B_{5,2}$ . The fractions in the almost-toric diagrams are the slopes of the segments.

which lies above the red curve on the diagram of the left of Figure 4. The number  $k \in \mathbb{N}$  indicates the number of nodes, and thus  $k = 1$  for *any* vertex appearing in a mutation of  $(\mathbb{CP}^2, \omega_{\text{st}})$ .

**Remark 4.1** It is immediate that the closed 3-manifold is a lens space, as it admits a genus one Heegaard splitting, with the Heegaard surface given by a torus fiber of the almost-toric fibration. The precise  $n, m, k \in \mathbb{N}$  are determined by the slopes of the sides. In the case of one node  $k = 1$ , if one side has infinite slope, then the cut will have slope  $m/n$  and the second side shall have slope  $(nm - 1)/n^2$ .  $\square$

Figure 5 depicts two instances of the lens spaces that appear in the first two mutations for  $(\mathbb{CP}^2, \omega_{\text{st}})$ . For  $L(1, 1) \cong (S^3, \xi_{\text{st}})$  the arriving weights are 1 and 2, and for  $L(4, 1)$  the arriving weight is 5, confer Figure 2. The intersection of the tropical curve with this 3-dimensional contact manifold is generically a transverse link, with as many components as the weight of the leg. From the contact viewpoint, the construction of the light blue piece is now tantamount to finding a *symplectic* surface filling of a transverse link in  $(L(k \cdot n^2, k \cdot nm - 1), \xi_{\text{st}})$  inside the 4-dimensional symplectic filling given by the pre-image of the region in the almost-toric diagram which contains the cut and is bounded by the red curve. This transverse link can be readily described as a positive transverse push-off of a Legendrian link. In particular, an exact Lagrangian filling for such a Legendrian link yields an embedded symplectic surface for its transverse push-off.

In general, a Legendrian link does not admit exact Lagrangian fillings and, even if it does, their topology is constrained. Fortunately, the Legendrian links appearing in this context are obtained by taking the  $w$ -copy Reeb push-off of the attaching boundary of the defining 2-handle for the 4-dimensional symplectic filling, where  $w \in \mathbb{N}, w \geq 2$ , is the arriving weight. For instance, a leg with weight 5 arriving to  $L(4, 1)$  with the slope as in Figure 2 intersects  $(L(4, 1), \xi_{\text{st}})$  at the positive transverse push-off of the 5-component Legendrian link in Figure 4 (Right). Since the Legendrian link consists of a  $w$ -copy of a Reeb push-off, it will always bound a  $w$ -punctured exact Lagrangian sphere in the symplectic filling given by these Legendrian handlebody diagrams. Indeed, performing  $(w - 1)$ -pinching moves, connecting the different components to one, yields the standard Legendrian unknot, which locally bounds a flat

Lagrangian disk. The  $w$ -punctured Lagrangian sphere is precisely obtained as this Lagrangian disk with  $(w - 1)$  Lagrangian 1-handles attached.

**Example 4.2** The simplest example of the above construction is building an almost-toric tropical curve for the standard toric diagram for  $(\mathbb{CP}^2, \omega_{st})$  with two cuts introduced in two of the toric vertices. Figure 6 depicts this situation.

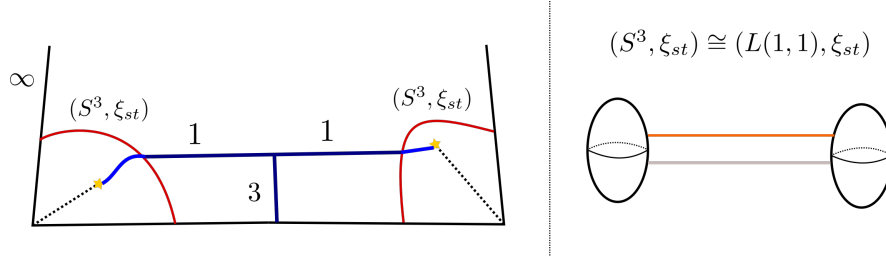


Figure 6: On the left, an almost-toric tropical complex projective line  $\mathbb{CP}^1 \subseteq \mathbb{CP}^2$  in the standard toric diagram, with two cuts introduced. On the right, the positive transverse push-off of the orange Legendrian knot yields the intersection of the tropical curve with the  $(S^3, \xi_{st})$  level set.

The transverse knot in this situation is the standard transverse unknot, with maximal self-linking number. It is depicted in *orange* in the Legendrian handlebody for the symplectic filling  $(\mathbb{D}^4, \omega_{st})$  given by one 1-handle and one 2-handle.  $\square$

Note that the topology of the resulting symplectic surface is that of a 2-sphere. Indeed, the tropical piece consists of a 2-sphere with  $(w_1 + w_2)$ -punctures, given by the weights  $w_1, w_2$  of the two legs which do not intersect the anti-canonical toric divisor. The local surface models introduced above, obtained by deforming the Lagrangian fillings to a symplectic surface, are two symplectic 2-disks with  $w_1$  and  $w_2$  punctures. The gluing of these pieces yields a closed symplectic 2-sphere.

In general, the lens spaces are of the form  $L(k \cdot n^2, k \cdot nm - 1)$  and, for  $k \geq 2$ , there might be a choice of Lagrangian filling. These different choices always allow us to adjust the homology class as desired. The reader is invited to work the case  $k = 2$  in detail, where the 4-dimensional symplectic filling contains a Lagrangian 2-sphere, along which one can Dehn twist. We believe this strategy generalizes and can be used to prove Theorem 3.12. Let us now turn gears towards the 4-dimensional approach, where the local models shall be constructed directly.

## 4.2 Almost-toric Fibrations

In this subsection, we succinctly discuss almost-toric diagrams and their associated *almost-toric fibrations*, henceforth abbreviated ATF [52], with the focus on visualizing symplectic surfaces, curves in complex dimension one, on a given ATF.

We refer the reader to Section 2 and [34, 52] for additional details. The necessary definition, [52, Definition 4.5] and [34, Definition 2.2], reads as follows:

**Definition 4.3** ([34, 52]) An *almost-toric fibration* of a symplectic 4-manifold  $(X, \omega)$  is a Lagrangian fibration  $\pi : (X, \omega) \rightarrow B$  such that any point of  $(X, \omega)$  there exists a Darboux neighborhood  $(x_1, y_1, x_2, y_2) \in (\mathbb{D}^4, \omega_{\text{st}})$ , with symplectic form  $\omega_{\text{st}} = dx_1 \wedge dy_1 + dx_2 \wedge dy_2$ , in which the map  $\pi$  has one of the following local normal forms:

$$\begin{aligned} \pi(x, y) &= (x_1, x_2), & \text{regular point,} \\ \pi(x, y) &= (x_1, x_2^2 + y_2^2), & \text{elliptic, corank one,} \\ \pi(x, y) &= (x_1^2 + x_2^2, x_2^2 + y_2^2), & \text{elliptic, corank two,} \\ \pi(x, y) &= (x_1 y_1 + x_2 y_2, x_1 y_2 - x_2 y_1), & \text{nodal or focus-focus,} \end{aligned}$$

with respect to some choice of coordinates near the image point in the almost-toric base  $B$ .  $\square$

For the nodal singularity, writing  $x = x_1 + ix_2$  and  $y = y_1 + iy_2$ , the almost-toric fibration  $\pi$  reads  $\pi(x, y) = \bar{x}y \in \mathbb{C}$ . The following remark is also relevant:

**Remark 4.4** By the Arnold-Liouville Theorem [3], given any point  $q$  in a regular fibre, there is a neighborhood of the form  $U \times T^2$ , with action-angle coordinates  $(p_1, p_2, \theta_1, \theta_2)$ ,  $(p_1, p_2) \in \mathbb{R}^2$  and  $(\theta_1, \theta_2) \in T^2 = \mathbb{R}^2/\mathbb{Z}^2$ , where the symplectic form  $\omega$  is  $dp_1 \wedge d\theta_1 + dp_2 \wedge d\theta_2$ . Here, we identify simultaneously  $U$  with a neighborhood of  $\pi(q)$  in  $B$ , as well as, a neighborhood of  $\mathbb{R}^2$ . Consider then a 1-cycle  $\gamma(t) = (\theta_1(t), \theta_2(t)) \in \pi^{-1}(q) = \mathbb{R}^2/\mathbb{Z}^2$  and move it along a curve  $\sigma(s)$  in  $U \subset \mathbb{R}^2$ , so we get the cylinder  $\Gamma(s, t) = (\sigma(s), \gamma(t))$  in the  $(p_1, p_2, \theta_1, \theta_2)$  coordinates. So, up to a choice of orientation,  $\Gamma(s, t)$  is symplectic iff  $\langle \sigma'(s) | \gamma'(t) \rangle \neq 0$ , for all  $t$ . In particular, if we fix the cycle with  $\gamma'(t) = |(a, b)\rangle$ ,  $(a, b) \in \mathbb{Z}^2$ , we are allowed to move in any direction in  $U$ , as long as we are never parallel to  $\langle (b, -a) |$ , in order to get a symplectic cylinder.  $\square$

The set  $B_0$  of regular values of  $\pi : X^4 \rightarrow B^2$ , carries naturally an affine structure, and circling around a node, i.e. the image of a nodal critical point, provides a monodromy for this affine structure, that is a shear with respect to some eigendirection associated to the node – see [34, 52] for details. In local action-angles coordinates (see Remark 4.4), where we have  $\pi|_V : V \cong U \times T^2 \rightarrow U \subset \mathbb{R}^2$ , with  $U \hookrightarrow B$ , this affine structure is identified with the lattice  $\mathbb{Z}^2 \subset \mathbb{R}^2 \cong T_b U$  for each  $b \in U$ .

As in Section 2, an ATF can be described by an almost-toric base diagram, which in section is denoted by  $P_X \subset \mathbb{R}^2$  (ATBD) [52, Section 5.2]. This is the reason for Definition 2.1. Indeed, in this paper an ATBD is depicted as a polytope, with nodes in the interior representing the nodal fibres, and cuts (represented by dashed segments) towards the edge, that encode the monodromy around the singular fibres.

**Remark 4.5** Figure 7 represents ATBD representing an ATF of  $(\mathbb{CP}^2, \omega_{\text{st}})$ , see also Figure 2 and Figure 1, and [55] for several ATBDs representing ATFs of Del Pezzo surfaces. In this article, we will always assume that a cut in the ATBD is a segment in the eigendirection of the monodromy of its associated node. That way we can define a homeomorphism  $B \rightarrow P_X$ , which is affine over  $B_0 \setminus \bigcup(\text{cuts})$ . To each cut, we associate a monodromy matrix in  $SL(2, \mathbb{Z})$ , representing, in the standard basis of  $\mathbb{R}^2$ , the monodromy associated to a counter-clockwise loop around the node.  $\square$

The symplectic curves we construct projects to a neighborhood of a graph embedded in the base of the ATF, in line with Mikhalkin's amoebas projecting to the neighborhoods of a tropical spine [44, 43, 48]. In our case, we have more flexibility since we only require the curve to be symplectic, not necessarily holomorphic. A series of recent works by several authors [37, 38, 47, 22] shows how to get Lagrangians from tropical data, which is also much more rigid then getting symplectic curves, as one would expect. To describe our symplectic surfaces we need to develop terminology in Subsection 4.3.

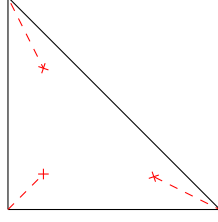


Figure 7: ATBD for  $\mathbb{CP}^2$ .

### 4.3 Symplectic-tropical curves

The central ingredient in Theorem 3.12 and in our argument in Subsection 3.3 is the notion of a *symplectic tropical curve* in an almost-toric diagram, which we abbreviate *STC*. This is the content of the following definition.

Let  $P_X \subset \mathbb{R}^2$  be an ATBD representing an ATF  $\pi : X \rightarrow B$  of a symplectic 4-manifold  $X$ . Let  $\Gamma$  be an oriented graph, with edges decorated by primitive  $\mathbb{Z}^2$  vectors and a multiplicity in  $\mathbb{Z}_{>0}$ . Given an oriented edge  $\gamma$  from a vertex  $b$  to a vertex  $c$ ,  $b$  is said to be negative and  $c$  positive, with respect to  $\gamma$ .

**Definition 4.6** A symplectic-tropical curve  $\mathcal{C} : \Gamma \rightarrow P_X$  is a  $C^0$ -embedding which satisfies the following conditions:

- (i) Vertices are either univalent (*boundary*), bivalent (*bending*) or trivalent (*interior*). The edges associated with boundary vertices shall be called *leaves*;
- (ii) All boundary vertices are negative.
- (iii) Images under  $\mathcal{C}$  of boundary vertices are either on the boundary of the polytope  $P_X$  or on a node. The images of bending vertices belong to the cuts (hence come endowed with an associated monodromy matrix). The images of interior vertices belong to the complement of cuts, nodes, and boundary;
- (iv)  $\mathcal{C}$  restricted to the (interior of) the edges is a  $C^\infty$ -embedding and tangent lines have lateral limits at each vertex, which are oriented according to the orientation of the corresponding edge. We call a vector on this limit tangent lines a *limit* vector;
- (v) If  $\mathbf{v}$  is a positively oriented vector tangent to the image of an edge under  $\mathcal{C}$ , with associated primitive vector  $\mathbf{w} \in \mathbb{Z}^2$ , then  $\langle \mathbf{v} | \mathbf{w} \rangle > 0$ ;
- (vi) For a boundary vertex over the boundary of  $P_X$ , the primitive  $\mathbb{Z}^2$ -vector associated to its corresponding leaf must be orthogonal to the boundary and pointing towards the interior of  $P_X$ . (The multiplicity of the edge can be arbitrary);
- (vii) For a boundary vertex over a node of  $P_X$ , the primitive  $\mathbb{Z}^2$ -vector  $\mathbf{w}$  associated to its corresponding leaf must be orthogonal to the cut, and its orientation is determined by (ii) and (v). (The multiplicity can be arbitrary);
- (viii) Let  $\gamma_1$  and  $\gamma_2$  be two edges meeting at a bending vertex, with monodromy matrix  $M$ . First, the bending vertex must be positive w.r.t. one edge and negative w.r.t. the other. Assume that we go counter-clockwise from  $\mathcal{C}(\gamma_1)$  to  $\mathcal{C}(\gamma_2)$ . If  $\mathbf{v}$  is a positively oriented limit vector for  $\mathcal{C}(\gamma_1)$  at this bending vertex, then  $M\mathbf{v}$  is a positively oriented limit vector for  $\mathcal{C}(\gamma_2)$ . Moreover, if  $\mathbf{w}$  is the

associated primitive vector to  $\gamma_1$ , then the associated primitive vector to  $\gamma_2$  must be  $(M^T)^{-1}\mathbf{w}$ . In this case, the multiplicity of  $\gamma_1$  and  $\gamma_2$  must be the same;

- (ix) For the three edges  $\gamma_j$ ,  $j = 1, 2, 3$ , associated to an interior vertex  $b$ , with associated vectors  $\mathbf{w}_j$  and multiplicity  $m_j$ , the following balancing condition must be satisfied:

$$(4-1) \quad \varepsilon_1 m_1 \mathbf{w}_1 + \varepsilon_2 m_2 \mathbf{w}_2 + \varepsilon_3 m_3 \mathbf{w}_3 = 0,$$

where  $\varepsilon_j = \pm 1$  according to  $b$  being positive or negative with respect to  $\gamma_j$ ,  $j = 1, 2, 3$ .  $\square$

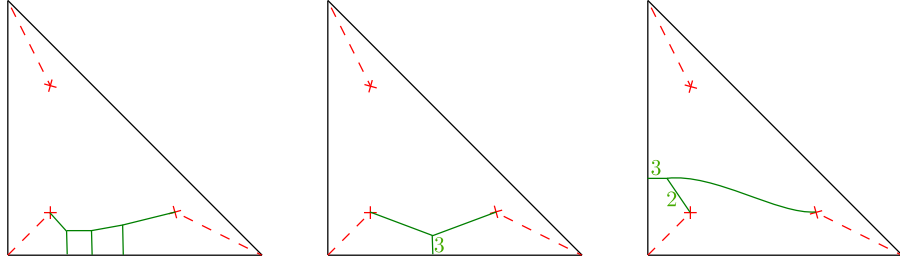


Figure 8: Examples of symplectic-tropical curves in an ATBD of  $\mathbb{CP}^2$ .

There are many conditions in Definition 4.6, the idea is the following. We travel along an edge with cycles, according to the multiplicity, represented by its associated vector, as in Remark 4.4. Condition (v) will guarantee that the surfaces are symplectic as we travel along the edges; condition (ix) implies that these cycles arriving at a vertex are null-homologous, which will allow us to glue them together (by a bounding null-homology); conditions (vi) and (vii) guarantee that the corresponding cycles collapse as we arrive at an edge, or can collapse at the nodal fiber; condition (viii) says that the map  $\Gamma \rightarrow B$  given by composing with the inverse of the homeomorphism  $B \rightarrow P_X$ , is actually smooth at the bending vertex, and the associated vector changes accordingly. The remaining pieces of notation is required to write the balancing condition (4-1) in a precise and consistent way.

We represent a symplectic-tropical curve by just drawing its image  $\mathcal{C}(\Gamma)$ , and labeling the multiplicity of each edge. The label is implicitly 1 if the edge is drawn unlabeled. Conditions (vi)–(ix), determine the associated vectors and multiplicity, up to the ambiguity given by the sign and orientation of the edges that are not leaves, which we basically ignore since they are just an artefact to write (ix) consistently. For instance, Figure 8 represents 3 different symplectic lines in an ATF of  $\mathbb{CP}^2$ . In the leftmost picture, the leaves are decorated with the associated vectors  $(1, -1)$ ,  $(0, 1)$  and  $(-1, -2)$ , accordingly, while the other two edges have labels  $\pm(1, 0)$  and  $\pm(1, 1)$ , the sign being determined by (ix) and how one decides to orient the edges.

The core constructive result in this section, which justifies Definition 4.6, is the following:

**Theorem 4.7** *Given  $\mathcal{C} : \Gamma \rightarrow P_X$  symplectic-tropical curve as above, and  $\mathcal{N} \subseteq P_X$  a neighborhood of  $\mathcal{C}(\Gamma)$ . Then there exists a closed symplectic curve<sup>2</sup>  $C$  embedded in  $X$ , projecting to  $\mathcal{N}$  under  $\pi : X \rightarrow B$ . In addition, the intersection of  $C$  with the anti-canonical divisor  $K_X \subseteq X$  defined by the boundary of  $P_X$  is given by the sum of the multiplicities of the corresponding boundary vertices.*  $\square$

<sup>2</sup>A real symplectic surface, i.e. two real dimensions.

In this context, we say that the symplectic surface  $C$  is represented by the symplectic-tropical curve  $\mathcal{C}(\Gamma)$ . See [52, Proposition 8.2] for a discussion on the anti-canonical divisor  $K_X \subseteq X$ . In order to prove Theorem 4.7, we need to construct local models near the nodes and the trivalent vertices. This is the content of the following subsections.

**Remark 4.8** We could consider embedding of graphs with interior vertices having valency greater than 3, and write a rather involved definition for symplectic-tropical curves. In this case, these graphs could be viewed as a limit of graphs as in Definition 4.6, and a result similar to Theorem 4.7 holds.  $\square$

### 4.3.1 Local model near the nodes

The interesting cases near the nodes is that we may arrive at a node with multiplicity  $k \in \mathbb{N}$  greater than 1. It is possible to address this using the transverse  $k$ -component links, as explained in Subsection 4.1. We shall now argue directly in the 4-dimensional symplectic domain and monitor the projections onto the ATBD. In principle, we would need to get  $k$  disjoint capping 2-disks with boundary in  $k$  copies of the collapsing cycle nearby a nodal singularity. That is not possible if we force the boundary of these 2-disks to be entirely contained in a torus fibre. In consequence, for  $k > 1$ , our 2-disks cannot project exactly over a segment under the projection  $\pi$ , but rather onto a 2-dimensional thickening of a segment in  $P_X$ .

Let us start with the local model for  $k = 1$ , where we are to collapse only one symplectic 2-disk at the singular point. Consider the local model of a nodal fibre as in Definition 4.3, and the complex notation  $\pi(x, y) = \bar{x}y$  for the almost-toric fibration the map  $\pi$ . Choose  $\varepsilon \in \mathbb{R}^+$  sufficiently small. In this case, the 2-disk

$$\sigma_1 = (re^{i\theta}, -ire^{i\theta}), \quad 0 \leq |r| \leq \varepsilon, \quad \theta \in [0, 2\pi]$$

is a symplectic 2-disk with boundary  $c(\theta) = (\varepsilon e^{i\theta}, -i\varepsilon e^{i\theta})$ , which is part of the symplectic line  $y = -ix$  and projects via  $\pi = \bar{x}y$  to the half-line  $i\mathbb{R}_{\leq 0}$ . Let us now discuss the case of higher  $k \in \mathbb{N}$ .

Let us introduce a second symplectic 2-disk in this neighborhood, disjoint from the above, so that its boundary is isotopic, and arbitrarily close, to the collapsing boundary cycle  $c(\theta)$  above. Fix a value  $\delta_2 \in \mathbb{R}^+$ , thought to be small with respect to  $\varepsilon^2$ , and a monotone non-increasing  $C^\infty$ -bump function  $\Psi_2(s)$  such that

$$\Psi_2(s) \equiv \delta_2 \text{ for } s \approx 0, \quad \Psi_2(s) \equiv 0 \text{ for } s \geq 1, \quad \Psi_2(s) > 0 \text{ for } s \in [0, \varepsilon^2].$$

By taking  $\delta_2$  sufficiently small, we can take  $\Psi$  as  $C^1$ -close to 0 as necessary. We can then guarantee that the line  $l_2 := \{y = -ix + \Psi_2(|x|^2)\}$  is still symplectic. Then our second disk  $\sigma_2$  is taken to be the intersection of the symplectic line  $l_2$  with the half-space defined by  $\text{im}(\bar{x}y) \geq -\varepsilon^2$ , where  $\text{im}$  denotes the imaginary part. Note that, by construction,  $\sigma_2 \cap \sigma_1 = \emptyset$ .

Now, in order to then construct  $k \in \mathbb{N}$  mutually disjoint symplectic 2-disks, with their boundary being isotopic and close to the collapsing boundary cycle  $c(\theta)$ , we only need to take  $\delta_k > \delta_{k-1} > \dots > \delta_2$ ,  $\delta_i \in \mathbb{R}^+$ ,  $2 \leq i \leq k$ , and the corresponding monotone non-increasing  $C^\infty$ -bump functions  $\Psi_k(s) > \Psi_{k-1}(s) > \dots > \Psi_2(s)$ , all sufficiently  $C^1$ -close to 0 so that the lines  $l_j := \{y = -ix + \Psi_j(|x|^2)\}$  are symplectic for  $j = 2, \dots, k$ . The symplectic 2-disk  $\sigma_j$  is then taken to be the intersection of the symplectic line  $l_j$  with the half-space  $\text{im}(\bar{x}y) \geq -\varepsilon^2$ . See Figure 9 (Left) for a depiction of the projections  $\pi(\sigma_j)$  of such symplectic 2-disks.

**Remark 4.9** The equations for the symplectic lines  $l_j$  imply that each 2-disk  $\sigma_j$ ,  $1 \leq j \leq k$ , intersects the Lagrangian plane  $x = y$  at a point where  $x = -ix + \Psi_j(|x|^2)$ , since by Pythagoras Theorem, we need  $\Psi_j(|x|^2) = \sqrt{2}|x|$ , which occurs since we have chosen  $\delta_j < \varepsilon^2$ .  $\square$

Note that the boundary  $\partial\sigma_j$  projects under  $\pi$  to a segment  $I_j$  normal to the half-line  $i\mathbb{R}_{\leq 0}$ . Now, using the fact that the lines  $l_j$  are isotopic to the line  $y = -ix$ , which topologically self-intersects once (e.g. relative to the boundary at infinity), we can deduce that the boundary  $\partial\sigma_j$  links  $\partial\sigma_1$  exactly once in the thickened annulus  $\pi^{-1}(I_k)$ , as illustrated in the rightmost picture of Figure 9.

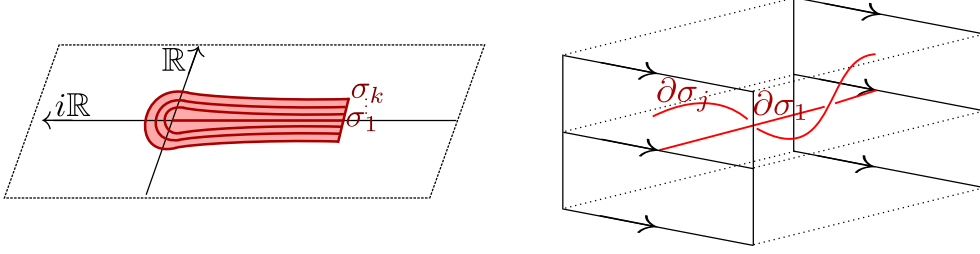


Figure 9: The left picture illustrates the projection of the  $\sigma_j$  disks. The right picture illustrates how  $\partial\sigma_j$  and  $\partial\sigma_1$  are linked in the thickened annulus  $\pi^{-1}(I_k)$ .

In proving Theorem 4.7, we may assume that the image of the leaves arrive at a node in a segment, which we can identify in our local model with a segment in  $i\mathbb{R}_{\leq 0}$ . The above discussion is then summarized in the following

**Proposition 4.10** Let  $\pi : X \longrightarrow B$  be an ATF, represented by an ATBD  $P_X$ , where we homeomorphically identify  $B$  with  $P_X$ . Let  $\gamma$  be a leaf of a symplectic-tropical curve  $\mathcal{C} : \Gamma \longrightarrow P_X$ , with boundary vertex over a node, multiplicity  $k \in \mathbb{Z}_{>0}$ , and  $\mathcal{N}$  a neighborhood of  $\mathcal{C}(\gamma) \subseteq B$ . Fix a point  $p \in \mathcal{C}(\gamma)$  close to the node with collapsing cycle  $\alpha \subset \pi^{-1}(p)$ .

Then we can associate  $k$  disjoint symplectic 2-disks  $\sigma_j$ ,  $1 \leq j \leq k$ , such that  $\pi(\sigma_j) \subset \mathcal{N}$ , with their boundary  $\partial\sigma_j$  arbitrarily close to  $\partial\sigma_1 = \alpha$ .  $\square$

### 4.3.2 Local modal near interior vertices

Condition (v) in Definition 4.6 and Remark 4.4 allows us to transport the boundary of the symplectic 2-disk  $\sigma_1$  in Proposition 4.10 along the image of the corresponding leaf until it is close to a interior node. (Note that if we hit a bending vertex, condition (viii) guarantees that we can keep moving the same cycle  $\partial\sigma_1$ , whose class in the first homology of the fibre is then represented by a different  $\mathbb{Z}^2$  vector according to the monodromy.) In addition, the boundaries  $\partial\sigma_j$  project to a segment normal to the leaf and, because of its closeness of to  $\partial\sigma_1$ , we can also transport it using cycles projecting under  $\pi$  to small segments normal to the leaf. In line with Remark 4.4, we can ensure that these surface remain symplectic.

At this stage, we need to construct a local model for a symplectic surface near a trivalent vertex  $b$ , using the data of (ix), that can be made to project to a given neighborhood of  $\mathcal{C}(b)$ . Moreover, it needs to glue with prescribed incoming cycles. For that, a first option is to rely on the article [44], where G. Mikhalkin uses O. Viro's patchworking ideas to construct families of hypersurfaces in  $(\mathbb{C}^*)^n$ , whose



amoebae converge to a given tropical hypersurface in  $\mathbb{R}^n$ , see [44, Remark 5.2]. In that manuscript, G. Mikhalkin actually views  $(\mathbb{C}^*)^n$  as the open strata of a closed toric variety, in particular having finite volume, so we can symplectically assume that it is indeed a local model. Given the nature of Theorem 4.7, we can assume that the symplectic-tropical curve arrives at the interior vertex in a tropical way, i.e., locally as segments  $\mathbf{v}_j = \mathbf{w}_j$ 's satisfying the balancing condition (4-1) of Definition 4.6.

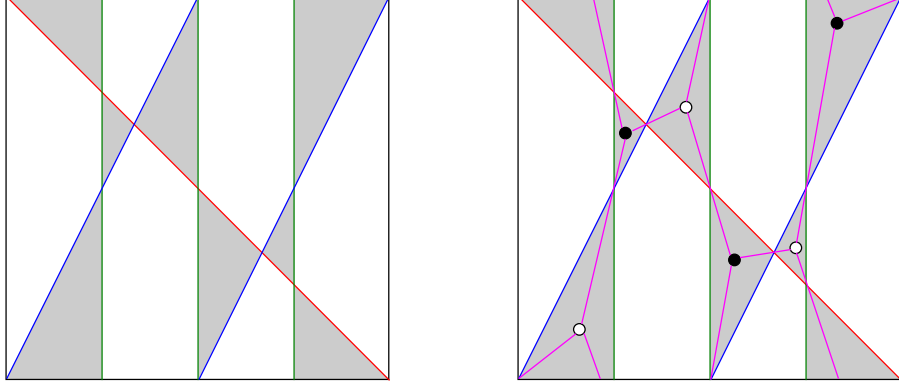


Figure 10: Collection of cycles in  $T^2$  satisfying the balancing condition (4-1) and its associated dimer. This cycles corresponds to the ones arriving at the interior vertex of the symplectic-tropical curve in the middle diagram of Figure 8. It represents the coamoeba in  $\mathcal{B}$  of the symplectic surface we will construct.

A second option, independent of [44], is using the following explicit local model. Over a small disk  $\mathcal{B} \subseteq B$  centered at an interior vertex  $b \in B$ , we have  $\pi^{-1}(\mathcal{B}) \cong \mathcal{B} \times T^2$ , and the fibration is given by the projection onto the first factor. The projection of the symplectic curve to the  $T^2$  factor is known as the coamoeba of that curve. We aim at first constructing what will be the coamoeba out of the balancing condition (4-1) and – out of that data – then building our local model for the symplectic curve. We want the surface to be so that its boundary projects to straight cycles, having only double crossings. Moreover, away from the pre-image of the double crossings, the rest of the surface will project injectively into polygons divided by the straight cycles. The homology classes of the boundary are represented by  $m_j$  disjoint copies of  $\varepsilon_j \mathbf{w}_j$ ,  $j = 1, 2, 3$ , where  $\mathbf{w}_j$ 's are the vectors associated with the interior vertex  $b$  and hence satisfy the balancing condition (4-1) from Definition 4.6 (ix). Figure 10 (Left) illustrates the amoeba of the local model we will build for the neighborhood of the interior vertex in the ATBD from Figure 8 (Center). The balancing condition associated with the interior vertex is  $(1, -1) + 3(0, 1) + (-1, -2) = 0$ .

The existence of the above mentioned configuration for the coamoeba is equivalent to the existence of a *dimer model*<sup>3</sup> embedded in  $T^2$ . We label each convex polygon of our coamoeba black and white, where a black polygon can only share a vertex with a white one. The vertices of the dimer model are then placed in the interior of the polygons according to their colours, and for each intersection of the boundary cycles we associate an edge, projecting inside the coamoeba. See Figure 10 (Right). Then the straight cycles are taken to be the collection of zigzag paths associated to the dimer. For concepts related to dimer models, including zigzag paths, and its relationship with coamoebas, we refer the reader to the recent works [10, 13, 20, 22]. Thus, from the discussion above, our aim is then to provide

<sup>3</sup>A dimer model [30] is a bipartite graph, and we name half of the vertices black and the other half white, so edges connect a black vertex to a white one.

a dimer model with prescribed set of homology classes for its collection of zigzag paths. Moreover, we want the zigzag paths to be straight. This is achieved in Proposition 4.12 below.

**Remark 4.11** If one does not require the paths to be straight, then the article [20, Section 6] constructs an algorithm to build a dimer model out of the prescribed classes for the collection of zigzag paths. (Again, with non-straight cycles.) Now, note that in [13, Example 4.1], an example of a collection of 5 classes in  $H_1(T^2)$  that cannot be realized by straight cycles, that are the zigzag paths of a dimer model, is given. Nevertheless, in case the collection of classes are given by copies of only 3 primitive classes, one can in fact construct a dimer model with straight set of zigzag paths, as shown in the upcoming Proposition 4.12. We believe this is likely well-known to experts but we did not find references in the literature.  $\square$

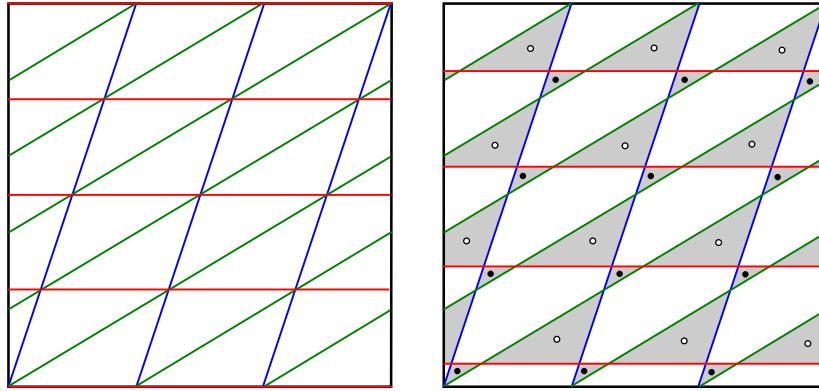


Figure 11: Construction of a dimer model with the prescribed collection  $4(1, 0) + (1, 3) + (-5, -3) = 0$  of zigzag paths.

**Proposition 4.12** Given  $\mathbf{w}_1, \mathbf{w}_2, \mathbf{w}_3 \in H_1(T^2; \mathbb{Z})$ , primitive classes satisfying

$$m_1 \mathbf{w}_1 + m_2 \mathbf{w}_2 + m_3 \mathbf{w}_3 = 0, \quad m_1, m_2, m_3 \in \mathbb{N}$$

there exists a dimer model in  $T^2$  with zigzag paths realised by  $m_j$  straight lines in the classes  $\mathbf{w}_j$ ,  $j = 1, 2, 3$ . Moreover, the component containing the vertices of the dimer can be taken to be triangles.

**Proof** Figure 11 essentially provides a proof by drawing. In detail, let us assume, without loss of generality, that  $\mathbf{w}_1 = (1, 0)$ , and let  $\mathbf{w}_2 = (a_2, b_2)$ ,  $\mathbf{w}_3 = (a_3, b_3)$ . Take the straight cycle  $[0, 1] \times \{0\}$  in  $T^2 = \mathbb{R}^2/\mathbb{Z}^2$ , in the class  $\mathbf{w}_1 = (1, 0)$ , and consider  $|m_2 b_2| = |m_3 b_3|$  equidistant points in  $[0, 1]$ . For  $j = 2, 3$ , take  $m_j$  straight lines with slope  $\mathbf{w}_j$ , passing through the first  $m_j$  points in the segment  $[0, 1]$ , and consider them as cycles in  $T^2 = \mathbb{R}^2/\mathbb{Z}^2$ . It can be seen that these lines intersect in heights which are multiples of  $1/m_1 \pmod{\mathbb{Z}}$ . For  $k = 0, \dots, m_1 - 1$ , take the cycles  $[0, 1] \times \{k/m_1\}$ , each of them intersecting the other straight lines in  $|m_2 b_2| = |m_3 b_3|$  triple points. In that way,  $T^2$  is divided into triangles, as illustrated in Figure 11 (Left). Then, moving the horizontal cycles slightly up, we build the required dimer, as shown in Figure 11.  $\square$

From this dimer model, constructed from the data of the balancing condition (4-1), we will now build a smooth surface in  $I \times T^2$ , where  $I = [-\epsilon, \epsilon]$ , with boundary  $m_j$  copies of cycles in class  $\mathbf{w}_j = \epsilon_j \mathbf{w}_j$  in  $H_1(I \times T^2; \mathbb{Z}) \cong H_1(T^2; \mathbb{Z})$ , living in heights  $-\epsilon, 0, \epsilon$  for  $j = 2, 1, 3$ , respectively.

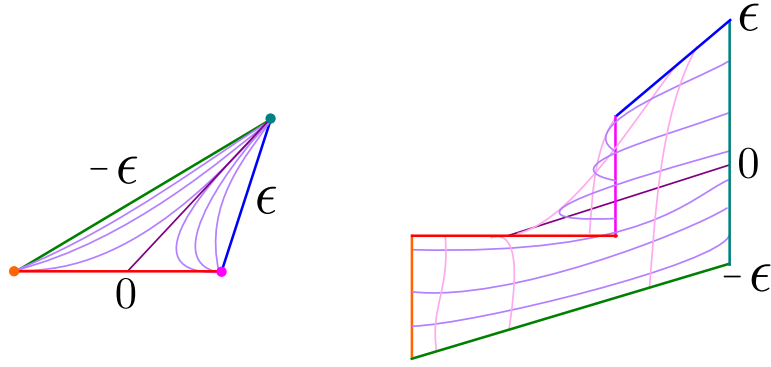


Figure 12: The smooth surface in  $I \times T^2$  associated to one of the triangles in the dimer model of Proposition 4.12. The coamoeba in the 2-torus  $T^2$  is depicted on the left, with the described foliation associated to  $f$ .

Consider the congruent white triangles and, in each, take a segment from its vertex given by the intersection of the cycles in the classes  $w_2$  and  $w_3$ , to the middle point of the opposite edge. We name the primitive direction of this segment  $f = (\alpha, \beta)$ , and abuse notation by calling  $f$  the segment itself. Consider then a smooth foliation of the triangle minus the vertices, so that following it gives an isotopy from the edge in the  $w_2$  cycle to half of the edge in the  $w_1$  cycle union the segment  $f$ , and then from the other half of the edge in the  $w_1$  cycle union the segment  $f$  to the the edge in the  $w_3$  cycle, as illustrated in Figure 12 (Left). Considering each leaf of the foliation as level sets of a smooth function  $\rho_2$  from the triangle triangle minus vertices to  $I$ , its graph embeds into  $I \times T^2$ , as in Figure 12 (Right). Now, taking a symmetric version of the foliation and function  $\rho_2$  on the black triangles of the dimer model, this ensures that the compactification of the union of the graphs is a smooth surface in  $I \times T^2$ , with the desired boundaries.

Note that this embedding can be made symplectic into the region  $\mathcal{B} \times T^2$ , the symplectic neighborhood of the pre-image of the interior vertex  $b$ , by embedding the segment  $I$  into  $\mathcal{B}$  in an appropriate direction. Nonetheless, we can also build our surface to project on the  $(p_1, p_2)$  coordinates onto amoebas, much like in the work of Mikhalkin [43, 44].

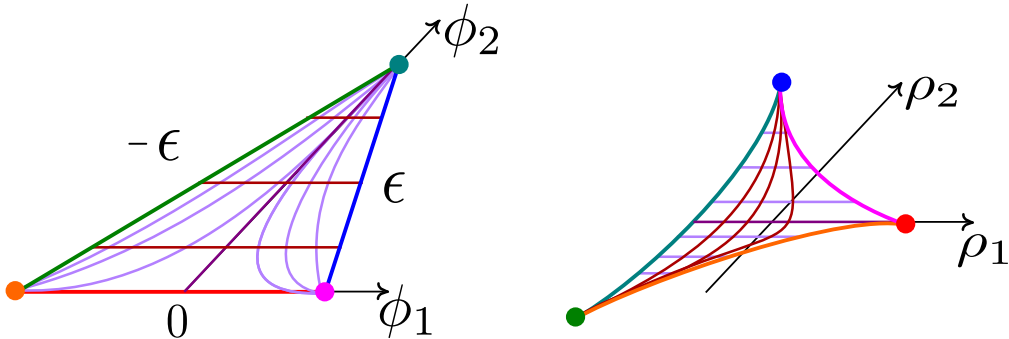


Figure 13: The depiction a triangular piece of the coamoeba (left) and the amoeba (right) of a symplectic surface near the interior vertex.

**Remark 4.13** For convenience, we shall now perform a change of local coordinates, from  $(p_1, \theta_1, p_2, \theta_2)$  to new coordinates  $(\rho_1, \phi_1, \rho_2, \phi_2)$ , where the symplectic form will be

$$dp_1 \wedge d\theta_1 + dp_2 \wedge d\theta_2 = d\rho_1 \wedge d\phi_1 + d\rho_2 \wedge d\phi_2.$$

This change the basis is performed in the  $T^2$  chart, going from  $\mathbf{e}_1 = (1, 0)$ , and  $\mathbf{e}_2 = (0, 1)$ , to  $\mathbf{e}_1$  and  $\mathbf{f} = (\alpha, \beta)$ . This corresponds to setting  $\phi_1 = \theta_1 - (\alpha/\beta) \cdot \theta_2$ , and  $\phi_2 = \theta_2/\beta$ , so  $\theta_1 \mathbf{e}_1 + \theta_2 \mathbf{e}_2 = \phi_1 \mathbf{e}_1 + \phi_2 \mathbf{f}$ . Setting  $\rho_1 = p_1$  and  $\rho_2 = \alpha p_1 + \beta p_2$  ensure that  $dp_1 \wedge d\theta_1 + dp_2 \wedge d\theta_2 = d\rho_1 \wedge d\phi_1 + d\rho_2 \wedge d\phi_2$ . These coordinates  $(\rho_1, \phi_1, \rho_2, \phi_2)$  shall now be used in the following proposition.  $\square$

We are now ready to construct all the required local models for the symplectic surfaces in Theorem 4.7. (These local models shall be connected in the subsequence Subsection 4.3.3.) This is the content of the following

**Proposition 4.14** Let  $\mathcal{C} : \Gamma \longrightarrow P_X$  be a symplectic-tropical curve in an ATF  $\pi : X \longrightarrow B$ , represented by an ATBD  $P_X$ ,  $b$  be an interior vertex and  $\mathcal{B}$  a small disk centred in  $b$ , whose boundary intersect  $\mathcal{C}(\Gamma)$  in the points  $p_1, p_2, p_3$ . Let  $\mathbf{w}_j$  be the associated vector corresponding to the edge containing  $p_j$ , for  $1 \leq j \leq 3$ , hence satisfying the balancing condition (4-1).

Then there exists a symplectic curve in  $X$ , projecting to  $\mathcal{B}$ , whose boundary projects to the points  $p_j$ , and represents cycles whose classes in  $H_1(\pi^{-1}(p_j); \mathbb{Z})$  are given by  $\mathbf{w}_j = \varepsilon_j \mathbf{w}_j$ ,  $1 \leq j \leq 3$ .

**Proof** Figure 13 illustrates how the embedding will look like in each of the (white) triangles, by describing the amoeba and coamoeba together. The interior vertex corresponds to  $(\rho_1, \rho_2) = (0, 0)$ , and we vary  $\rho_1$  in a small enough interval  $[-\delta, \delta]$ . The smooth surface we construct will be the projection to the  $(\rho_2, \phi_1, \phi_2)$  coordinates. Hence, our foliation in the triangle corresponds to the level sets of the coordinate  $\rho_2$ , i.e.  $\rho_2$  constant. Each edge of the triangle in the coamoeba have constant  $(\rho_1, \rho_2)$  coordinates corresponding to the vertices of the amoeba. Using the same name for the edges, as for their homology classes, we choose  $\rho_1$ , so that,  $\rho_1(\mathbf{w}_3) = \rho_1(\mathbf{w}_2) < 0 \leq \rho_1(\mathbf{w}_1)$ . The  $\rho_1$  coordinate decreases as we move along the  $\rho_2$  level sets from bottom to top. Also, as we vary  $\phi_1$  positively in the horizontal segments ( $\phi_2$  constant) in the triangle, we choose  $\rho_1$  so that its variation is non-negative for  $\rho_2 \leq 0$  and non-positive for  $\rho_2 \geq 0$ ; also the  $\rho_2$ -coordinate varies positively. We also note that the segments in our smooth surface that projected to the vertices of the triangle in  $T^2$ , will project to the boundary of the amoeba in  $\mathcal{B}$ .

Now, in order to check the symplectic condition for the above surface, we probe with the paths  $\xi^1, \xi^2$ . The former path is given by following the horizontal segment ( $\phi_2$  constant) in the triangle, and the later is given by following the  $\rho_2$  level sets in the triangle. Denoting by  $d\rho_i^j$  and  $d\phi_i^j$  the coordinates of  $d\rho_i$  and  $d\phi_i$ , along the  $j$ -th path, for  $i, j = 1, 2$ , we have that,

$$d\rho_1^1 = \begin{cases} \geq 0 & \text{if } \rho_2 \leq 0 \\ \leq 0 & \text{if } \rho_2 \geq 0 \end{cases}, \quad d\phi_1^1 \geq 0, \quad d\rho_2^1 > 0, \quad d\phi_2^1 = 0,$$

$$d\rho_1^2 < 0, \quad d\phi_1^2 = \begin{cases} \geq 0 & \text{if } \rho_2 \leq 0 \\ \leq 0 & \text{if } \rho_2 \geq 0 \end{cases}, \quad d\rho_2^2 = 0, \quad d\phi_2^2 > 0.$$

So we get that:

$$(4-2) \quad \omega(\partial\xi^1, \partial\xi^2) = \begin{vmatrix} d\rho_1^1 & d\phi_1^1 \\ d\rho_1^2 & d\phi_1^2 \end{vmatrix} + \begin{vmatrix} d\rho_2^1 & d\phi_2^1 \\ d\rho_2^2 & d\phi_2^2 \end{vmatrix} > 0.$$

as desired, where  $\partial\xi^i$  is the tangent vector to the  $\xi^i$  curve. An analogous embedding is defined for the black triangles, with the same amoeba image on the  $(\rho_1, \rho_2)$  projection, and we obtain a smooth embedding of the surface as required.

**Remark 4.15** Note that we could simply take  $\rho_1 \equiv 0$  over the surface, and it would still satisfy (4-2). Hence we can indeed get a symplectic embedding of our surface over a fixed interval in  $\mathcal{B}$ .

Finally, notice that we chose our amoeba (with small  $\delta$ ) so that the tangency of the amoeba at the vertices are far from being orthogonal to the corresponding  $\mathbf{w}_j$  direction. Let  $\mathcal{H}_j$  be the half-plane whose boundary line is normal to  $\mathbf{w}_j$ , passes through  $b$ , and contains the vertex of the amoeba corresponding to  $\mathbf{w}_j$ . The symplectic conditions (4-2) and (v) from Definition 4.6, ensures that the path in  $\mathcal{C}(\Gamma)$  associated to  $\mathbf{w}_j$  is in  $\mathcal{H}_j$ . Hence, we can connect this path to the corresponding  $p_j$  via a path still satisfying the condition of never being orthogonal to  $\mathbf{w}_j$ .  $\square$

### 4.3.3 Connecting the local models

In the subsection we conclude Theorem 4.7 by gluing together the local models provided in Proposition 4.10 and Proposition 4.14 above.

The local model at an interior vertex gives us a  $m_j$  copies of the boundary corresponding to  $\mathbf{w}_j$ , equidistant in our parametrisation of  $T^2$ . We now follow the path that passes through  $p_j$ , as in Proposition 4.14:

- If it hits another interior vertex, we just follow this constant cycles and the surfaces glue naturally.
- If it hits a boundary vertex over the boundary of  $P_X$ , we build the surface again by keeping the cycles constant, and the cycles smoothly collapses to a point since near the boundary of  $P_X$  we have a toric model.

Now, due to the nature of the boundaries coming out of Proposition 4.10, we need to do additional work in order to glue to the local models given by Proposition 4.10, as follows (recall Figure 9).

To connect  $k$  straight cycles, which we color in red, to  $k$  curling cycles, which we color blue – see again Figure 9 – we consider dimers as the ones illustrated in Figure 14. The figures depicts the cases  $k = 3$  and 4, and readily generalizes for any  $k \geq 1$ . Independent of  $k$ , the components containing the vertices of these dimer models are either a bi-gon, a 3-gon or a 4-gon. The analysis for getting a symplectic embedding for each of these pieces, especially the 3-gons and the bi-gons, is similar to the one we made in the proof of Proposition 4.14, and we employ the analogous terminology now.

**Remark 4.16** The main difference is that the  $\rho_2$  coordinate at most of the pieces of the blue cycles is not constant, but this was not crucial for getting the symplectic curve in Proposition 4.14. This makes the boundary of the surface project into segments, rather than points.  $\square$

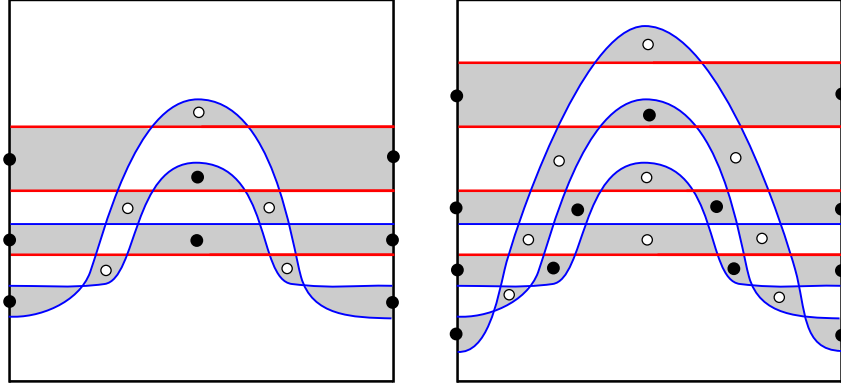


Figure 14: Dimer models for connecting the boundaries of the disks, for the local model of a boundary vertex at a node, to straight cycles.

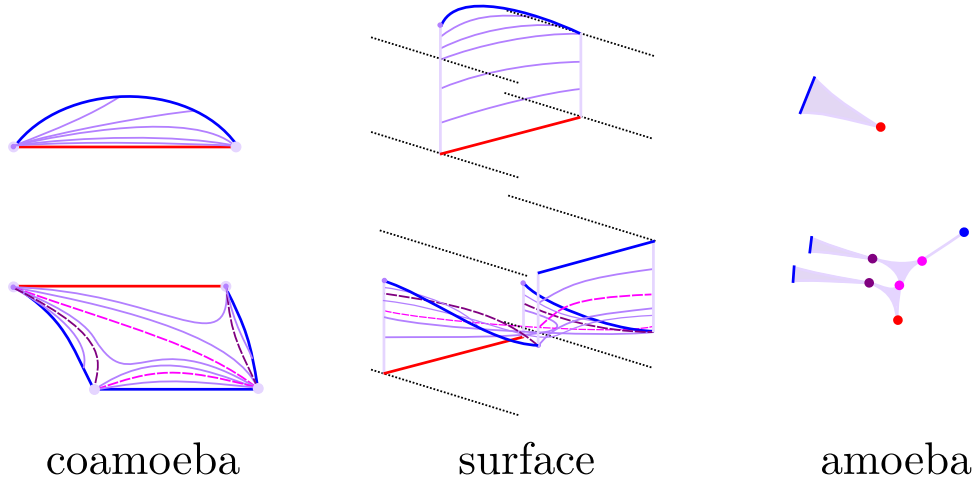


Figure 15: Coamoebas, surfaces and amoebas corresponding to different pieces of the dimer model illustrated in Figure 14. The 4-gon is subdivided into two 3-gons and two bigons indicated by the dashed curves.

To replicate the analysis in the proof of Proposition 4.14 to the 4-gons, it is better to subdivide it into two 3-gons and two bigons. Figure 15 illustrates the coamoebas (with some  $\rho_2$  level sets depicted), the corresponding piece of the smooth surface and the amoeba should look like. Remark 4.15 still holds and we could actually view the amoeba picture as straight segments, but the blue boundaries would still project to sub-segments.

Now, we do not know that the boundaries  $\partial\sigma_j$ 's, who live in the product of an interval with  $T^2$ , project exactly in the pattern as depicted in Figure 14, for  $2 \leq j \leq k$ . The only information we have is that they are mutually linked and that the projections intersect each horizontal cycle generically twice. Nevertheless, this is in fact not a problem, since for each one of them we can draw the actual projection and the corresponding generic curve as in Figure 14.

These curves will generate a dimer, either one annulus or two bi-gons. Hence, we can connect them with a smooth symplectic surface. The condition,  $\Psi_k(s) > \Psi_{k-1}(s) > \dots > \Psi_2(s)$  we required in

the discussion before the statement of Proposition 4.10, ensures that we can place these surfaces inside mutually disjoint thickened tori for  $2 \leq j \leq k$ . This explains how to patch the boundaries  $\partial\sigma_j$ 's to straight cycles for our  $(\theta_1, \theta_2)$  coordinates on the torus.

Finally, the cycles built in Proposition 4.14 are equidistant in our coordinates for  $T^2$ , but the straight cycles we just built are sufficiently close to  $\partial\sigma_1$  (In this metric sense, Figure 14 is misleading for visual purposes.). Using the notation of Proposition 4.14, we promptly see that this is not a problem, since we can move apart these close cycles – thought to be given by  $\phi_2$  constant – until their projection to  $T^2$  become equidistant, by moving only in the corresponding  $\rho_2$  direction. The symplectic condition (4–2) is readily checked, by taking the first curve the horizontal ones in the coamoeba part, and the second curves vertical ones, so  $d\rho_1^1 = d\rho_1^2 = 0$ ,  $d\rho_2^1 = d\rho_2^2 > 0$ ,  $d\phi_2^2 = 0$ .

All these connecting surfaces can be made to project into sufficiently small regions in the almost-toric fibrations, in particular inside the neighborhood  $\mathcal{N}$  of our given symplectic-tropical curve  $\mathcal{C}(\Gamma)$ . This concludes the proof of Theorem 4.7.  $\square$

From now on, we will ease notation by calling  $\mathcal{C}$  the symplectic-tropical curve obtained in Theorem 4.7 from  $\mathcal{C} : \Gamma \rightarrow P_X$ . At this stage, Theorem 4.7 allows us to construct symplectic surfaces  $C(\mathcal{C}) \subseteq X$  associated to symplectic-tropical curves  $\mathcal{C} \subseteq B$ , for an almost-toric fibration  $\pi : X \rightarrow B$ . The upcoming Subsection 4.4 shall now address the general combinatorics appearing in the ATBD associated to Del Pezzo surfaces, which are crucial for the construction of the required symplectic-tropical curves used in our prove of Theorem 1.3 in Section 3.

#### 4.4 Combinatorial background for triangular shaped ATFs

From [55], consider the ATBD of triangular shape for a Del Pezzo surface containing the  $\Theta_{p,q,r}^{n_1,n_2,n_3}$  monotone Lagrangian torus as a visible fibre, i.e., not inside a cut. This is related to the Markov type equation:

$$(4-3) \quad n_1 p^2 + n_2 q^2 + n_3 r^2 = G p q r$$

where  $G = \sqrt{d n_1 n_2 n_3}$ ,  $d$  is the degree of the corresponding Del Pezzo. These equations yield the Diophantine equations in Subsection 3.2. In [55], it is shown that  $n_1 p^2$ ,  $n_2 q^2$  and  $n_3 r^2$  correspond to the determinant of the primitive vectors associated with the corners of the corresponding ATBD.

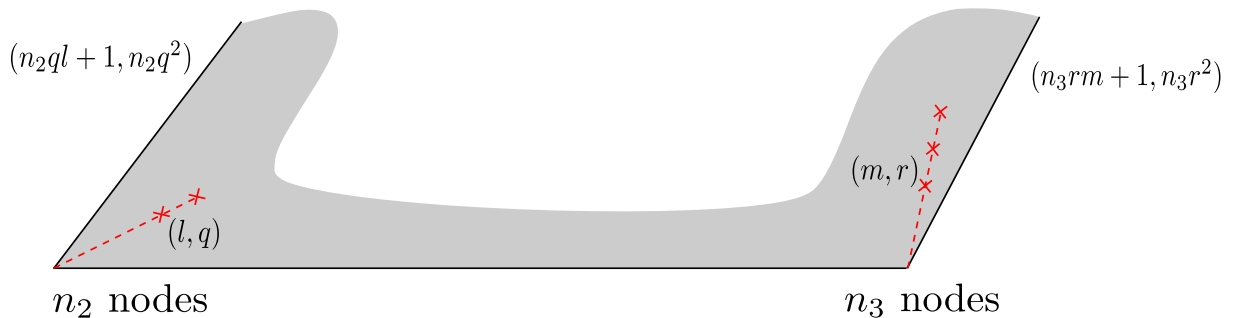


Figure 16: Corners of ATBDs



Forcing the common edge of the corners corresponding to  $n_2q^2$  and  $n_3r^2$  to be horizontal, we get that the cuts and the primitive vectors of the remaining edges are as illustrated in Figure 16, where we name  $(l, q)$  and  $(m, r)$  the direction of the cuts – compare with [52, Figure 13] and [54, Proposition 2.2, Figure 2]. The condition that the third determinant is  $n_1p^2$  then becomes:

$$(4-4) \quad \begin{vmatrix} n_2ql - 1 & n_3rm + 1 \\ n_2q^2 & n_3r^2 \end{vmatrix} = n_2n_3r^2ql - n_3r^2 - n_2n_3q^2rm - n_2q^2 = n_1p^2$$

This yields the equalities

$$n_2n_3r^2ql - n_2n_3q^2rm = n_3r^2 + n_2q^2 + n_1p^2 = Gpqr$$

and upon dividing by  $n_2n_3qr$ , we obtain

$$(4-5) \quad rl - qm = \frac{Gp}{n_2n_3}.$$

Equation (4-5) is used to build symplectic-tropical curves in the  $\varepsilon$ -neighborhood depicted in Figure 16.

#### 4.4.1 Symplectic-Tropical Curves in the Edge Neighborhood $\mathfrak{N}$

Let  $\mathfrak{B}$  be a neighborhood of an edge union associated cuts of an ATBD, as illustrated in Figure 16. Let  $\mathfrak{N}$  denote the preimage of  $\mathfrak{B}$  in  $X$ . By studying the combinatorics of the ATF, we show that we can construct a symplectic-tropical curve (Definition 4.6) inside  $\mathfrak{B}$ , and by Theorem 4.7, there is a corresponding symplectic curve in  $\mathfrak{N}$ . These symplectic curves will have the same intersection with the anti-canonical divisor as the rational curves highlighted in Figure 1. Their homology classes can differ from the rational curves listed in  $\mathcal{H}$  (Figure 1), by the classes of the Lagrangian spheres projecting in between two nodes inside  $\mathfrak{N}$ . In order to obtain them in the desired homology class, we will need to modify our curves in the pre-image of the neighborhood of the cuts, containing the Lagrangian spheres. This second correction is done in the next Subsection 4.4.2.

The collapsing cycle corresponding to the node associated with the cut  $(l, q)$ , respectively  $(m, r)$ , is represented by the orthogonal vector  $(q, -l)$ , respectively  $(-r, m)$ . Consistent with Definition 4.6 (vii), consider a symplectic-tropical curve with: one interior vertex; one leaf going towards one of the nodes with  $(q, -l)$  collapsing cycle, with multiplicity  $r$ ; another going towards one of the nodes with  $(-r, m)$  collapsing cycle, with multiplicity  $q$ ; and the third going towards the bottom edge, with multiplicity  $\frac{Gp}{n_2n_3}$ .

These choices satisfy the balancing condition (4-1) of Definition 4.6 (ix), since from (4-5):

$$(4-6) \quad r(q, -l) + q(-r, m) + \frac{Gp}{n_2n_3}(0, 1) = (0, 0).$$

Hence we get a symplectic-tropical curve in  $\mathfrak{N}$  by Theorem 4.7.

Let us understand the behaviour of a family of these curves as we deform our Del Pezzo surface towards the corresponding limit orbifold. From the proof of [55, Theorem 4.5], and considering both the limit orbifold and the limit orbiline  $\mathcal{A}$  corresponding to the limit of horizontal line in Figure 16, we get that the intersection of  $\mathcal{A}$  with the anticanonical divisor  $[\mathcal{A}] + [\mathcal{B}] + [\mathcal{C}]$ , where  $[\mathcal{B}]$  and  $[\mathcal{C}]$  are the classes of the other orbilines, is:

$$(4-7) \quad [A] \cdot ([A] + [B] + [C]) = \frac{n_1 p^2 (n_3 r^2 + n_2 q^2 + n_1 p^2)}{n_1 n_2 n_3 p^2 q^2 r^2} = \frac{Gp}{n_2 n_3 q r}$$

Note that  $qr$  times this number is the one found in Equation (4-5). Hence, the symplectic-tropical curve we construct limit to a orbi-curve in the class  $qr\mathcal{A}$ . In particular, for the symplectic-tropical curve to be a smoothing of that orbi-line in the class  $\mathcal{A}$ , we must have  $q = 1$  and  $r = 1$ . Indeed, by looking at the intersection with the Lagrangian spheres, we will see that the actual smoothing (in case  $qr = 1$ ) is given by a *deformed* symplectic-tropical curve.

#### 4.4.2 Deforming Symplectic-Tropical Curves

As explained in the previous subsection, we need to be able to have control of the intersection number of our symplectic-tropical curve  $\mathcal{C}$  with the Lagrangian 2-spheres that appear naturally for a pair of nodes lying inside the same cut. For that, let us prove Proposition 4.17, with the following notation.

Let  $\mathcal{C} : \Gamma \rightarrow P_X$  be a symplectic-tropical curve in a ATF of  $X$ , represented by the ATBD  $P_X$  and  $\mathcal{N}$  a neighborhood of  $\mathcal{C}(\Gamma)$ , as before. Consider a class of  $n$  nodes of the ATBD inside the same cut, so that at least one of the nodes is in  $\mathcal{C}(\Gamma)$  and let  $\mathcal{M}$  be a neighborhood of the cut. Let  $S_1, \dots, S_{n-1}$  be Lagrangian spheres projecting inside the cut to consecutive segments between the nodes. Also name  $S_0 = S_n = \emptyset$ . Let  $m$  be the sum of the multiplicities of the leaves arriving at these  $n$  nodes, and choose  $d < n$  nodes, where  $m \equiv d \pmod n$ .

**Proposition 4.17** There is a symplectic curve projecting into  $\mathcal{N} \cup \mathcal{M}$  with the property that it its intersection with  $S_1 \cup \dots \cup S_{n-1}$  is precisely the  $d$  chosen nodes.  $\square$

The reminder of this subsubsection is devoted to the proof of Proposition 4.17. The idea is that, since  $m - d = kn$ , we can place  $\sigma_j$  disks for Proposition 4.10, for  $2 \leq j \leq k + 1$  at all the  $n$  nodes. Naming  $n_1, \dots, n_n$  be the  $n$  nodes in a cut, in order, and  $S_i$  a Lagrangian sphere projecting to the cut between the consecutive nodes  $n_i, n_{i+1}$ , we see that the signed intersection of  $S_i$  with the collection of  $kn$  disks is zero, since the  $S_i$  sphere only intersects the  $k$  disks around the  $n_i$  and  $n_{i+1}$  nodes, with opposite signs. Thus, it is clear that, at least smoothly, we can pairwise cancel these intersections. Nevertheless, before that, we need to connect the disks.

Let us focus now on how to construct in Lemma 4.18 a symplectic pair of pants  $\mathcal{P}$  that we can glue to the boundary of a pair of  $\sigma_j$  symplectic 2-disks near the  $n_i$  and  $n_{i+1}$  nodes.

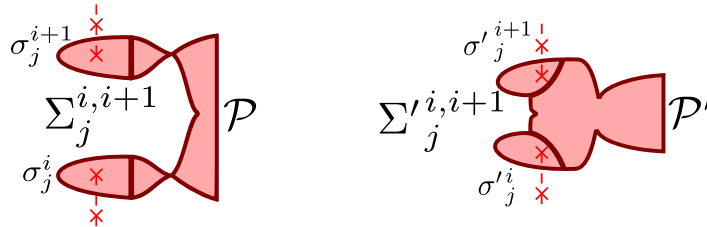


Figure 17: Amoebas of the surfaces  $\Sigma_j^{i,i+1}, \Sigma'_j^{i,i+1}$ .

**Lemma 4.18** *There is a symplectic disk  $\Sigma_j^{i,i+1}$  in the cut neighborhood  $\mathcal{M}$ , containing the two symplectic 2-disks  $\sigma_j^i$  and  $\sigma_j^{i+1}$  disks as a subset, with boundary in a thickened 2-torus  $\mathbb{T}$ , and whose class is two times the collapsing class of the nodes via the identification  $H_1(\mathbb{T}; \mathbb{Z}) \cong H_1(T^2; \mathbb{Z})$ .*

Denote by  $\mathcal{P}$  the pair of pants which is the closure of  $\Sigma_j^{i,i+1} \setminus (\sigma_j^i \cup \sigma_j^{i+1})$ . □

Figure 17 shows on the left the amoeba corresponding to the  $\Sigma_j^{i,i+1}$  surface. The idea is to then isotope it to a different surface  $\Sigma_j^{i,i+1}$  with boundary still in  $I \times T^2$ , such that the intersection with the Lagrangian 2-sphere  $S_i$  is empty.

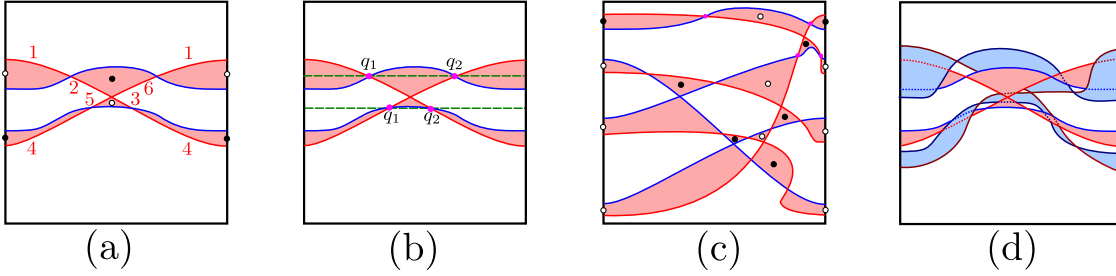


Figure 18: (a) A dimer model for the symplectic pairs of pants  $\mathcal{P}$ . (b) Dimer model for  $\mathcal{P}'$ , illustrating the cycles in the  $S_i$  Lagrangian sphere, over the intersection between the boundary of the amoeba of  $\mathcal{P}'$  and the amoeba of  $S_i$  (a segment between the nodes). (c) The dimer model for the part of the surface  $\Sigma_j^{i,i+3}$  connecting the boundary of the  $\sigma_j$  disk in the  $n_{i+3}$  node with the boundary of  $\Sigma_j^{i,i+2}$ . (d) Coamoeba of 2 non-intersecting  $\mathcal{P}'$ s. The suggested height is with respect to the  $p_2$  coordinate.

**Proof of Lemma 4.18** Let us assume the cut is vertical, and thus the collapsing cycles is given by a  $\theta_2$ -constant curve in the  $(\theta_1, \theta_2)$  coordinates of  $T^2$ . Making a change of action-angles coordinates, if needed, we may assume that the collapsing cycles corresponding to the  $n_i$  nodes are slightly phased-out. We thus draw the  $T^2$  projection of the boundary of the  $\sigma_j$  2-disks, recalling that it links once the horizontal cycle in a thickened torus that they live in (recall construction before Proposition 4.10). We color these boundaries blue, and draw a dimer model that indicates the coamoeba of the pair of pants  $\mathcal{P}$  we will construct, as illustrated in the first picture of Figure 18. We will color the other boundary of  $\mathcal{P}$  red. We number the components of the red curve in the dimer model of Figure 18 (Left) as indicated, and sketch the profile of its  $p_2$  coordinate as indicated in Figure 19.

The  $\partial\sigma_j$  curves can be taken sufficiently close to the collapsing cycle  $\partial\sigma_1$ , so we assume its  $\theta_2$  variation is small enough with respect to the difference  $p_1$  between the coordinate of the red curve and the  $p_1$  coordinate of the blue curve. (Essentially, we take them small with respect to the size of  $\mathcal{M}$ .)

The dimer model we are considering consists of two bi-gons and two tri-gons. We carefully analyze the  $(p_1, p_2)$ -coordinates we associate to these pieces, to ensure that get a symplectic pair of pants  $\mathcal{P}$  connecting the blue boundaries to the red one. The corresponding amoebas, together with the  $\theta_1$ - and  $\theta_2$ -level sets, are indicated in Figure 20 (Middle). There is a curve in the amoeba corresponding to the vertices of the bi-gon, that will be crucial in further analysis. This curve shall be named the *pink* curve, and in this case it is a horizontal segment.

Following analogous convention for the analysis of amoebas and coamoebas as in the proof of Proposition 4.14, with  $\rho_i$  corresponding to  $p_i$  and  $\phi_i$  to  $\theta_i$ , we take the first curve  $\xi^1$  corresponding to a

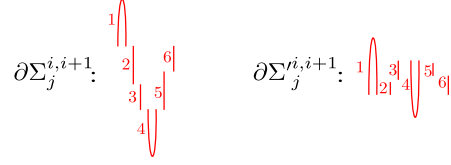


Figure 19: The profile of the  $p_2$  coordinate as we move along  $\partial\Sigma_j^{i,i+1}$ ,  $\partial\Sigma_j^{i,i+1}$ . The numbering corresponding to the ones on the leftmost picture of Figure 18.

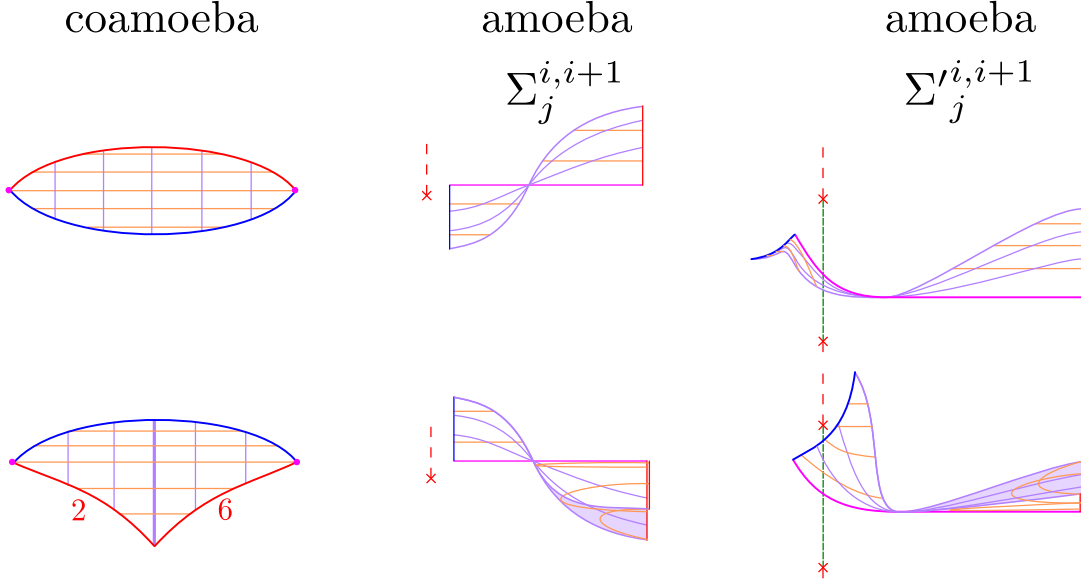


Figure 20: Amoebas of the pieces of the pair of pants  $\mathcal{P}$  and  $\mathcal{P}'$  for the surfaces  $\Sigma_j^{i,i+1}$ ,  $\Sigma_j^{i,i+1}$ .

$\theta_2$ -level set, oriented with  $d\theta_1^1 > 0$  and the second curve  $\xi^2$  corresponding a  $\theta_1$ -level set, with the orientation such that the  $p_1$  coordinate is decreasing, i.e.,  $dp_1^2 < 0$ .

First, let us study the bi-gon pieces. We assume that the  $\theta_2$  variation is sufficiently small for the red curve as well, so if we fix the norm of  $dp^2$  as we travel, we then have  $d\theta_2^2$  is small enough away from the vertices. As indicated in Figure 20, we choose  $\xi^1$  so that  $dp_2^1 = 0$  and  $d\theta_2^1 = 0$ . As we move along  $\xi^1$  at the bottom of the bi-gon, the  $p_1$  coordinate increases up to the middle of the horizontal curve at coamoeba and decreases from the middle until the end. The logic is reversed as we move to the top of the bi-gon. So,  $\omega(\partial\xi^1, \partial\xi^2) = -d\theta_1^1 dp_1^2 > 0$  (recall equation (4-2)), as desired. The limit case where  $\theta_2$  obtains the maximum and the minimum in the bi-gon can be analyzed by replacing the  $\xi^1$  curve by the respective red and blue curves. Since it also corresponds to maximum and minimum of the  $p_2$  coordinate, we still have  $dp_2^1 = 0$  and  $d\theta_2^1 = 0$ , ensures positivity of  $\omega(\partial\xi^1, \partial\xi^2)$ .

Second, we now turn our attention to the tri-gon, as depicted in Figure 20. We first notice that the  $p_2$  coordinates associated with the bottom vertex of the tri-gon, must be different for the edge labeled 2 and the edge labeled 6, the later being greater than the former, recall Figures 18 and 19. This implies that we must not only consider one curve with that corresponding  $\theta_2$ -coordinate constant, but rather a

family of curves. The shaded region in the bottom-middle picture of Figure 20 indicates the image of this curves under the  $(p_1, p_2)$ -projection. The analysis at the top of this part of the coamoeba is similar to before, with  $dp_2^1 = 0$  and  $d\theta_2^1 = 0$  and  $\omega(\partial\xi^1, \partial\xi^2) = -d\theta_1^1 dp_1^2 > 0$ . (Note that we do not remain stationary with  $d\theta_1^1 = 0$  at the top part of the coamoeba.) At the bottom part, we do have  $dp_2^1 > 0$  as  $\xi^1$  travels from the 2 curve to the 6 curve and we also have  $d\theta_2^2 > 0$ , as we are traveling from the red curve to the blue curve along  $\xi^2$ , with  $dp_1^2 < 0$ . That way, since  $d\theta_1^1 \geq 0$ , we have

$$\omega(\partial\xi^1, \partial\xi^2) = -d\theta_1^1 dp_1^2 + d\theta_2^2 dp_2^1 > 0.$$

Gluing analogous models for the for the bottom part of the diagram in a consistent way provides our symplectic pair of pants.  $\square$

We now move towards the construction of the surface  $\Sigma_j^{i,i+1}$  that does not intersect the Lagrangian sphere  $S_i$ . Given our choice of coordinates, the Lagrangian sphere projects into a vertical segment in the  $(p_1, p_2)$  factor. In order to keep working with the same coordinates in the region we want to do the modification of our curve: we modify the ATBD, without changing our ATF, simply by reversing the direction of the cuts associated with the nodes  $n_{i+1}, \dots, n_n$  (this operation was named *transferring the cut* in [54]). Note that we already made this operation in Figures 17, 20. The rightmost diagrams of Figure 20 represents the projection of  $S_i$  by a dashed segment, which is different than the one we use to represent the cuts. Let us set  $(p_1, p_2) = (0, 0)$  the middle point of this dashed segment.

From Remark 4.9, we see that  $\sigma_j^i$  and  $\sigma_j^{i+1}$  both intersect  $S_i$  once, and with opposite signs. We consider disks  $\sigma_j^i$  and  $\sigma_j^{i+1}$ , obtained from  $\sigma_j^i$  and  $\sigma_j^{i+1}$  by carving out a neighborhood of the intersection point with  $S_i$ , with their  $(p_1, p_2)$  projection as illustrated in Figure 17 (Right). We keep coloring their boundary blue, and their coamoeba projection is similar to the ones we just analyzed, as it is sufficiently close to the corresponding collapsing cycle with constant  $\theta_2$ -coordinate. Thus, we can also build a dimer model as in Figure 18 (Left), to build a pair of pants  $\mathcal{P}'$ , and we also color the other boundary of  $\mathcal{P}'$  red.

Recall that we named a pink curve, and the  $(p_1, p_2)$  image of the vertices corresponding to the intersection of the blue and red curves in the coamoeba coordinates  $(\theta_1, \theta_2)$ , which we will refer to as pink vertices. It will play the following role in our construction. As before, we focus on the top part of the coamoeba, the bottom part being symmetric under the reflection around the  $p_2 = 0$  coordinate (or at least having a symmetric behaviour, since our coamoeba picture is not symmetric.) Then the pink curve corresponding to the top bi-gon will be the graph of a non-increasing convex function  $p_2(p_1)$ , starting at a point with  $p_1 < 0$ ,  $p_2 > 0$ , becoming negative before  $p_1$  becomes 0, and eventually becoming constant at some point where  $p_1 > 0$ . Hence the pink curve for the bottom bi-gon will intersect this at some point with negative  $p_1$  coordinate. We call  $x$  the endpoint in the  $p_2$ -constant segment, with smallest  $p_1$ -coordinate. For that to happen, the  $p_2$ -coordinate of the red curve needs to move different as we move along the different parts of the coamoeba, as indicated in Figure 19. So it maintains the property that the  $p_2$ -coordinate at the common point of the segments labeled 2 and 3 is smaller than the one corresponding to the 5 and 6 segments. We also need to ensure the following. Consider the point of intersection between the  $(p_1, p_2)$  projection of the top blue curve and the projection of  $S_i$ . Look at the  $\theta_2$ -coordinate of the circle of  $S_i$  over this point, and consider its intersections  $q_1, q_2$  with the blue curve. We draw the coamoeba profile of the red curve so that  $q_1, q_2$  are precisely the pink vertices, as illustrated in Figure 18 (Center). We make analogous choices for drawing the red curves at the bottom of the coamoeba.

We are now in shape to prove the following lemma.

**Lemma 4.19** *There is a symplectic disk  $\Sigma_j^{i,i+1}$  in the cut neighborhood  $\mathcal{M}$ , disjoint from the Lagrangian 2-sphere  $S_i$ , containing the  $\sigma_j^i$  and  $\sigma_j^{i+1}$  symplectic 2-disks as a subset, with boundary in a thickened torus  $\mathbb{T}$ , whose homology class is twice the collapsing class of the nodes via the identification  $H_1(\mathbb{T}; \mathbb{Z}) \cong H_1(T^2; \mathbb{Z})$ .*

*Denote by  $\mathcal{P}'$  the pair of pants which is the closure of  $\Sigma_j^{i,i+1} \setminus (\sigma_j^i \cup \sigma_j^{i+1})$ .*

**Proof** As in the previous proof, we will draw in the  $(p_1, p_2)$ -coordinates the level sets of the  $\theta_2$  and  $\theta_1$  coordinates, naming the former  $\xi^1$  and the later  $\xi^2$ . Let us start looking at the bi-gon, and describe the projection of the  $\xi^1$  curve in the amoeba. Each curve starting close to the  $\theta_2$  minimum, up to a certain height  $b$  (to be specified), will have a horizontal projection, with the maximum of the  $p_1$  coordinate corresponding to the half of the  $\theta_1$  coordinate of  $\xi^1$ . This last property remains the same, even when we start at a height greater than  $b$ , but then, the image becomes a graph of a non-increasing function  $p_2(p_1)$ , eventually limiting to the part of the pink curve that stops at  $x$ , as illustrated in the top-right picture of Figure 20. We assume that the derivative is smaller in norm to the derivative of the graph giving the pink curve. For the top part of the coamoeba, the  $\xi^1$  curves have constant  $p_2$  coordinates, with the minimum of the  $p_1$  coordinate happening at the middle of the  $\theta_1$  coordinate. The amoeba projection of the  $\xi^2$  curves are also indicated in top-right picture of Figure 20. In particular, analyzing the symplectic condition for the top of the coamoeba part, is essentially done as in the proof of Lemma 4.18, compare top-middle and top-right pictures of Figure 20.

To ensure the symplectic condition at the bottom of the coamoeba, we need to carefully choose the point  $b$ , recalling that we can choose the red curve so that the  $\theta_2$  variation is small enough compared with the  $\theta_1$  variation. Away from the points in  $\xi^1$  with maximum  $p_1$  coordinate, let us move in the  $\xi^i$  curves with the normalised condition of  $|dp_1^i| = 1$ . The variation  $d\theta_2^2$  then will be bounded by an extremely small constant (w.r.t. the  $\theta_1$  diameter the coamoeba). We take a constant  $b$ , high enough to ensure that  $\omega(\partial\xi^1, \partial\xi^2) = d\theta_1^1 - dp_2^1 d\theta_2^2 > 0$ , recalling that we forced  $dp_2^1$  to be zero for points at  $\theta_2$  heights smaller than  $b$  and  $|dp_2^1|$  is bounded by the maximum slope of the pink curve. In the points in  $\xi^1$  with maximum  $p_1$  coordinate, we simply have  $dp_2^1 = 0$  and  $\omega(\partial\xi^1, \partial\xi^2) = -d\theta_1^1 dp_1^2 > 0$ . We let the reader check the positivity for the limiting points at the pink curve.

Let us now move to the tri-gon part of the coamoeba. For the top part we choose a height  $c$  in the coamoeba, playing a similar role as  $b$  in the above paragraph. If the  $\theta_2$  coordinate of  $\xi^1$  is bigger than  $c$ , we take the amoeba part to have constant  $p_2$  coordinate. So if the  $\theta_2$  coordinate is not smaller than  $c$ , we have  $dp_2^1 = 0$  and  $\omega(\partial\xi^1, \partial\xi^2) = -d\theta_1^1 dp_1^2 > 0$ . The analysis regarding the symplectic condition is done as in the last paragraph for the part corresponding to the  $\theta_2$  coordinate smaller than  $c$ . For the bottom part, recall that the  $p_2$  coordinate corresponding to the part 2 of the coamoeba of the red curve is smaller than the one corresponding to the part 6. So we can take  $dp_2^1 > 0$ . The analysis now is similar to the analogous part in the proof of Lemma 4.18. We have  $d\theta_1^1 \geq 0$  (being zero at the middle of the  $\xi^1$  curves whose  $\theta_2$  coordinate is not bigger than the pink vertices),  $dp_2^1 > 0$ ,  $d\theta_2^1 = 0$ ,  $dp_1^2 < 0$ ,  $d\theta_1^2 = 0$ ,  $d\theta_2^2 > 0$ , since we move on  $\xi^2$  from the red curve to the blue curve.

The fact that we chose the pink curve to cross  $p_1 = 0$  with negative  $p_2$  coordinate promptly ensures that the coamoeba region of  $S_i$  corresponding to the segment given by the intersection of  $p_1 = 0$  with amoeba of the bi-gon, does not intersect the bi-gon itself. For the tri-gon part, looking at the amoeba projection, we see that  $S_i$  does not intersect the region of the surface corresponding to the bottom of the tri-gon. The fact that we chose the coamoeba of our red curve so that the pink vertices coincide with the points  $q_1, q_2$ , ensures that the part of the surface whose coamoeba correspond to top of the tri-gon does not intersect the Lagrangian  $S_i$  as well, as required.

□

**Remark 4.20** There is a smooth way to isotope the boundary of  $\mathcal{P}$  to the boundary of  $\mathcal{P}'$ , and following that, a smooth way to isotope the amoebas of  $\Sigma_j^{i,i+1}$  to the ones of  $\Sigma_j^{i,i+1}$ , see again Figure 20, as well as the small differences on the coamoebas. Hence, we can isotope from  $\Sigma_j^{i,i+1}$  to  $\Sigma_j^{i,i+1}$ , with their boundaries restricted to a thickened torus  $\mathbb{T} = I \times T^2$ . □

Now we see that the symplectic surface  $\Sigma_j^{i,i+1}$  intersects the Lagrangian 2-sphere  $S_{i+1}$  once in a point belonging to  $\sigma_j^{i+1}$ . In an analogous fashion to Lemma 4.19, we can chop out of  $\Sigma_j^{i,i+1}$  the intersection point with  $S_{i+1}$  and then glue its boundary, the boundary of  $\sigma_j^{i+2}$  (where we remove the intersection of  $\sigma_j^{i+2}$  with  $S_{i+1}$ ), and the boundary of a new chosen “red curve” in a thickened torus that has three times the homology of the collapsing cycle in this thickened torus, with a new pair of pants. Naming the former two curves blue, the first step would be to construct a dimer model between the blue curves and the red curve, so that the behaviour on the region that it could intersect  $S_{i+1}$  is the same as the one analyzed in Lemma 4.19. Denote this surface by  $\Sigma_j^{i,i+2}$ . We can iterate this process and consider symplectic surfaces  $\Sigma_j^{i,i+k}$  in the cut neighborhood  $\mathcal{M}$ , that do not intersect  $S_i, \dots, S_{i+k-1}$ , and has boundary on a thickened torus, whose homology class is  $k+1$  times the collapsing cycle. This process leads to the following:

**Lemma 4.21** *There exists a symplectic disk  $\Sigma_j^{1,n}$  inside  $\mathcal{M}$ , not intersecting the Lagrangian set  $\bigcup_{i=1}^{n-1} S_i$ , and whose boundary lies on a thickened torus  $I \times T^2$ , with boundary class being  $n$  times the class of the collapsing cycle.*

**Proof** We build this surface iteratively as indicated above, starting with  $\Sigma_j^{1,2}$ . The algorithm to build the red curve and the corresponding dimer model is illustrated for going from  $\Sigma_j^{1,3} \cup \sigma_j^4$  to  $\Sigma_j^{1,4}$  in the third diagram of Figure 18. We chose the red curve to cross in consecutive chambers of the complement of the curves given by the coamoeba projection of the blue curves, which we recall is the boundary of the disconnected surface obtained by chopping out the intersections of  $\Sigma_j^{1,i} \cup \sigma_j^{i+1}$  with  $S_i$ . We do it so that the top part of the dimer, corresponding to one bi-gon and two tri-gons have the same configuration as in Lemma 4.19, including the points analogous to  $q_1, q_2$ . Recalling Remark 4.20, we can think that we first glue a pair of pants  $\mathcal{P}$  as before for the boundaries of  $\Sigma_j^{1,i} \cup \sigma_j^{i+1}$  and then isotope to our desired surface  $\Sigma_j^{1,i+1}$ , with the modifications happening in the same framework as in the proof of Lemma 4.19. □

Now we should inductively build the surfaces  $\Sigma_j^{1,n}$ , for  $j$  going from 1 to  $k$ , making sure these surfaces do not intersect. Recall that the boundaries of  $\sigma_j$  and  $\sigma_{j+1}$  are linked in the thickened 3-dimensional neighborhood. We can achieve non-intersection by adjusting the crossings of blue and red curves between different amoebas, and the  $p_2$  coordinate. Thus we can ensure the required non-intersection just by looking at the  $(\theta_1, \theta_2, p_2)$  projection of the surfaces. The case  $n = 2$  is illustrated in Figure 18 (d). We can then get the other  $d$  disks, carrying the collapsing cycle from the respective nodes to boundary of the same thickened torus. They project to curves inside the amoeba of the  $\Sigma_j^{1,n}$  disks, see Figure 21. After doing that, still within the cut neighborhood  $\mathcal{M}$ , we can connect the boundaries of the  $\Sigma_j^{1,n}$  surfaces,  $j = 1, \dots, k$  and of the  $d$  disks into  $m = kn + d$  straight cycles and redistribute these cycles over curves connecting to our symplectic-tropical curve  $\mathcal{C}(\Gamma)$ , as we did in the Section 4.3.3.



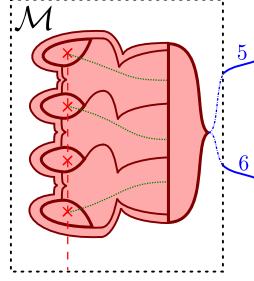


Figure 21: Final amoeba for the symplectic disk in the case of a symplectic-tropical curve arriving at  $n = 4$  nodes with multiplicity  $m = 5 + 6 = 11$ , so  $k = 2$  and  $d = 3$ . For visual purposes, we illustrate the amoeba of  $k = 2$  surfaces as if one envelopes the other, when in fact both have the same amoebas.

Figure 21 illustrates the amoeba image of this local model of a deformed symplectic-tropical curve, when  $n = 4$ ,  $m = 11$ , so  $k = 2$  and  $d = 3$ . This finishes the proof of Proposition 4.17.  $\square$

We can glue all these local models now, as we did in Section 4.3.3, to get deformed symplectic-tropical curves, intersecting Lagrangian spheres only at prescribed nodes, with the number determined by the total multiplicity and the number of nodes at a given cut.

#### 4.5 Required Symplectic-Tropical Curves in the $\mathfrak{N}$ for Theorem 1.3

Consider the triangular-shaped ATFs of  $\mathbb{CP}^2$ ,  $\mathbb{CP}^1 \times \mathbb{CP}^1$ ,  $Bl_3(\mathbb{CP}^2)$  and  $Bl_4(\mathbb{CP}^2)$ , [55] with one smooth corner, i.e., satisfying a Markov type equation of the form

$$(4-8) \quad 1 + n_2 q^2 + n_3 r^2 = Gqr.$$

Let  $\mathfrak{N}$  be a neighborhood of the edge opposite the frozen smooth vertex, introduced in Section 4.4.1. The results of the previous subsections yield the following

**Theorem 4.22** *Each homology class of the symplectic divisors highlighted in Figure 1 can be realized as a symplectic-tropical curve in  $\mathfrak{N}$ .*

**Proof** First note that for the equations associated with  $\mathbb{CP}^2$ ,  $\mathbb{CP}^1 \times \mathbb{CP}^1$ ,  $Bl_3(\mathbb{CP}^2)$  and  $Bl_4(\mathbb{CP}^2)$ , the quantity  $G/n_2 n_3$  is respectively, 3, 2, 1, 1, which is the intersection number of the symplectic divisors in the corresponding spaces with the anti-canonical divisor. Thus, Theorem 4.7 and Section 4.4.1 suffice for the case of  $\mathbb{CP}^2$ . For the remaining cases, one needs to ensure the correct intersection with the Lagrangian spheres. This can be achieved case by case using that

$$1 + n_2 q^2 \equiv 0 \pmod{n_3}, \quad 1 + n_3 r^2 \equiv 0 \pmod{n_2}.$$

For instance, in the case of  $Bl_4(\mathbb{CP}^2)$ , we get  $q^2 \equiv -1 \pmod{5}$ , so  $q \equiv 2$ , or  $3 \pmod{5}$ . Take the divisor of Figure 1 that intersects two Lagrangian spheres. Following the mutations in [55, Figure 17], at the triangular-shape ATBD [55, Figure 17 ( $A_4$ )], these spheres become the top and bottom spheres, of the 4-chain of Lagrangian spheres. If  $q \equiv 2 \pmod{5}$ , apply Proposition 4.17 taking the 2 intersections to the top and bottom node. If  $q \equiv 3 \pmod{5}$ , we arrive at the three interior nodes instead, having the same intersection number with the Lagrangian spheres. One can check that the sign is correct by looking at the first instance when  $q = 2$  and observe that the mutations  $q \rightarrow 5r - q$  switch between  $q \equiv 2 \pmod{5}$  and  $q \equiv 3 \pmod{5}$  (the first case  $q = 2$  is depicted as  $A_1$  in Figure 23).  $\square$

## 4.6 Further Deformations of Symplectic Tropical Curves

In this subsection we introduce a series of additional techniques regarding symplectic-tropical curves, that will allow us to visualize chains of them inside an ATF. When we say a chain of symplectic curves, we imply that the total intersection between them is equal to the geometric intersection. Thus, it is not enough to simply construct, for each curve in the chain a STC, as we did in the previous sections, as we want to *geometrically* realize the homological intersection. We start with a simple observation:

**Remark 4.23** First, for  $i = 1, 2$ , let  $\mathcal{C}_i$  denote two STCs as in Definition 4.6. Let  $C_i$  denote a STC in  $X$  represented by  $\mathcal{C}_i$  as in Theorem 4.7, and let  $\gamma_i$  be an edge of  $\mathcal{C}_i$ . If  $\gamma_1$  and  $\gamma_2$  homology class of the torus, any intersection between  $\mathcal{C}_1(\gamma_1)$  and  $\mathcal{C}_2(\gamma_2)$ , can be taken to be empty as an intersection of the symplectic surface  $C_1$  and  $C_2$ , since we can just assume we carry disjoint cycles in the same homology class.  $\square$

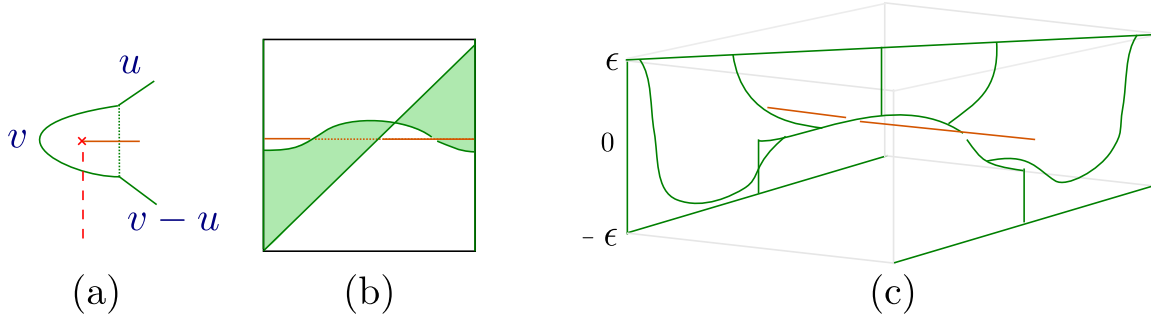


Figure 22: (a) The amoeba of a STC given by a  $\sigma_j$  disk (from Proposition 4.10), glued along the boundary with two cycles intersecting once  $\partial\sigma_j$ ; (b) The coamoeba of the gluing surface; (c) A depiction of how the surface looks like inside a thickened torus.

We will also need the following:

**Proposition 4.24** Consider a thickened torus  $\mathbb{T} = [-\epsilon, \epsilon] \times T^2$ , as the pre-image of a segment in the regular part of a base of an ATF. Let  $\alpha$  be a straight cycle in  $\{0\} \times T^2$  represented by  $v \in H_1(\mathbb{T}; \mathbb{Z}) \cong H_1(T^2; \mathbb{Z}) \cong \mathbb{Z}^2$ ,  $\beta$  be a cycle in the class  $v$  that wraps around once  $\alpha$ , and  $\gamma_{\pm}$  be a straight cycle in  $\{\pm\epsilon\} \times T^2$ , represented by  $u_{\pm}$ , with  $\det u \wedge v = \pm 1$ , and  $u_- = u_+ - v$ .

Then there exists a symplectic pair of pants in the complement in  $\mathbb{T} \setminus \alpha$ , with boundary  $\gamma_- \cup \beta \cup \gamma_+$ .

**Proof** Use the dimer model represented in Figure 22 (b) to build a symplectic surface as in Section 4.3.2, making sure that the 0 level set of the height function ( $\rho_2$  in Proposition 4.14) is disjoint from the straight cycle  $\alpha$ . The end result is depicted in Figure 22 (c).  $\square$

**Remark 4.25** Applying this result for  $\partial\sigma_j$ , the boundary of a disk  $\sigma_j$  as in Proposition 4.10, we see that we can pass with all  $\sigma_l$ , with  $l < j$  (the ones with boundary closer to  $\alpha = \partial\sigma_1$ ) through the middle of the surface constructed in Proposition 4.24. The amoeba of this process is depicted in Figure 22 (a).

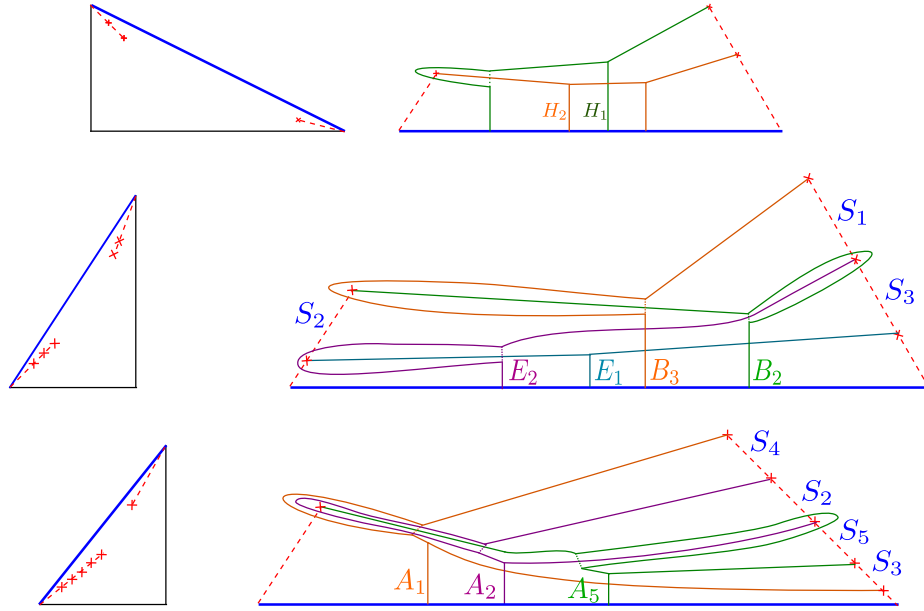


Figure 23: STCs in classes  $H_1$ ,  $H_2$  in a specific ATBD of  $\mathbb{CP}^1 \times \mathbb{CP}^1$ , in the exceptional classes  $E_1$ ,  $E_2$ ,  $B_2 = H - E_1 - E_3$  and  $B_3 = H - E_1 - E_2$  in an ATBD of  $Bl_3(\mathbb{CP}^2)$ , and in the exceptional classes  $A_1 = H - E_1 - E_4$ ,  $A_2 = E_4$ , and  $A_5 = E_1$  in an ATBD of  $Bl_4(\mathbb{CP}^2)$ .

In Figure 23, we apply the above Remark 4.25 to visualise STCs in the neighborhood  $\mathfrak{N}$  of highlighted edge of the ATF of  $\mathbb{CP}^1 \times \mathbb{CP}^1$  depicted in the top corner of Figure 1. They are representative of the classes  $H_1 = [\mathbb{CP}^1 \times \{\text{point}\}]$  and  $H_2 = [\{\text{point}\} \times \mathbb{CP}^1]$ . Remarks 4.25, 4.23, are used to visualize a 4-chain of STCs in the neighborhood  $\mathfrak{N}$  of highlighted edge of the ATF of  $Bl_3(\mathbb{CP}^2)$  of triangular shape depicted in Figure 1. The homology classes for the spheres in this 4-chain are the ones corresponding to the highlighted edges of the toric diagram for  $Bl_3(\mathbb{CP}^2)$  in Figure 1. Figure 23 also shows a 3-chain of symplectic spheres in the ATBD of  $Bl_4(\mathbb{CP}^2)$  of [55, Diagram (A<sub>4</sub>)]. Their classes corresponds to the highlighted 3-chain in the first diagram of  $Bl_4(\mathbb{CP}^2)$  in Figure 1.

Now, we can iteratively apply Remark 4.25 in the neighborhood of one or more nodes. We are going to use simplified pictures, for visual purposes. For instance, Figure 24 (a) shows a simplified depiction of two nonintersecting STCs near two nodes of a cut in an ATF, with associated vector  $v$ . Surrounding each node, we see a  $\sigma_j$  type curve, where we applied Remark 4.25  $a$  times around each node and then unite their amoebas using Remark 4.23. Figure 24 (b) shows an alternative version, where we took  $2b$  curves around a unique node in associated with the vector  $w$ , and applied Remarks 4.25, 4.23 to get two disjoint symplectic curves.

Let us now shift our focus to what happens as we approach the local model nearby a trivalent vertex of an STC, with two (or more) sets of curves satisfying the balancing condition (4-1). The first observation is that if you arrive with two sets of cycles with total homology represented by  $v \in \mathbb{R}^2$  and want to glue them to sets of cycles with homology  $w$  and  $-w - v$ , using two non-intersecting surfaces, the price you pay is that the cycles corresponding to  $w$  and  $-w - v$  in the boundary of the second surface, must link

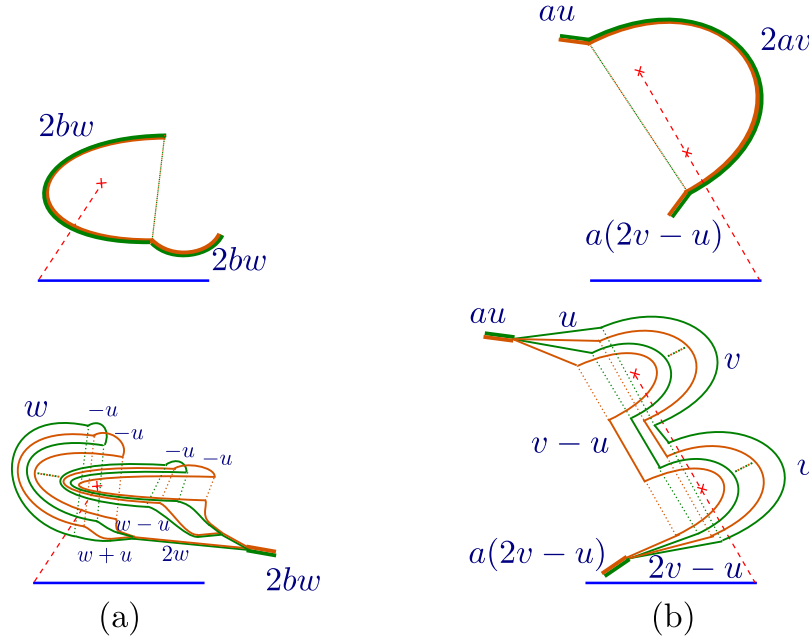


Figure 24: Simplified pictures for the STC discussed above.

the corresponding boundaries on the first surface a total amount<sup>4</sup> of  $\mathbf{w} \wedge \mathbf{v}$ . We define precisely what we mean by cycles linking within the regular part of a Lagrangian torus fibration:

**Definition 4.26** Let  $\mathbb{D}$  be a 2-disk, fix a point  $o \in \mathbb{D}$  and take two disjoint 1-cycles  $\alpha, \sigma$  in  $\mathbb{D} \times T^2$  away from  $\{o\} \times T^2$ . We view  $\sigma$  as a cycle in  $H_1(\mathbb{D} \times T^2 \setminus \alpha; \mathbb{Z}) \cong H_1(T^2; \mathbb{Z}) \oplus \mathbb{Z}$ , where the first summand corresponds to  $\{o\} \times T^2 \hookrightarrow \mathbb{D} \times T^2 \setminus \alpha$ .

By definition, the *linking* between  $\sigma$  and  $\alpha$  is the projection of the class  $[\sigma] \in H_1(\mathbb{D} \times T^2 \setminus \alpha; \mathbb{Z})$  onto the (rightmost)  $\mathbb{Z}$ -factor. The sign involves a choice of generator for the  $\mathbb{Z}$  cycle, that we assume the same, when dealing with more than one 1-cycle relative to  $\alpha$ .  $\square$

Let us summarize the above discussion into the following statement:

**Proposition 4.27** Consider the local model for a symplectic surface near the interior vertex constructed in Proposition 4.14, associated to the balancing condition  $m_1 \mathbf{w}_1 + m_2 \mathbf{w}_2 + m_3 \mathbf{w}_3 = 0$ . Consider the number  $d = m_1 m_2 |\mathbf{w}_1 \wedge \mathbf{w}_2|$  and  $d = \delta_1 + \delta_2$ , a two partition  $\delta_1, \delta_2 \in \mathbb{Z}_{\geq 0}$ .

Then there exists another disjoint symplectic surface in the same local neighborhood such that the boundaries satisfies the following two conditions:

- The  $m_3$  boundaries associated to  $\mathbf{w}_3$  are parallel copies of the corresponding boundaries of the original curve inside the same torus fibre;
- The boundaries associated to  $\mathbf{w}_1$  and  $\mathbf{w}_2$  link the corresponding boundaries of the original curve, in the sense of Definition 4.26,  $\delta_1$  and  $\delta_2$  times, respectively.

<sup>4</sup>For us  $\mathbf{w} \wedge \mathbf{v}$  denotes the determinant of the two vectors in  $\mathbb{R}^2$ .

**Proof** We start with the dimer model for the original surface constructed in Proposition 4.14. Recall that we used  $(\rho_1, \rho_2)$  coordinates for the amoeba description, with  $\rho_2 \in [-\epsilon, \epsilon]$ . We will construct another dimer model for our second surface, and build the amoeba as in Sections 4.3.2, 4.3.3, 4.4.2.

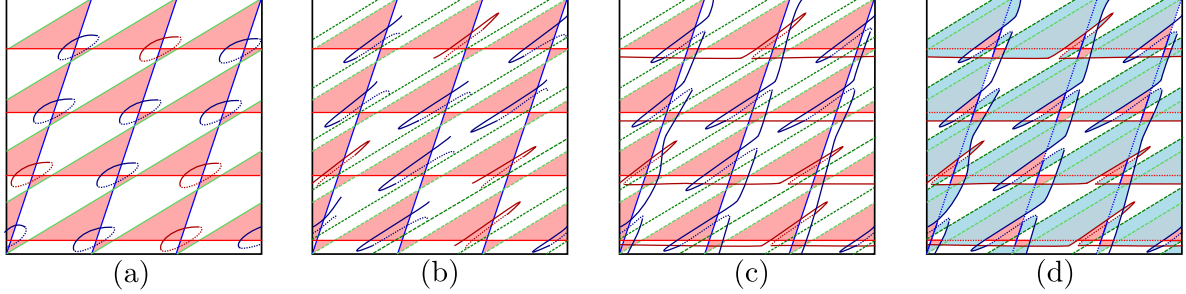


Figure 25: Near an interior vertex of determinant  $d$ , there are disjoint symplectic curves with the total linking of their boundaries equal to  $d$ . This series of diagrams illustrate the algorithm to get the disjoint surfaces.

In the intersection of these two dimer models we will record the  $\rho_2$ -coordinate of the new curve in the dimer model, to be less than  $-\epsilon$  or greater than  $\epsilon$ . This will be indicated in the same diagram, as follows. If coamoeba regions of the two surfaces intersect, the boundary of the lower region will be denoted by a dotted segment in the intersection. Figure 25 (d) illustrates two non-intersecting surfaces via their coamoeba projection. By the work developed in Sections 4.3.2, 4.3.3, 4.4.2, the construction of such dimer model, with the additional  $\rho_2$  information, will be enough to ensure that we obtain two disjoint symplectic surfaces.

As before we take  $w_1 = (1, 0)$ , and we use the following algorithm to construct the dimer model, which concludes Proposition 4.27.

*Algorithm for the Dimer Model:*

- Step 1 Color the  $w_1$  cycles red,  $w_2$  cycles blue,  $w_3$  cycles green.
- Step 2 For each of the  $|d| = m_1 m_2 |w_1 \wedge w_2|$  intersections between the red and blue cycles of the original curve, draw cycles linking both blue and red cycles, as illustrated in Figure 25 (a), in the same pattern. Color  $\delta_1$  of them red and the other  $\delta_2$  of them blue.
- Step 3 Consider a new green cycle, parallel to the original green, constructed as a positive shift in, say, the  $\phi_2$  coordinate of the amoeba (the  $\phi_i$ -coordinates being the coamoeba coordinates as in the notation of Proposition 4.14).
- Step 4 Replace the red/blue links of Step 2, by chains of the same color, “linking” the corresponding original curve, with one end on the new green cycle and crossing the original blue and red cycle twice, to the left of the new green cycle. The first crossing is above and the second below the original dimer, with respect to the  $\rho_2$  coordinate, as illustrated in Figure 25 (b).
- Step 5 For each red/blue linking chain, we connect its “tail” with the “head” of the adjacent chain of the same color, using a red/blue 1-chain parallel to the original chain of the same color, forming the new red/blue cycles as illustrated in Figure 25 (c).
- Step 6 Paint the regions that were created by the new green, red and blue cycles, passing below or above the original dimer accordingly, as illustrated in Figure 25 (d).

□

**Remark 4.28** We could allow linkings for the  $w_3$  cycles, provided the total linking is still  $d$ . This is not needed for our purposes, and it would make the construction algorithm more intricate. □

**Remark 4.29** After getting the two surfaces of Proposition 4.27, one can actually run an analogous algorithm to get yet a third, fourth and  $n$ -th surfaces, disjoint from the previous ones, with boundary so that the green cycle is parallel to the previous green cycles, and the red/blue cycles links each red/blue cycles of the previous surfaces  $\delta_1/\delta_2$  times. For that, one just needs to replicate the intersection pattern of the  $n$ -th red/blue curve, with the previous  $(n - 1)$  ones. □

Now assume that we arrive at the surface near the interior node, constructed in Proposition 4.14, with  $m_3$  straight (green)  $w_3$  cycles, parallel to the original one, and  $m_1$  (red)  $w_1$  cycle, linking the original curve  $c$  times. We can adjust the new red curves, so that the curves arrive linking the dimer model over one red/blue vertex as in Figure 26 (a).

**Proposition 4.30** Considering the above setup and  $d \in \mathbb{N}$  as in Proposition 4.27. Then there exists a symplectic surface connecting the  $m_3$   $w_3$ -cycles (green) and  $m_1$   $w_1$ -cycles (red), with  $m_2$   $w_2$ -cycles (blue), linking the original  $w_2$ -cycles  $(c + d)$  times.

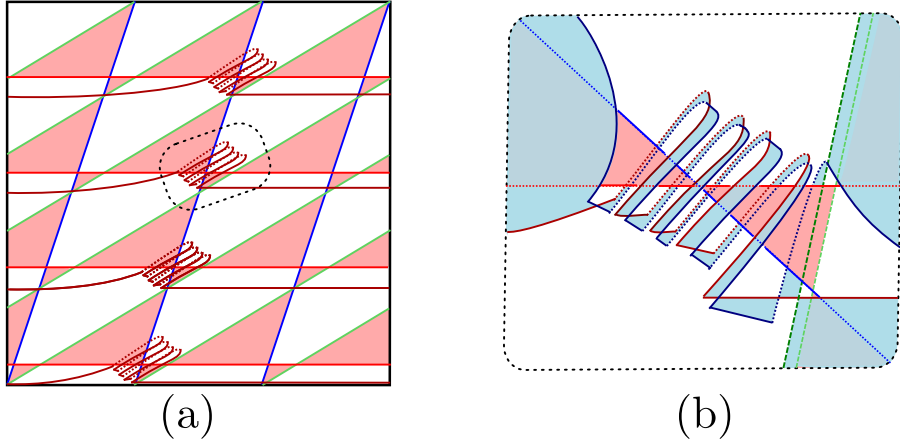


Figure 26: How linking can change for non-intersecting symplectic surfaces near the interior vertex of a STC. Picture (b) is a zoomed version around the node with red links. The blue curve is a bit rotated for visual purposes.

**Proof** At each vertex having the linking of the red curves, we construct a local model as illustrated by Figure 26 (a) and (b). We note that the new blue chain links the original blue at the red linking number plus 1. In Figure 26, the red cycles are linking 4 times and the new blue cycle links 5 times the original blue cycle. (A generalization of the picture is clear.) Now we add blue links to the remaining intersections of the originals blue and red curves, as in Step 2 of the algorithm of Proposition 4.27. Then we can run Step 5, Step 6 of the above algorithm in an analogous fashion, noting that the local model of Figure 26 (b) is well adapted for that. □

**Remark 4.31** As in Remark 4.29, if we assume that we arrive with another set of  $m_1$  red cycles linking the previous ones  $c$  times, and a set of  $m_3$  parallel green cycles, we can – after an initial adjustment, concentrating the several red links in one node as before – locally construct the new blue link, linking both previous blue link equal to the local red linking number plus one. Close to the boundary of the local region, the third local surface will lay above the previous two. This can also be iterated  $n$  times, so that the local behaviour glues well with the  $n$ -th iteration of the algorithm, described in Remark 4.29.  $\square$

## 4.7 Getting chains of symplectic-tropical curves

Let us apply the results of Section 4.6 to construct the required chains of symplectic tropical curves used in Theorem 3. There are three cases, corresponding to  $\mathbb{CP}^1 \times \mathbb{CP}^1$ ,  $Bl_3(\mathbb{CP}^2)$  and  $Bl_4(\mathbb{CP}^2)$ , which we now analyze.

### 4.7.1 The case of $\mathbb{CP}^1 \times \mathbb{CP}^1$ .

Consider the triangular-shaped ATF of the symplectic monotone  $\mathbb{CP}^1 \times \mathbb{CP}^1$ , with a smooth corner, associated to a solution of the Diophantine equation

$$1 + q^2 + 2r^2 = 4qr.$$

Let  $\mathfrak{N}$  be a neighborhood of the edge opposite the smooth corner – where the frozen vertex is located – and consider its associated cuts, as in Section 4.4.1.

**Proposition 4.32** There is a 2-chain of symplectic-tropical curves inside the edge neighborhood  $\mathfrak{N}$ , such that the associated symplectic curves belong to the classes  $H_1$  and  $H_2$ , and have total intersection number one, i.e., equal to their topological intersection.

**Proof** For that, we need to revisit the specific combinatorics in this situation. In this case, the associated Markov type equation of interest is  $1 + q^2 + 2r^2 = 4qr$ . From Equation (4–5), we see that the determinant between the associated vectors  $v = (-r, m)$  and  $w = (q, -l)$  is  $v \wedge w = 2$ . It follows from the corresponding Vieta jumping (Proposition 3.9) that  $q = 2a + 1$  and  $r = 2b + 1$  are odd. Hence, we can rewrite the balancing condition as:

$$(4-9) \quad qv + rw + 2(0, 1) = v + w + 2u = 0$$

where  $u = av + bw + (0, 1)$ . We readily see that  $w \wedge u = u \wedge v = 1$ . In consequence, we are allowed to use the vectors  $\pm u$ , with each of the vectors  $v$  and  $w$  as in Proposition 4.24. Finally, we look at

$$u \wedge (0, 1) = -\frac{q-1}{2}r + \frac{r-1}{2}q = \frac{r-q}{2}.$$

Assume that  $q > r$ , so that  $u$  points to the left. Then we deduce that

$$2v - u \wedge (0, 1) = \frac{q-5r}{2} < 0,$$

because  $1 + 2r^2 = q(4r - q)$ , so  $q < 4r$ .

Now, Figure 27 is a depiction of the chain of symplectic spheres in  $\mathfrak{N}$  in classes  $H_1$  and  $H_2$ . The intersection is depicted by a star. The top picture records the homology classes of the cycles corresponding to each edge. The bottom picture records the linking between the two cycles obtained by applying



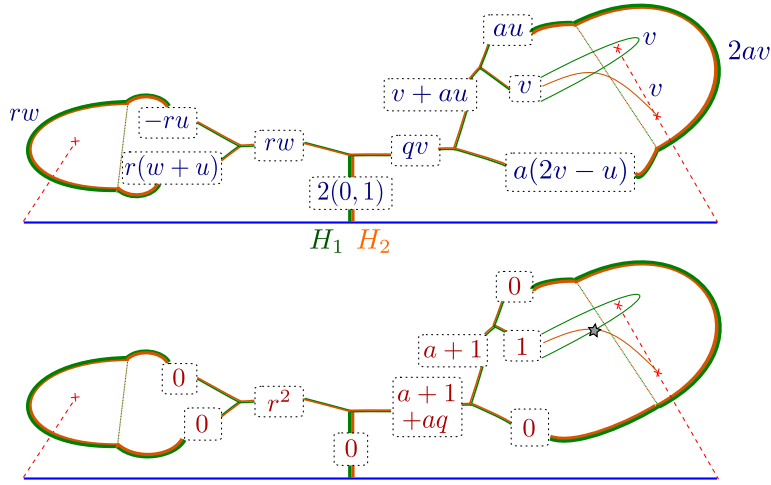


Figure 27: STCs in classes  $H_1, H_2$  in a neighborhood  $\mathfrak{N}$  of the edge opposite to the smooth corner in a arbitrary ATF of  $\mathbb{CP}^1 \times \mathbb{CP}^1$  associated with a solution of  $1 + q^2 + 2r^2 = 4qr$ .

Propositions 4.27 and 4.30. We note that we get the Markov equation as a compatibility equation for the interior vertex associated with the  $2(0, 1)$  cycles. Indeed, since  $qv \wedge rw = 2qr$ , we must have

$$2qr = r^2 + a + 1 + aq = \frac{2r^2 + q - 1 + 2 + (q - 1)q}{2} = \frac{2r^2 + q^2 + 1}{2}.$$

In the case  $r > q$ , we replace the vector  $u$  by  $-u$  in Figure 27, and note that  $u \wedge (0, 1) > 0$  and

$$2v + u \wedge (0, 1) = \frac{-q - 3r}{2} < 0.$$

The case  $r = q$  is depicted in Figure 23. □

**Remark 4.33** The construction obtained by the above picture in Figure 27 is equivalent to the construction of two (geometrically) disjoint copies of the  $H_1$  class, to which we can apply a Dehn twist with respect to the visible Lagrangian 2-sphere. □

#### 4.7.2 The case of $Bl_3(\mathbb{CP}^2)$ .

Let us now consider a triangular-shaped ATF for the symplectic 4-manifold  $Bl_3(\mathbb{CP}^2)$ , with a smooth corner, associated to a solution of the Diophantine equation

$$1 + 2q^2 + 3r^2 = 6qr,$$

$\mathfrak{N}$  a neighborhood of the edge opposite the smooth corner, and its associated cuts, as in Section 4.4.1. In the case, the required chain of symplectic surfaces reads:

**Proposition 4.34** There exists a 4-chain of symplectic-tropical curves inside the edge neighborhood  $\mathfrak{N}$  whose associated symplectic curves lie in the exceptional classes  $E_1, E_2, B_2 = H - E_1 - E_3$  and  $B_3 = H - E_1 - E_2$ , and intersection between two of them equals their geometric intersection.

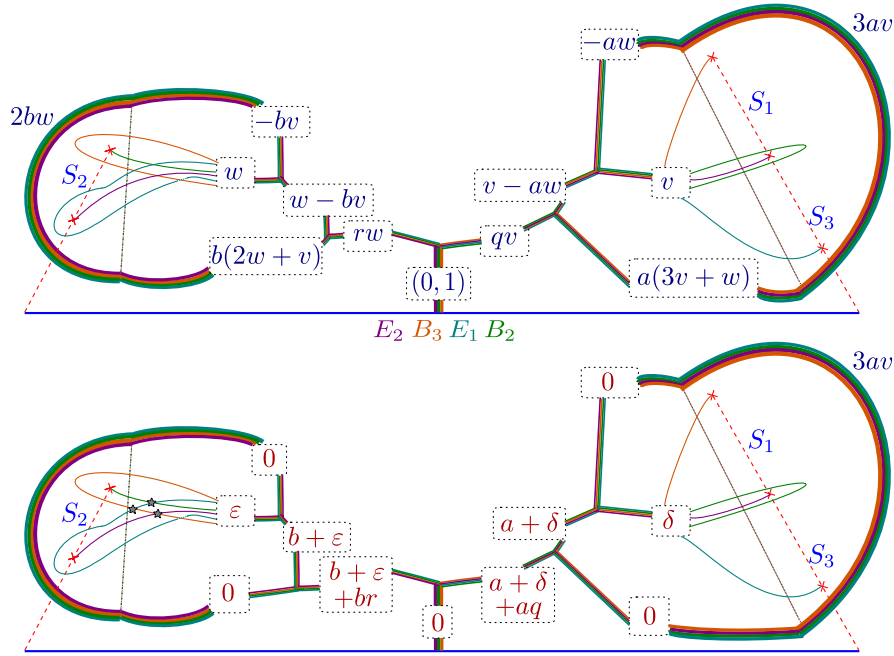


Figure 28: STCs in classes  $E_1$ ,  $E_2$ ,  $B_2$  and  $B_3$  in a neighborhood  $\mathfrak{N}$  of the edge opposite to the smooth corner in a arbitrary ATF of  $Bl_3(\mathbb{CP}^2)$  associated with a solution of  $1 + 2q^2 + 3r^2 = 6qr$ .

**Proof** From Equation (4–5), we deduce that the determinant between associated vectors  $v = (-r, m)$  and  $w = (q, -l)$  is  $v \wedge w = 1$ . From the corresponding Vieta jumping (Proposition 3.9), we obtain that  $q^2 \equiv -1 \pmod{3}$ , and thus  $q \equiv 1$  or  $2 \pmod{3}$ , and  $r \equiv 1 \pmod{2}$ .

Figure 28 illustrates the case  $q = 3a + 1$ ,  $r = 2b + 1$ . As before, the intersection is depicted by a star in the bottom picture, and occurs exactly as we change the linking number between cycles. The top picture records the homology classes of the cycles corresponding to each edge. The bottom picture records the linking between the two cycles by applying Propositions 4.27 and 4.30. In this case, the linking numbers  $\delta$  and  $\varepsilon$ , will depend on the curves we are taking into account. We have that  $\varepsilon, \delta \in \{0, 1\}$  and  $\delta + \varepsilon = 1$ . The compatibility condition becomes:

$$qr = b + \varepsilon + br + a + \delta + aq = \frac{3(r-1)(r+1) + 6 + 2(q-1)(q+1)}{6} = \frac{3r^2 + 2q^2 + 1}{6}$$

Figure 29 illustrates the second case  $q = 3a + 2$ ,  $r = 2b + 1$ . In this case, we have  $\varepsilon \in \{0, 1\}$ ,  $\delta \in \{1, 2\}$  and  $\delta + \varepsilon = 2$ , where the compatibility becomes:

$$qr = b + \varepsilon + br + 2a + \delta + aq = \frac{3(r-1)(r+1) + 12 + 2(q-2)(q+2)}{6} = \frac{3r^2 + 2q^2 + 1}{6},$$

as required. This concludes the construction for the case of  $Bl_3(\mathbb{CP}^2)$ .

□

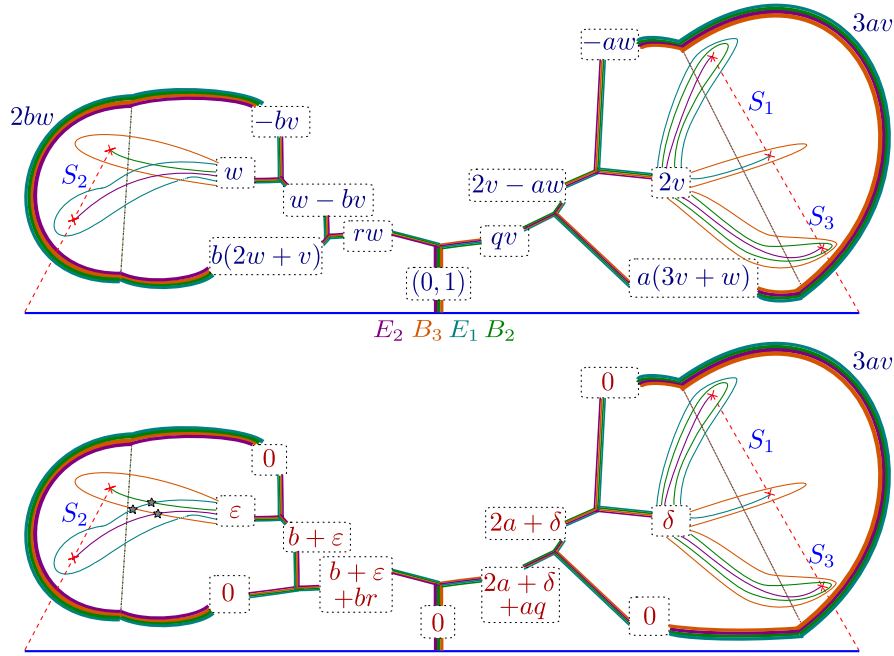


Figure 29: STCs in classes  $E_1$ ,  $E_2$ ,  $B_2$  and  $B_3$  in a neighborhood  $\mathfrak{N}$  of the edge opposite to the smooth corner in a arbitrary ATF of  $Bl_3(\mathbb{CP}^2)$  associated with a solution of  $1 + 2q^2 + 3r^2 = 6qr$ .

#### 4.7.3 The case of $Bl_4(\mathbb{CP}^2)$ .

Finally, we consider a triangular-shaped ATF for the symplectic surface  $Bl_4(\mathbb{CP}^2)$ , with a smooth corner, associated to a solution of the Diophantine equation

$$1 + q^2 + 5r^2 = 5qr,$$

$\mathfrak{N}$  a neighborhood of the edge opposite the smooth corner, together with the associated cuts, as in Section 4.4.1. The required chain of symplectic curves is obtained in the following

**Proposition 4.35** There exists a 3-chain of symplectic-tropical curves inside the edge neighborhood  $\mathfrak{N}$  whose associated symplectic curves belong to the exceptional classes  $A_1 = H - E_1 - E_4$ ,  $A_2 = E_4$ , and  $A_5 = E_1$ , and their pairwise intersections equal their geometric intersections.

**Proof** Let us revisit the specific combinatorics of the situation: the associated Markov type equation of interest is  $1 + q^2 + 5r^2 = 5qr$ , and from Equation (4–5), the determinant between the associated vectors  $v = (-r, m)$  and  $w = (q, -l)$  is  $v \wedge w = 1$ . As above, Proposition 3.9 shows that  $q^2 \equiv -1 \pmod{5}$ , and thus  $q \equiv 2$  or  $3 \pmod{5}$ . Figure 30 shows the case  $q = 2 + 5a$ .

As before, we have the compatibility associated with the  $(0, 1)$  cycles, using  $qv \wedge rw = qr$ , and giving the associated Diophantine equation:

$$qr = r^2 + 2a + 1 + aq = \frac{5r^2 + (q-2)(q+2) + 5}{5} = \frac{5r^2 + q^2 + 1}{5}.$$

For the second case, Figure 31 shows the case  $q = 3 + 5a$ , and the compatibility becomes:

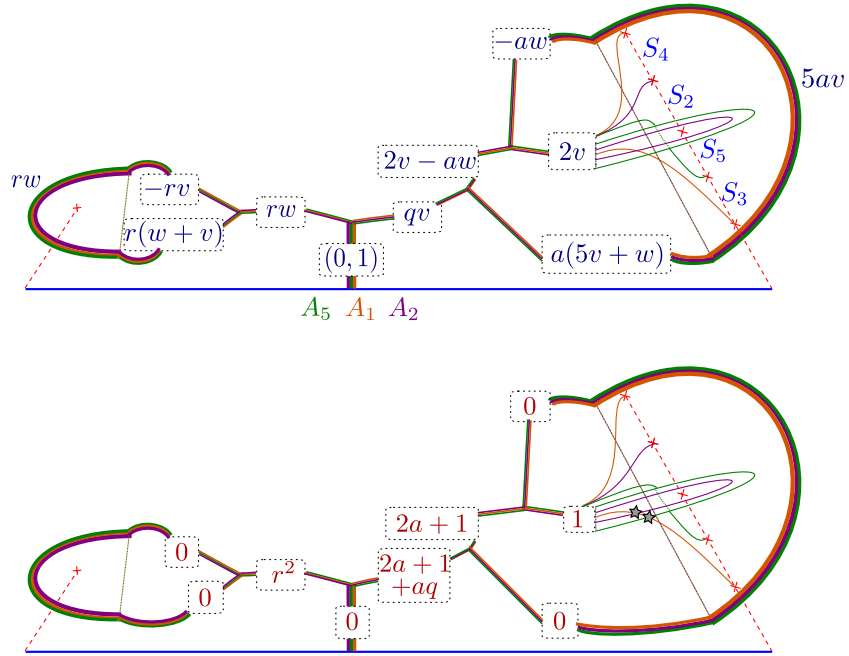


Figure 30: STCs in classes  $A_1$ ,  $A_2$  and  $A_5$  in a neighborhood  $\mathfrak{N}$  of the edge opposite to the smooth corner in a arbitrary ATF of  $Bl_4(\mathbb{CP}^2)$  associated with a solution of  $1 + q^2 + 5r^2 = 5qr$ .

$$qr = r^2 + 3a + 2 + aq = \frac{5r^2 + (q-3)(q+3) + 10}{5} = \frac{5r^2 + q^2 + 1}{5}.$$

This concludes the verification for the case of  $Bl_4(\mathbb{CP}^2)$ .  $\square$

## 5 Quiver Combinatorics and Ellipsoid Embeddings

The aim of this section is to discuss the connection between the numerics of sharp ellipsoid embeddings and the arithmetic of cluster algebras. Let  $M \cong \mathbb{Z}^2$  be the character lattice of the algebraic torus  $(\mathbb{C}^*)^2$ , and  $N = \text{Hom}(M, \mathbb{Z})$  its dual lattice. Let us fix a 4-dimensional symplectic toric variety  $X_\Delta = (X, \omega)$  with fan  $\Delta \subseteq N$ , up to  $\text{GL}_2(\mathbb{Z})$ -equivalence. Following the strategy presented in this article, the first question we are addressing is the existence of a sharp symplectic embedding

$$i : E(1, a) \longrightarrow (X, \omega),$$

for values of  $a \in \mathbb{R}^+$ . For the cases in which the symplectic embedding  $i$  exists, the second question is addressing the existence of a symplectic embedding

$$\iota : E(1, a) \longrightarrow (X \setminus D, \omega), \quad a \in \mathbb{R}^+,$$

where  $D \subseteq (X, \omega)$  is a symplectic divisor. This second part can be solved as in Subsection 3.3, and the arithmetic coincides for the sequence of absolute sharp embeddings  $\{i_n\}$  and its relative  $\{\iota_n\}$  counterpart. Thus onwards, only the problem of ellipsoid embeddings into closed toric varieties is addressed. Let us now provide an algebraic recipe for potentially finding convergent sequences

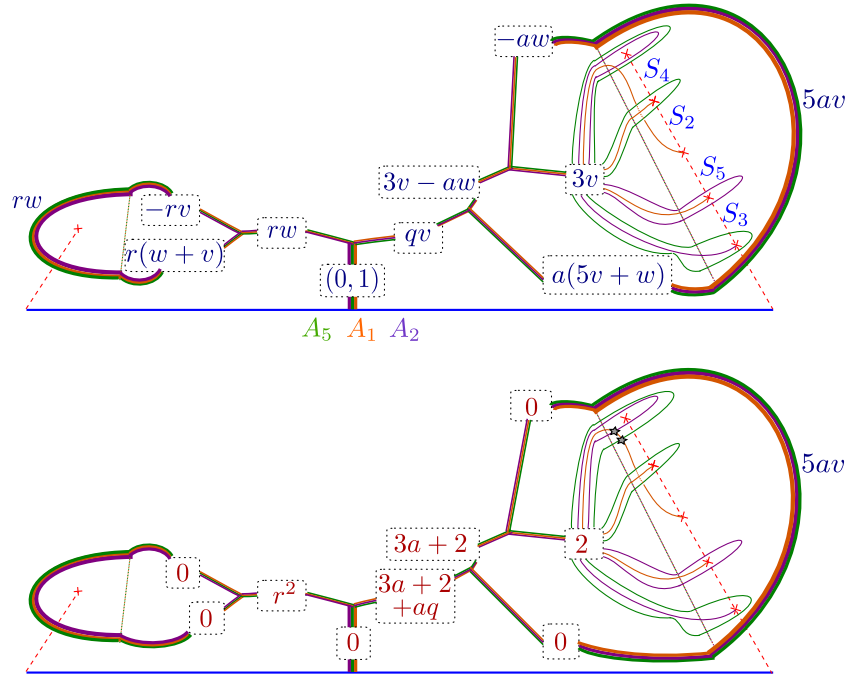


Figure 31: STCs in classes  $A_1$ ,  $A_2$  and  $A_5$  in a neighborhood  $\mathfrak{N}$  of the edge opposite to the smooth corner in a arbitrary ATF of  $Bl_4(\mathbb{CP}^2)$  associated with a solution of  $1 + q^2 + 5r^2 = 5qr$ .

$\{\alpha_n\}_n \in \mathbb{N}$  of positive real numbers such that  $E(1, \alpha_n)$  sharply embeds into  $(X, \omega)$ , constructing sharp points for an infinite staircase.

For that, let us introduce a cluster algebra  $C_\Delta$  associated to the fan  $\Delta \subseteq N$  [1, 29]. Let  $E = |E(\Delta)|$  be the number of edges of the fan  $\Delta$ . The initial seed for  $C_\Delta$  is given by the following quiver  $Q_\Delta$ :

1. The vertices of  $Q_\Delta$  are in bijection with the edges  $\{e_1, \dots, e_E\}$  of the fan  $\Delta$ ,
2. The number of arrows between to vertices  $v_i, v_j$ , associated to edges  $e_i, e_j$  is given by

$$\max\{\rho_i \wedge \rho_j, 0\}$$

where  $\rho_i$  is the primitive normal vector of the edge  $e_i$ ,  $1 \leq i, j \leq E$ .

Thus, the cluster variables for this seed are indexed by the edges  $\{e_1, \dots, e_E\}$  of the fan, and the skew-symmetric exchange matrix  $B$  is given by the exterior products of the two primitive normal vectors associated to each pair of edges. Cluster mutation consists of quiver mutation in pair with a mutation of the cluster variables. By definition, the cluster algebra  $C_\Delta$  associated to  $\Delta$  is generated by all the cluster variables of all the seeds obtained by mutating our initial seed.

## 5.1 The algebraic recipe

The fan associated to an ellipsoid, or rather its compactification to a weighted projective space, is triangular. Given that the problem we address is that of ellipsoid embeddings, the first ingredient in our recipe is a sequence  $\mu_1, \dots, \mu_s$  of mutations which brings  $\Delta$  to a triangular fan  $\Delta_0$ . These mutations

are specified by an ordered choice of possibly repeated vertices  $v_1, \dots, v_s$ ,  $v_i \in V(Q)$ ,  $1 \leq i \leq s$ , in the quiver. Given that the fan  $\mu_s(\dots(\mu_1(\Delta)))$  is triangular, the sequence of mutations  $\mu_1, \dots, \mu_s$  specifies a partition of  $V(Q)$  into three sets  $V(Q) = T_1 \cup T_2 \cup F$ , where  $T_1, T_2$  are determined by which edge of  $\mu_s(\dots(\mu_1(\Delta)))$  they are sent to and the set  $F$  consists of the set of vertices which are not mutated at in the list  $\mu_1, \dots, \mu_s$ .

Given the quiver  $Q$ , declare the subset  $F \subseteq V(Q_\Delta)$  to be frozen vertices, i.e. coefficient variables for the associated cluster algebra. Evaluate the cluster variables in  $T_1 \cup T_2$  to their initial value for a minimal Markov triple  $(1, q, r)$ ,  $q, r \in \mathbb{N}$ , where the cluster variables for  $T_1$  are set to  $q$  and those of  $T_2$  to  $r$ . The recipe now starts from  $\mu_s(\dots(\mu_1(Q)))$  and reads as follows:

- (i) Mutate at *all* the vertices  $v \in T_1$ ,
- (ii) Mutate at *all* the vertices  $v \in T_2$ ,
- (iii) Repeat Steps (i) and (ii).

First, it is relevant to observe that the order in which you mutate the vertices in a given set  $T_1$ , or  $T_2$ , does not matter. This is algebraically interesting, given that these vertices are not necessarily disjoint, but geometrically clear.

Second, at the  $k$ th iteration of the recipe,  $k \in \mathbb{N}$ , the cluster variables associated to the vertices  $v \in T_1$  have all the same value  $T_1(k)$ , and the cluster variables associated to the vertices  $v \in T_2$  have all the same value  $T_2(k)$ . The required sequence is given by

$$a_n = T_1\left(\frac{n+1}{2}\right), \quad \text{if } n \text{ odd}, \quad a_n = T_2\left(\frac{n}{2}\right), \quad \text{if } n \text{ even},$$

and the infinite stair case has sharp ellipsoid embeddings points at  $\alpha_n$  being the appropriate Maslov successive quotients of  $\{a_n\}$ . This yields a cluster algebra perspective to the numerics in Subsection 3.2. Let us give the necessary detail for the almost-toric basis in the second row of Figure 1.

**Example 5.1** Let  $(X, \omega) = X(\mathcal{P}) = Bl_3(\mathbb{CP}^2)$  be the monotone delPezzo surface  $dP_3$ , corresponding to the symplectic (almost)-toric 4-manifold represented by the leftmost almost-toric base in the second row of Figure 1. The toric fan  $\Delta_{dP_3}$  associated to this moment polytope is generated by the vertices  $\{(1, 0), (0, 1), (-1, 0), (0, -1), (-1, 1), (1, -1)\}$ . The quiver  $Q_\Delta$  is depicted in Figure 32.

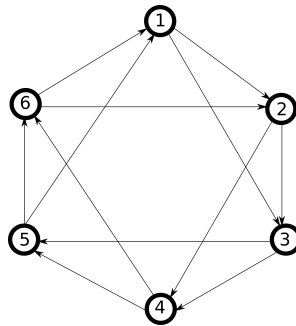


Figure 32: Quiver associated to the fan of  $Bl_3(\mathbb{CP}^2)$ .

Let  $\mu_1, \mu_2, \mu_3$  be the ordered mutations at the vertices  $v_1, v_5$  and  $v_2$ , so  $s = 3$  in this example. The toric fan  $\Delta_{dP_3}$  becomes a triangular fan after these three mutations. Indeed, the fan  $\mu_3(\mu_2(\mu_1(\Delta_{dP_3})))$  is that of  $\mathbb{P}(1, 2, 3)$ . The partition of the vertex set  $Q_{\Delta_{dP_3}}$  is:

$$T_1 = \{3, 5\}, \quad T_2 = \{1, 2, 4\}, \quad F = \{6\}.$$

Let us now follow the algebraic recipe above. First, initialize the six cluster variables

$$x_1 = x_2 = x_3 = x_4 = x_5 = x_6 = 1.$$

In what follows, we write the mutations for the cluster variables without specifying the mutation in the quiver, which is assumed to occur as well in each mutation. For instance, Figure 33 draws the quiver after mutating at the variables  $x_1, x_5$  and  $x_2$ , in this order.

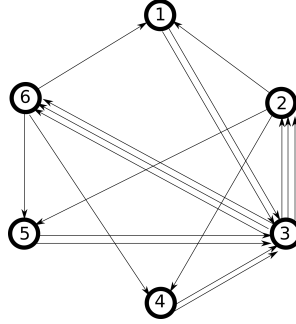


Figure 33: Quiver associated the fan of the symplectic toric 4-manifold  $Bl_3(\mathbb{CP}^2)$  after applying the three mutations  $\mu_1, \mu_2, \mu_3$  at vertices  $v_1, v_5$  and  $v_2$  respectively.

The first three mutations are at  $x_1, x_5$  and  $x_2$ , with resulting cluster variables (still) being:

$$\left\{ \begin{array}{ll} x_1 = 1, & x_3 = 1 \\ x_2 = 1, & x_5 = 1 \\ x_4 = 1, & x_6 = 1 \end{array} \right\},$$

but the current seed is that associated to the quiver in Figure 33. In this precise seed, we start mutating according to the steps. First, we mutate at  $x_1, x_2, x_4$ , and we obtain:

$$\left\{ \begin{array}{ll} x_1 = 1, & x_3 = 1 \\ x_2 = 1, & x_5 = 1 \\ x_4 = 1, & x_6 = 1 \end{array} \right\},$$

Then we mutate at the variables  $x_3, x_5$ , which leads to

$$\left\{ \begin{array}{ll} x_1 = 1, & x_3 = 2 \\ x_2 = 1, & x_5 = 2 \\ x_4 = 1, & x_6 = 1 \end{array} \right\},$$

Mutating at  $x_1, x_2, x_4$  sets the cluster variables to

$$\left\{ \begin{array}{ll} x_1 = 1, & x_3 = 2 \\ x_2 = 3, & x_5 = 2 \\ x_4 = 3, & x_6 = 1 \end{array} \right\}.$$



The next few numerical seeds of these iterative process are:

$$\left\{ \begin{array}{l} x_1 = 3, \quad x_3 = 7 \\ x_2 = 3, \quad x_5 = 7 \\ x_4 = 3, \quad x_6 = 1 \end{array} \right\} \mapsto \left\{ \begin{array}{l} x_1 = 11, \quad x_3 = 7 \\ x_2 = 11, \quad x_5 = 7 \\ x_4 = 11, \quad x_6 = 1 \end{array} \right\} \mapsto \left\{ \begin{array}{l} x_1 = 11, \quad x_3 = 26 \\ x_2 = 11, \quad x_5 = 26 \\ x_4 = 11, \quad x_6 = 1 \end{array} \right\} \mapsto \left\{ \begin{array}{l} x_1 = 41, \quad x_3 = 26 \\ x_2 = 41, \quad x_5 = 26 \\ x_4 = 41, \quad x_6 = 1 \end{array} \right\},$$

and the first few values of the sequence  $a_n$  are:

$$\{a_n\} = \{1, 1, 1, 2, 3, 7, 11, 26, 41, 97, 153, 362, 571, 1351, 2131, 5042, 7953, 18817, 29681, \dots\}.$$

The cluster variable mutation is dictated by the transformation:

$$x_{n+3} = \frac{x_{n+1}x_{n+2}+1}{x_n},$$

and satisfies the linear recurrence  $x_n = 4x_{n-2} - x_{n-4}$ . This is Sequence A005246 in the Sloane notation. Consider the Maslov weighted sequence

$$A_n = \left\{ \begin{array}{ll} A_n = 2a_n^2, & n \text{ odd,} \\ A_n = 3a_n^2, & n \text{ even.} \end{array} \right\}$$

This is the sequence associated to the balanced quivers and exactly matches our arithmetic in Subsection 3.2. In particular, the sharp points of the infinite stairs associated to the toric diagram are given by the consecutive quotients for  $\{A_n\}$ , which tend to  $2 + \sqrt{3}$ .  $\square$

## References

- [1] Mohammad Akhtar, Tom Coates, Sergey Galkin, and Alexander M. Kasprzyk. Minkowski polynomials and mutations. *SIGMA Symmetry Integrability Geom. Methods Appl.*, 8:Paper 094, 17, 2012.
- [2] Mohammad E. Akhtar and Alexander M. Kasprzyk. Mutations of fake weighted projective planes. *Proc. Edinb. Math. Soc.* (2), 59(2):271–285, 2016.
- [3] V.I. Arnol’d. *Mathematical methods of classical mechanics*, volume 60 of *Graduate Texts in Mathematics*. Springer-Verlag, New York, [1989]. Translated from the 1974 Russian original by K. Vogtmann and A. Weinstein, Corrected reprint of the second (1989) edition.
- [4] Matthew Strom Borman, Tian-Jun Li, and Weiwei Wu. Spherical Lagrangians via ball packings and symplectic cutting. *Selecta Math. (N.S.)*, 20(1):261–283, 2014.
- [5] Keon Choi, Daniel Cristofaro-Gardiner, David Frenkel, Michael Hutchings, and Vinicius Gripp Barros Ramos. Symplectic embeddings into four-dimensional concave toric domains. *J. Topol.*, 7(4):1054–1076, 2014.
- [6] David A. Cox, John B. Little, and Henry K. Schenck. *Toric varieties*, volume 124 of *Graduate Studies in Mathematics*. American Mathematical Society, Providence, RI, 2011.
- [7] Dan Cristofaro-Gardiner. Symplectic embeddings from concave toric domains into convex ones. *J. Differential Geom.*, 112(2):199–232, 2019.
- [8] Dan Cristofaro-Gardiner. Ehrhart polynomials and symplectic embeddings of ellipsoids. *Journal Lon. Math. Soc.*, 112, 2020.
- [9] Dan Cristofaro-Gardiner, Tara S. Holm, Alessia Mandini, and Ana Rita Pires. Infinite staircases and reflexive polygons. *arXiv*, 2020.

- [10] B. Feng, Y.-H. He, K. D. Kennaway, and C. Vafa. Dimer models from mirror symmetry and quivering amoebae. *Adv. Theor. Math. Phys.*, 12(3):489–545, 2008.
- [11] Vladimir V. Fock and Alexander B. Goncharov. Cluster ensembles, quantization and the dilogarithm. *Ann. Sci. Éc. Norm. Supér. (4)*, 42(6):865–930, 2009.
- [12] Sergey Fomin and Andrei Zelevinsky. Cluster algebras. I. Foundations. *J. Amer. Math. Soc.*, 15(2):497–529, 2002.
- [13] J. Forsgård. On dimer models and coamoebas. *Ann. Inst. Henri Poincaré D*, 6(2):199–219, 2019.
- [14] David Frenkel and Dorothee Müller. Symplectic embeddings of 4-dim ellipsoids into cubes. *J. Symplectic Geom.*, 13(4):765–847, 2015.
- [15] William Fulton. *Introduction to toric varieties*, volume 131 of *Annals of Mathematics Studies*. Princeton University Press, Princeton, NJ, 1993. The William H. Roever Lectures in Geometry.
- [16] Marco Golla and Laura Starkston. The symplectic isotopy problem for rational cuspidal curves. *arXiv*, 2020.
- [17] A. L. Gorodentsev and A. N. Rudakov. Exceptional vector bundles on projective spaces. *Duke Math. J.*, 54(1):115–130, 1987.
- [18] M. Gromov. Pseudo holomorphic curves in symplectic manifolds. *Invent. Math.*, 82(2):307–347, 1985.
- [19] Mark Gross. *Tropical geometry and mirror symmetry*, volume 114 of *CBMS Regional Conference Series in Mathematics*. Published for the Conference Board of the Mathematical Sciences, Washington, DC; by the American Mathematical Society, Providence, RI, 2011.
- [20] Daniel R. Gulotta. Properly ordered dimers,  $R$ -charges, and an efficient inverse algorithm. *J. High Energy Phys.*, (10):014, 31, 2008.
- [21] Paul Hacking and Yuri Prokhorov. Smoothable del pezzo surfaces with quotient singularities. *Compos. Math.*, 146(1):169–192, 2010.
- [22] Jeff Hicks. Tropical Lagrangians and Homological Mirror Symmetry. *arXiv:1904.06005*, 2019.
- [23] Richard Hind. Lagrangian unknottedness in Stein surfaces. *Asian J. Math.*, 16(1):1–36, 2012.
- [24] Michael Hutchings. Embedded contact homology and its applications. In *Proceedings of the International Congress of Mathematicians. Volume II*, pages 1022–1041. Hindustan Book Agency, New Delhi, 2010.
- [25] Michael Hutchings. Quantitative embedded contact homology. *J. Differential Geom.*, 88(2):231–266, 2011.
- [26] Michael Hutchings. Beyond ECH capacities. *Geom. Topol.*, 20(2):1085–1126, 2016.
- [27] Nathan Owen Ilten. Deformations of smooth toric surfaces. *Manuscripta Math.*, 134(1-2):123–137, 2011.
- [28] Nathan Owen Ilten and Robert Vollmert. Deformations of rational  $T$ -varieties. *J. Algebraic Geom.*, 21(3):531–562, 2012.
- [29] Alexander Kasprzyk, Benjamin Nill, and Thomas Prince. Minimality and mutation-equivalence of polygons. *Forum Math. Sigma*, 5:e18, 48, 2017.
- [30] P. W. Kasteleyn. Graph theory and crystal physics. In *Graph Theory and Theoretical Physics*, pages 43–110. Academic Press, London, 1967.
- [31] J. Kollár and N. I. Shepherd-Barron. Threefolds and deformations of surface singularities. *Invent. Math.*, 91(2):299–338, 1988.
- [32] Francois Lalonde and Dusa McDuff. The classification of ruled symplectic 4-manifolds. *Math. Res. Lett.*, 3(6):769–778, 1996.
- [33] Weonmo Lee, Yong-Geun. Oh, and Renato Vianna. Asymptotic behavior of exotic Lagrangian tori  $T_{a,b,c}$  in  $\mathbb{CP}^2$  as  $a + b + c \rightarrow \infty$ . *arXiv:1904.11775*, 2019.

- [34] Naichung Conan Leung and Margaret Symington. Almost toric symplectic four-manifolds. *J. Symplectic Geom.*, 8(2):143–187, 2010.
- [35] Jun Li, Tian-Jun Li, and Weiwei Wu. The symplectic mapping class group of  $\mathbb{C}P^2 \# n \overline{\mathbb{C}P^2}$  with  $n \leq 4$ . *Michigan Math. J.*, 64(2):319–333, 2015.
- [36] Tian-Jun Li and Weiwei Wu. Lagrangian spheres, symplectic surfaces and the symplectic mapping class group. *Geom. Topol.*, 16(2):1121–1169, 2012.
- [37] Cheuk Yu Mak and Helge Ruddat. Tropically constructed Lagrangians in mirror quintic threefolds. *arXiv:1904.11780*, 2019.
- [38] Diego Matessi. Lagrangian pairs of pants. *arXiv:1802.02993*, 2018.
- [39] Dusa McDuff. Rational and ruled symplectic 4-manifolds. In *Geometry of low-dimensional manifolds, 2 (Durham, 1989)*, volume 151 of *London Math. Soc. Lecture Note Ser.*, pages 7–14. Cambridge Univ. Press, Cambridge, 1990.
- [40] Dusa McDuff. The structure of rational and ruled symplectic 4-manifolds. *J. Amer. Math. Soc.*, 3(3):679–712, 1990.
- [41] Dusa McDuff. Symplectic embeddings of 4-dimensional ellipsoids. *J. Topol.*, 2(1):1–22, 2009.
- [42] Dusa McDuff and Felix Schlenk. The embedding capacity of 4-dimensional symplectic ellipsoids. *Ann. of Math. (2)*, 175(3):1191–1282, 2012.
- [43] Grigory Mikhalkin. Amoebas of algebraic varieties and tropical geometry. In *Different faces of geometry*, volume 3 of *Int. Math. Ser. (N. Y.)*, pages 257–300. Kluwer/Plenum, New York, 2004.
- [44] Grigory Mikhalkin. Decomposition into pairs-of-pants for complex algebraic hypersurfaces. *Topology*, 43(5):1035–1065, 2004.
- [45] Grigory Mikhalkin. Enumerative tropical algebraic geometry in  $\mathbb{R}^2$ . *J. Amer. Math. Soc.*, 18(2):313–377, 2005.
- [46] Grigory Mikhalkin. Tropical geometry and its applications. In *International Congress of Mathematicians. Vol. II*, pages 827–852. Eur. Math. Soc., Zürich, 2006.
- [47] Grigory Mikhalkin. Examples of tropical-to-Lagrangian correspondence. *Eur. J. Math.*, 5(3):1033–1066, 2019.
- [48] Grigory Mikhalkin. Spines for amoebas of rational curves. *arXiv:1906.04500*, 2019.
- [49] Alexei N. Rudakov. Markov numbers and exceptional bundles on  $P^2$ . *Izv. Akad. Nauk SSSR Ser. Mat.*, 52(1):100–112, 240, 1988.
- [50] Alexei N. Rudakov. Exceptional vector bundles on a del pezzo surface. In *Algebraic geometry and its applications (Yaroslavl, 1992)*, Aspects Math., E25, pages 177–182. Friedr. Vieweg, Braunschweig, 1994.
- [51] Felix Schlenk. Symplectic embedding problems, old and new. *Bull. Amer. Math. Soc. (N.S.)*, 55(2):139–182, 2018.
- [52] Margaret Symington. Four dimensions from two in symplectic topology. In *Topology and geometry of manifolds (Athens, GA, 2001)*, volume 71 of *Proc. Sympos. Pure Math.*, pages 153–208. Amer. Math. Soc., Providence, RI, 2003.
- [53] Michael Usher. Infinite staircases in the symplectic embedding problem for four-dimensional ellipsoids into polydisks. *Algebr. Geom. Topol.*, 19(4):1935–2022, 2019.
- [54] R. Vianna. Infinitely many exotic monotone Lagrangian tori in  $\mathbb{C}P^2$ . *J. Topol.*, 9(2):535–551, 2016.
- [55] R. Vianna. Infinitely many monotone Lagrangian tori in del Pezzo surfaces. *Selecta Math. (N.S.)*, 23(3):1955–1996, 2017.
- [56] Renato Vianna. Infinitely many exotic monotone Lagrangian tori in  $\mathbb{C}P^2$ . *J. Topol.*, 9(2):535–551, 2016.

- [57] Renato Vianna. Infinitely many monotone Lagrangian tori in del Pezzo surfaces. *Selecta Math. (N.S.)*, 23(3):1955–1996, 2017.

*University of California Davis, Dept. of Mathematics, Shields Avenue, Davis, CA 95616, USA*

*Institute of Mathematics, Federal University of Rio de Janeiro (UFRJ), Rio de Janeiro, Brazil*

[casals@math.ucdavis.edu](mailto:casals@math.ucdavis.edu), [renato@im.ufrj.br](mailto:renato@im.ufrj.br)